

**PRODUCTION OF HYDROGEN VIA HYDROLYSIS USING  
ALUMINUM WASTE CAN POWDER COMPOSITES FOR CARBON  
DIOXIDE METHANATION**

By

**LIM SENG TAT**

A dissertation submitted to the Department of Environmental Engineering  
Faculty of Engineering and Green Technology,  
Universiti Tunku Abdul Rahman,  
in partial fulfillment of the requirements for the degree of  
Master of Engineering Science  
February 2022

## TABLE OF CONTENTS

	<b>Page</b>
<b>ABSTRACT</b>	<b>ii</b>
<b>ACKNOWLEDGEMENTS</b>	<b>iii</b>
<b>APPROVAL SHEET</b>	<b>iv</b>
<b>LIST OF TABLES</b>	<b>v</b>
<b>LIST OF FIGURES</b>	<b>vi</b>
<b>LIST OF ABBREVIATIONS</b>	<b>vii</b>
<b>CHAPTER</b>	
<b>1.0 INTRODUCTION</b>	<b>1</b>
1.1 World's Energy Consumption and Fuel Shares	1
1.2 Carbon Dioxide Mitigation	5
1.3 Hydrogen as the Future Fuel	7
1.4 Aluminum Waste Can	8
1.5 Problem Statement	9
1.6 Research Objectives	11
1.7 Novelty	11
1.8 Scope of Study	12
1.9 Organization of thesis	13
<b>2.0 LITERATURE REVIEW</b>	<b>15</b>
2.1 Introduction	15
2.2 Hydrogen Production	15
2.2.1 Methane Steam Reforming (SMR)	16
2.2.2 Water-gas Shift Reaction (WGSR)	17

2.2.3	Coal Gasification (CG)	18
2.2.4	Electrolysis of Water (EW)	19
2.2.5	Biomass Gasification (BG)	25
2.2.6	Photovoltaic (PV) Electrolysis	25
2.2.7	Wind Turbine Electrolysis System (W-EL)	26
2.2.8	Hydropower Electrolysis System (H-EL)	26
2.3	Aluminum-water Reaction	29
2.3.1	Activation of Aluminum in Alkaline Condition	30
2.3.2	Mechano-chemical Activation of Aluminum in Neutral Condition	33
2.3.3	Hydrogen Production using Aluminum Waste Cans	35
2.4	Current Trends of Greenhouse Gases and Carbon Dioxide	45
2.5	Technologies of Carbon Dioxide Capture	48
2.6	Carbon Dioxide Methanation	52
<b>3.0</b>	<b>MATERIALS AND METHODS</b>	57
3.1	Introduction	57
3.2	Materials, Chemicals and Equipment	59
3.3	Preparation of Waste Can Powder	65
3.3.1	Disintegration of Waste Can Strips	65
3.3.2	Activation of Aluminum Waste Can Powder	66
3.4	Hydrolysis Setup	68
3.4.1	Hydrolysis Process Optimization	69
3.4.2	Gibbs Free Energy Calculation	70
3.5	Carbon Dioxide Methanation	71
3.5.1	Preparation of Methanation Catalyst	73
3.5.2	Catalytic Activity Calculation	75
3.6	Characterization	76
3.6.1	X-ray Diffraction Analysis	76
3.6.2	Particle Size Distribution Analysis	76
3.6.3	Brunauer-Emmet-Teller Surface Area	77
3.6.4	Field Emission Scanning Electron Microscopy	78
3.6.5	Energy-dispersive X-ray Fluorescence Spectroscopy	78

<b>4.0</b>	<b>RESULTS AND DISCUSSIONS</b>	<b>79</b>
4.1	Introduction	79
4.2	Disintegration of Aluminum Waste Cans	79
4.3	Optimization of Hydrolysis Process	82
4.3.1	Effect of Different Type of Alkaline Solutions	83
4.3.2	Effect of Different Water Source	84
4.3.3	Effect of Reaction Temperatures	86
4.4	Comparison of Hydrogen Production Via Commercial Aluminum and AWCP	87
4.5	Characterization of AWCP	88
4.5.1	BET Active Surface Area and Pore Characteristics	88
4.5.2	X-ray Fluorescence Spectroscopy (XRF)	92
4.5.3	X-ray Diffraction Analysis (XRD)	93
4.3.4	Field Emission Scanning Electron Microscopy (FESEM)	95
4.6	Hydrolysis Performance of Binary Aluminum Composites	96
4.7	Characterization of Binary AWCP Composites	100
4.7.1	X-ray Diffraction Analysis (XRD)	101
4.7.2	Field Emission Scanning Electron Microscopy (FESEM)	102
4.7.3	BET Active Surface Area	103
4.8	Hydrolysis Performance of Aluminum Ternary Composites	104
4.9	Characterization of Ternary AWCP Composites	109
4.9.1	X-ray Diffraction Analysis (XRD)	109
4.9.2	Field Emission Scanning Electron Microscopy (FESEM)	110
4.9.3	BET Active Surface Area Analysis	112
4.10	Gibbs Free Energy	112
4.11	Batch Carbon Dioxide Methanation	115
4.12	Continuous Carbon Dioxide Methanation	120
4.12.1	Continuous Carbon Dioxide Methanation via 5 min Refeed	120

<b>5.0</b>	<b>CONCLUSION AND RECOMMENDATION</b>	125
	5.1 Conclusion	125
	5.2 Recommendation for Future Work	128
	<b>LIST OF REFERENCES</b>	129-140
	<b>APPENDICES</b>	141-152
	<b>LIST OF PUBLICATIONS</b>	153

## **ABSTRACT**

### **PRODUCTION OF HYDROGEN VIA HYDROLYSIS USING ALUMINUM WASTE CAN POWDER COMPOSITES FOR CARBON DIOXIDE METHANATION**

**Lim Seng Tat**

Hydrogen ( $H_2$ ) is a promising solution to conventional fossil fuel energy because it gives near-zero carbon emission and contains high calorific value. Recently methanation of carbon dioxide ( $CO_2$ ) using  $H_2$  is gaining interest. Many studies have focused on catalyst optimization of the methanation process. However, no studies have been performed to study methanation using clean  $H_2$ . The common methanation process uses commercial  $H_2$  gas, which is more expensive and therefore not commercially feasible. Therefore, a clean and sustainable  $H_2$  production method is needed for methanation. Aluminum waste can powder (AWCP) which was synthesized by novel disintegration method was used in hydrolysis reaction to produce  $H_2$  gas. Different types of alkaline solutions, different types of water sources, and different durations of disintegration time were investigated to study their effects on hydrolysis. AWCP and selected pure metals (i.e., Zinc (Zn), Tin (Sn), Magnesium (Mg) and Indium (In)) were mechanochemically activated by the ball milling method to synthesize binary AWPC composites (i.e., AWCP/Zn, AWCP/Sn, AWCP/Mg and AWCP/In) and ternary AWCP composites (i.e., AWCP/Sn/Mg and

AWCP/Sn/In) to maximize H<sub>2</sub> production by forming microgalvanic cells. Branauer-Emmet-Teller (BET) analysis proved that disintegration method using medicine blender is novel as Field Emission Scanning Electron Microscopy (FESEM) confirmed uneven fresh surfaces that are flaky in structure compared to pore-like structure of commercial Al. This method increased the BET surface area of the AWCP composites and contributed to a higher H<sub>2</sub> yield due to ball-to-ball and ball-to-jar collisions during the ball milling process, which helped water to penetrate Al more effectively. The addition of pure metals to AWCP could reduce the total reaction time significantly. Binary AWCP (3% Sn), produced 1360 ml/g H<sub>2</sub> in 240 s. However, ternary AWCP (3% Sn-3% Mg) produced 1320 ml / g of H<sub>2</sub> in 660 s. XRD analysis confirmed the formation of intermetallic phases in AWCP (3%Sn – 3% Mg). Upon optimizing the H<sub>2</sub> production, the gas was tested to produce methane (CH<sub>4</sub>) using CO<sub>2</sub> in a catalytic system. In batch methanation, AWCP (3% Sn-3% Mg) generated much higher CH<sub>4</sub> because it had a longer total reaction time and allowed longer residence time for H<sub>2</sub> and CO<sub>2</sub> to react. The pure AWCP (100%) produced the highest CH<sub>4</sub> production due to low gas hourly space velocity (GHSV). For continuous methanation, AWCP (3% Sn) yielded the highest amount of CH<sub>4</sub> despite high GHSV because a lot of unreacted H<sub>2</sub> was left for further reaction continuously. In this study, a feasible and sustainable clean generation of H<sub>2</sub> for use in methanation was successfully achieved.

## **ACKNOWLEDGEMENT**

I would like to express my deepest appreciation to my supportive and experienced supervisor (Prof. Dr. Sumathi Sethupathi) and co-supervisor (Dr. Tan Kok Tat) who have been of tremendous support of this research. They have been providing technical and theoretical assistant on this research throughout the process.

Secondly, I would like to thank Universiti Tunku Abdul Rahman for the research grant provided throughout this study which helped me to sustain all the expenses throughout this research.

Thirdly, I would like to thank Universiti Putra Malaysia for the friendliness which allowed me to utilize and made full use of their laboratory equipment and facilities throughout the research.

## APPROVAL SHEET

This dissertation/thesis entitled “**PRODUCTION OF HYDROGEN VIA HYDROLYSIS USING ALUMINUM WASTE CAN POWDER COMPOSITES FOR CARBON DIOXIDE METHANATION**” was prepared by LIM SENG TAT and submitted as partial fulfillment of the requirements for the degree of Master of Engineering Science at Universiti Tunku Abdul Rahman.

Approved by:

\_\_\_\_\_  
(Prof. Dr. Sumathi Sethupathi)

Date: \_\_\_\_\_

Supervisor

Department of Environmental Engineering

Faculty of Engineering and Green Technology

Universiti Tunku Abdul Rahman

\_\_\_\_\_  
(Dr. Tan Kok Tan)

Date: \_\_\_\_\_

Co-supervisor

Department of Petrochemical Engineering

Faculty of Engineering and Green Technology

Universiti Tunku Abdul Rahman

## LIST OF TABLES

Table		Page
2.1	Specifications of three major types of electrolyzers	20
2.2	Conventional techniques to produce H <sub>2</sub> , its advantages and limitations	21-22
2.3	H <sub>2</sub> production systems with modifications and its results	23-24
2.4	Technical data for various H <sub>2</sub> production methods	28
2.5	Hydrolysis performance of Al and its alloys in alkaline conditions	37-38
2.6	Hydrolysis performance of Al and its alloys in neutral conditions	39-42
2.7	Advantages and disadvantages of post-combustion technology	51
2.8	A review of past methanation experiments	55-56
3.1	List of materials	59-61
3.2	List of equipment used for the study	62-64
3.3	Composition of binary and ternary AWCP	67
3.4	Details of the parameter studied for hydrolysis optimization	70
4.1	BET surface area and the pore characteristics of disintegrated AWCP	90
4.2	EDXRF analysis of disintegrated AWCP produced from 100 PLUS waste cans	93
4.3	The major peaks (degree) and its corresponding intensity (a.u.) for both disintegrated AWCP and commercial Al	94

4.4	H <sub>2</sub> production performance analysis of AWCP and binary AWCP composites	98-99
4.5	BET surface area of binary AWCP composites	104
4.6	H <sub>2</sub> production performance analysis of AWCP and ternary AWCP composites	106
4.7	Comparison of research outcomes with literature work	108
4.8	BET surface area of ternary AWCP composites	112
4.9	Hydrolysis results, final temperature and respective Gibbs free energy of AWCP samples.	114
4.10	Standard-state enthalpy of formation and absolute entropy data	114
4.11	CH <sub>4</sub> total production and catalytic activity for batch methanation based on 0.5g sample without refeed	119
4.12	CH <sub>4</sub> total production and catalytic activity for continuous methanation based on 0.5g sample with refeed every 5 min for 1 hr	124

## LIST OF FIGURES

Figures		Page
1.1	Global total energy consumption from 1990-2017 in MT	2
1.2	Global fuel shares of total energy supply in 2018	3
1.3	Global fuel shares of electricity production by fuel in 2017	4
1.4	Global CO <sub>2</sub> emissions from fuel combustion by region in 2017	5
1.5	Thermochemical and electrochemical routes for CO <sub>2</sub> hydrogenation to form valuable products	7
2.1	Total GHGs emissions (GT of CO <sub>2</sub> equivalent) from 1970-2012	45
2.2	Total GHGs emissions in 2017 (equivalent to 6,457 GT CO <sub>2</sub> emissions)	46
2.3	World's total CO <sub>2</sub> emission (GT) from 1960-2014	47
2.4	Shares of total 1297 patents on solid sorbents, membrane and solvent	48
2.5	Overview of post-combustion carbon capture technologies	50
3.1	Overall workflow	58
3.2	Water displacement apparatus set-up for Al hydrolysis for H <sub>2</sub> production	68
3.3	Schematic diagram of CO <sub>2</sub> methanation process utilizing H <sub>2</sub> produced from the AWCP/NaOH/H <sub>2</sub> O reaction	71
3.4	Actual methanation rig facility at PutraCAT Lab, Universiti Putra Malaysia	72

3.5	Procedural steps for 15 wt % Ni/PSAC catalyst synthesis via wetness impregnation method	74
4.1	Particle size distribution of AWCP after (a) 1 min (b) 5 min, (c) 10 min, (d) 15 min, (e) 20 min disintegration and (f) commercial Al.	81
4.2	Hydrolysis performance of disintegrated AWCP using different type of alkaline solutions	84
4.3	Hydrolysis performance of disintegrated AWCP using different types of water sources	85
4.4	Hydrolysis performance of disintegrated AWCP at different reaction temperatures (°C)	86
4.5	Hydrogen production of disintegrated AWCP versus commercial Al powder	88
4.6	N <sub>2</sub> adsorption/desorption of AWCP after 20 min of disintegration time	92
4.7	The major peaks for Al material (degree) and its corresponding intensity (a.u.) for AWCP and commercial Al	94
4.8	FESEM images of (a) commercial Al and (b) AWCP at 20K magnification	95
4.9	H <sub>2</sub> production graph of AWCP binary composites: a) AWCP/Sn, b) AWCP/Mg, c) AWCP/In and d) AWCP/Zn	97
4.10	The XRD patterns of binary AWCP (3% Sn) composite	101
4.11	FESEM micrographs of AWCP (3% Sn) composite at X1500 magnification (a) and at X500 magnification (b); with EDS mappings of AWCP (c) and Sn (d)	103
4.12	H <sub>2</sub> production graph over time of AWCP ternary composites (a) AWCP/Sn/Mg and (b) AWCP/Sn/In	105
4.13	The XRD patterns of AWCP (3% Sn-3% Mg) ternary composite	110
4.14	FESEM micrographs of AWCP (3% Sn-3% Mg) ternary composite at ×1500 magnification (a) and X500 magnification (b); with EDS mappings of AWCP (c), Mg (d) and Sn (e)	111

4.15	Total H <sub>2</sub> and CH <sub>4</sub> production profile for batch CO <sub>2</sub> methanation for selected AWCP samples	118
4.16	(a) H <sub>2</sub> production and (b) CH <sub>4</sub> production (μmol) from continuous CO <sub>2</sub> methanation based on every 5-min re-feed for 1 hr using AWCP (100%), AWCP (97%), AWCP (94%), AWCP (3% Sn) binary composite, and AWCP (3% Sn - 3% Mg) ternary composite	123

## LIST OF ABBREVIATIONS

Al	Aluminum
AWCP	Aluminum waste can powder
BET	Brunauer-Emmett-Teller
CO <sub>2</sub>	Carbon dioxide
FESEM	Field emission scanning electron microscopy
GC	Gas chromatography
GHGs	Greenhouse gases
H <sub>2</sub>	Hydrogen
In	Indium
CH <sub>4</sub>	Methane
Mg	Magnesium
N <sub>2</sub>	Nitrogen
PSA	Particle size analysis
NaOH	Sodium hydroxide
Sn	Tin
H <sub>2</sub> O	Water
XRF	X-ray fluorescence
XRD	X-ray diffraction
Zn	Zinc

## **CHAPTER 1**

### **INTRODUCTION**

#### **1.1 World's Energy Consumption and Fuel Shares**

The world's total energy consumption has increased from 8,457 MT (1990) to 13,576 MT (2017). Figure 1.1 shows the total global consumption of energy from 1990 to 2017 in MT (1 MT is equivalent to 42 GJ or 11,630 kWh). Global Energy Statistical Yearbook (2019) disclosed the United States and China being the primary contributors to increase in global energy production. However, there was a decrease in energy production in European Union (EU) due to reduced electricity generation from nuclear energy sources, depleted oil and gas resources, and most importantly, climate policies that determined the end of electricity generation using coal. Younas et al. (2019) also discussed the world's energy demand and expected the demand to reach about 48 % (20,538 MT) in the upcoming 20 years. It is to be noted that, most of the energy currently being used is primarily supplied by the conventional fossil fuels which generally produces significant amounts of carbon footprint. Meanwhile, Malaysia is expected to consume about 100 MT by 2030 (Ghani et al., 2019).

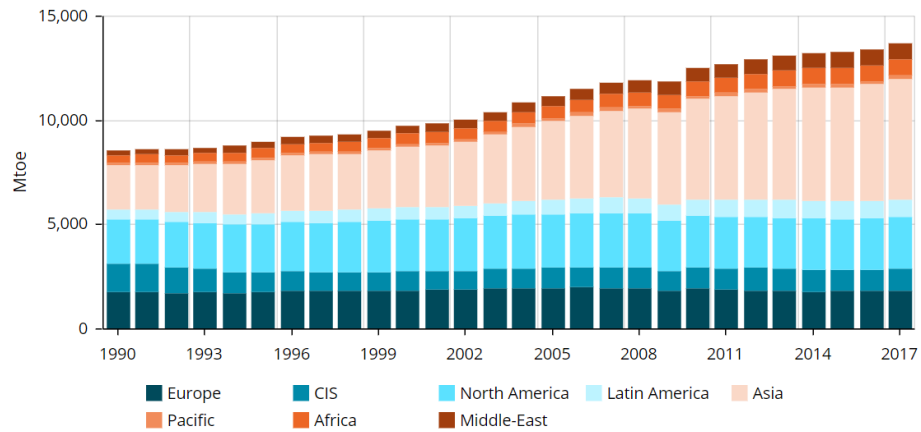


Figure 1.1: Global total energy consumption from 1990-2017 in MT (Global Energy Statistical Yearbook, 2019).

Figure 1.2 shows the global total primary energy supply fuel shares in 2018. It was reported that the conventional fossil fuels comprised of natural gas, oil and coal primarily accounted for about 79.4 % of world's total primary energy supply; 9.6 % from nuclear energy; 2.3 % from hydropower; 6.1 % from other renewable energy and waste; and 2.6 % from the others (Key World Energy Statistics, 2019).

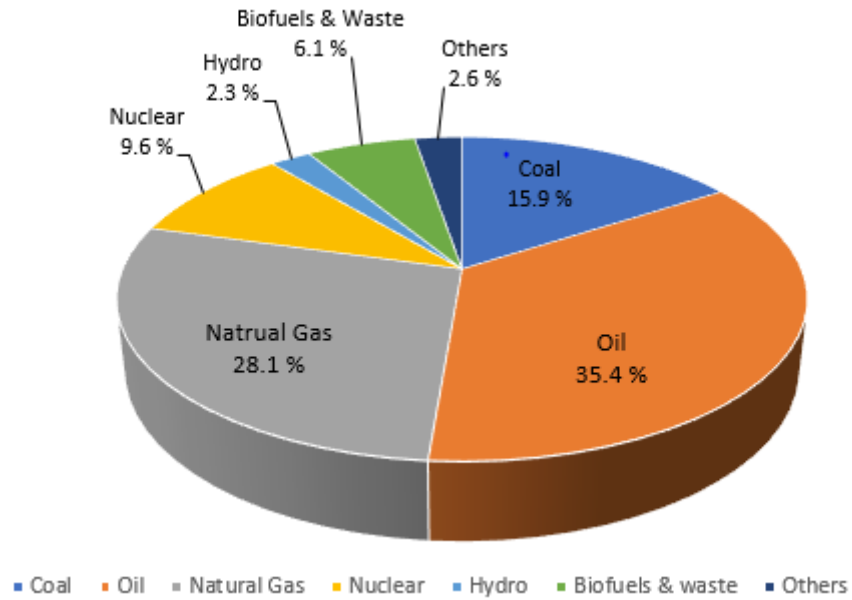


Figure 1.2: Global fuel shares of total energy supply in 2018 (Key World Energy Statistics, 2019).

Whereas, Figure 1.3 shows the global electricity production fuel shares in 2017. The conventional fossil fuels (fossil thermal) were responsible for 64.8 % of total electricity generation; 10.3 % from nuclear power; 15.9 % from hydropower; and 9.0 % from the other sources (Key World Energy Statistics, 2014).

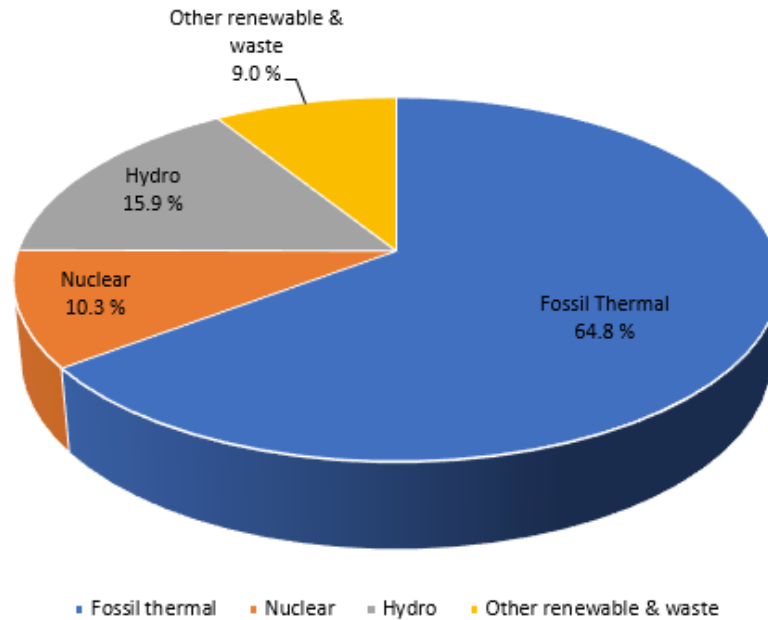


Figure 1.3 Global fuel shares of electricity production by fuel in 2017 (Key World Energy Statistics, 2019).

Figure 1.4 shows the global CO<sub>2</sub> emissions by fuel combustion by region in 2017. The Organization for Economic Cooperation and Development (OECD) comprised of 35.3 % world's emissions; 28.3 % from China; 12.7 % from non-OECD Asia; 7.5 % from non-OECD Europe and Eurasia; 5.4 % from Middle East; 3.9 % from Bunkers; and 3.2 % from non-OECD Americas (Key World Energy Statistics, 2019). On the other hand, CO<sub>2</sub> emissions per capita increased from 1.33 tons (year 1971) to 7.98 tons of (year 2020) at annual increment rate of 3.8% (Knoema, 2022). The above data has clearly shown that fossil fuels are still in high demand compared to renewable energy. Moreover, CO<sub>2</sub> mitigation is required with immediate effect to reduce CO<sub>2</sub> level as much as possible to prevent further damage to the earth.

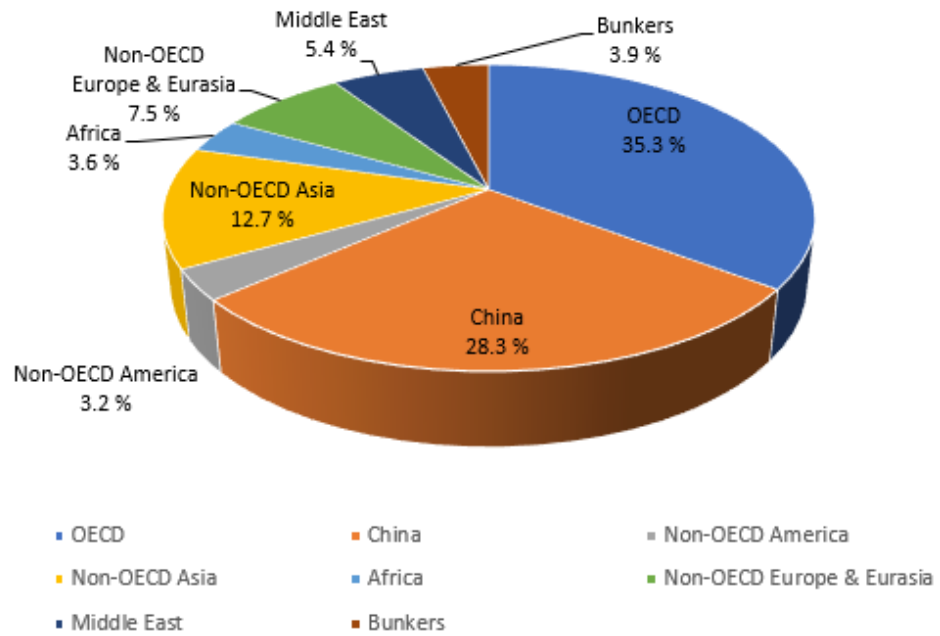


Figure 1.4: Global CO<sub>2</sub> emissions from fuel combustion by region in 2017 (Key World Energy Statistics, 2019).

## 1.2 Carbon Dioxide Mitigation

The above-mentioned data has clearly supported the environmental crisis related to carbon emissions. Thus, CO<sub>2</sub> mitigation is urgently required to resolve this global issue. Many nations have come in consensus to solve this carbon emissions under the Paris Agreement, adopted by 55 countries (which are responsible for about 55 % of global emissions) to work towards the same goal, which is to fight climate change globally. This urges all scientists and researchers to find out green and sustainable methods to produce energy to meet the global requirements at the same time.

Effective solutions are needed to resolve the global environmental problems. Carbon capture and storage (CCS) and CO<sub>2</sub> transformation into value-added products were promising solutions for carbon emissions mitigation (Younas et al., 2016). CCS captures CO<sub>2</sub> gas from a point source of any type of industrial plants such as cement factories, iron and steel, and chemical sectors. Metz et al (2005) stated incorporating CCS in a conventional power plant to reduce CO<sub>2</sub> emissions by 80-90 %. There are different CCS configurations of technologies such as oxy combustion, cryogenic combustion and pre-combustion and post-combustion. According to Jacquemin, Beuls and Ruiz (2010), high cost and transportation difficulties are some of the drawbacks of these CCS technologies.

Due to the major drawbacks of CCS, another promising CO<sub>2</sub> mitigation solution worth investigating is CO<sub>2</sub> transformations into value-added products. Many researches have been focusing on CO<sub>2</sub> conversions; for instance, to produce methane (CH<sub>4</sub>) which is one of the important fuels in power generation in many industries. Other than CH<sub>4</sub>, CO<sub>2</sub> can be converted to many other products such as oxalic acid, dimethyl ether (DME), alkyl formates, alkyl formamides, carbon monoxide (CO), syngas or synthesis gas (mixture of H<sub>2</sub>, CO and CO<sub>2</sub>), and methanol through thermochemical or electrochemical route (Younas et al., 2016). Figure 1.5 indicates value-added products that can be formed from thermochemical and electrochemical routes via CO<sub>2</sub> hydrogenation. CO<sub>2</sub> transformation to CH<sub>4</sub>, called Sabatier reaction or CO<sub>2</sub> methanation worthwhile to be explored and researched. The reason is that the CO<sub>2</sub> methanation utilizes the waste CO<sub>2</sub> or CO from the point sources in any manufacturing or process plants, the CH<sub>4</sub> that is generated will not directly go into the atmosphere. Instead

of that, the CH<sub>4</sub> generated will be utilized as a fuel to produce energy. As a result, this will further increase the energy efficiencies of the plants and reduce overall energy consumptions.

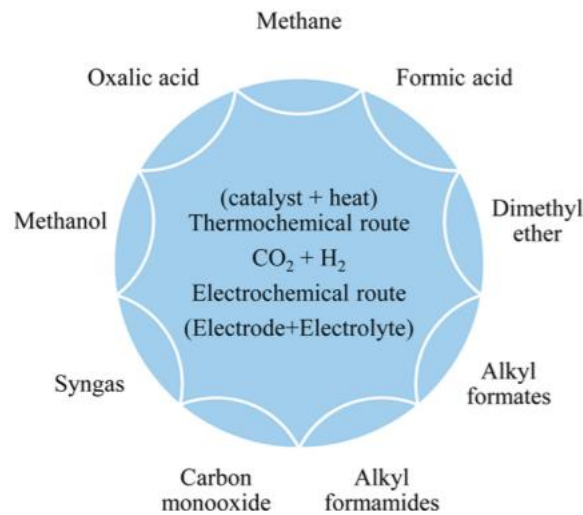


Figure 1.5: Thermochemical and electrochemical routes for CO<sub>2</sub> hydrogenation to form valuable products (Younas et al., 2016).

### 1.3 Hydrogen as the Future Fuel

Although conventional fossil fuels have been playing a dominant role in production of global energy, H<sub>2</sub> has also been making significant contributions to the energy systems. Most importantly, H<sub>2</sub> is clean and near zero or zero carbon emissions. Now that the environmental issue is a global concern, H<sub>2</sub> energy is promising alternative solution in the energy transition. The demand for H<sub>2</sub> is growing while the primary source for the H<sub>2</sub> production currently is fossil-based fueled. H<sub>2</sub> has many uses in many sectors. H<sub>2</sub> is used in refining

and production of ammonia, methanol and steel. El-Emam and Ozcan (2019) mentioned the world's H<sub>2</sub> consumption is approximately 65 million tonnes annually. In Malaysia, Sarawak has introduced H<sub>2</sub> fuel cell buses in an attempt to initiate the green public transport. These aforementioned buses are manufactured by Foshan Feishi Automobile Manufacture Co. Ltd. in China. It can travel a distance of 300 km with consumption of 20 kg H<sub>2</sub>. The H<sub>2</sub> came from the Integrated H<sub>2</sub> Production Plant and refueling station built by Sarawak's Energy in collaboration with the renowned industrial gas maker, Linde EOX Sdn Bhd. The H<sub>2</sub> is produced via an electrochemical process converting water into H<sub>2</sub> gas through electrolysis of water (Al-Ogaili et al., 2021). It is crucial for the authorities and government bodies to acknowledge the contribution of H<sub>2</sub> to the energy transition that is in effective implementation, conventional fossil fuels will deplete one day, the transition to a renewable energy is inevitable.

#### **1.4 Aluminum Waste Cans**

Aluminum has been widely used for packaging of food and beverage products, transportation, and building all over the world due to aluminum is having many desirable properties including its light-weight (Wang et al., 2014). Elsarrag, Elhoweris and Alhorr (2017) reported global aluminum production at approximately 61 million MT annually. Aluminum waste cans can be readily recycled. However, Ben (2019) reported the problem of aluminum recycling on a global scale. Significant amount of aluminum waste is disposed of in landfill despite its reusability potential. Disposal of aluminum waste into the landfills

does not pose a problem initially as they can be dormant for a long time. However, the possibility of contacting with water at high pressures can generate  $H_2$  in the landfill posing risk of combustion and explosion (Elsarrag, Elhoweris and Alhorr, 2017). This could lead to landfill fires and toxic emissions that may affect the health of nearby communities. On top of that, only about 10 – 15 % of aluminum waste are being recycled globally (Ben, 2019) Additionally, the smelting of cans in aluminum waste recycling also posed inefficiencies contributing to recycling issues such as production of salt cake, a combination of aluminum nitrides, oxides, metals and salts which are expensive to be recycled (Ben, 2019). The aluminum waste cans are potential raw materials in production of green and renewable high-purity  $H_2$  gas in view of replacing or integrating with the high carbon-footprint steam reforming process which conventionally generates  $H_2$  currently. This study aims to resolve recycling of aluminum waste and its potential to generate green  $H_2$  gas.

## **1.5 Problem Statement**

Increasing demand for energy, aluminum waste dumping and the rapid climatic change due to the increasing amount of atmospheric  $CO_2$  have been deeply associated with current global warming conditions. In view of increasing demand of energy, the dependency of current conventional fossil fuels would not be sustainable as they are not renewable, depleting from time to time, and are high in carbon footprint.

Aluminum waste dumping and if the initiatives of aluminum waste recycling is not started immediately, it would lead to another associated global emission of pollutants. All these contributions directly or indirectly contribute towards the increase of atmospheric CO<sub>2</sub> which will lead to global warming and climatic change. All these are evitable if efforts on finding green solutions are being made on a global scale.

Besides, considerable efforts have been made in capturing CO<sub>2</sub> from major sources and converting it to a valuable fuel, methane (CH<sub>4</sub>) in a process called methanation or Sabatier reaction. The researchers are currently using commercial H<sub>2</sub> for methanation and emphasized on the optimization of catalysts; commonly, nickel-based catalysts (Zhang et al., 2014; Mutz et al., 2015; Jia et al., 2019). The commercial H<sub>2</sub> produced from conventional methods are of high carbon footprint and H<sub>2</sub> has higher calorific value compared to that of CH<sub>4</sub> gas. This results in loss of energy efficiency. Therefore, methanation using commercial H<sub>2</sub> gas is not feasible and sustainable.

The aim of this research is to optimize the production of H<sub>2</sub> gas from Al waste cans and test its potential for CO<sub>2</sub> methanation to produce value-added CH<sub>4</sub>. The expected output of this study is an economic, green and sustainable H<sub>2</sub> production system from Al waste cans and a potential source of H<sub>2</sub> for CO<sub>2</sub> methanation.

## **1.6 Research Objectives**

The research objectives are highlighted below:

1. To synthesize the aluminum waste can powder via disintegration and investigate the effect of hydrolysis process using different alkaline solutions, water sources, and duration of disintegration time for AWCP.
2. To analyze the performance of binary and ternary AWCP composites for hydrolysis.
3. To evaluate the performance of binary and ternary AWCP composites for CO<sub>2</sub> methanation via batch and continuous study.

## **1.7 Novelty**

There are many research works reported in the literature for CO<sub>2</sub> methanation using H<sub>2</sub>. However, none has been reported using H<sub>2</sub> produced from aluminum-water reaction. Many other activation methods to increase H<sub>2</sub> production from aluminum-water reaction have been reported using commercial Al powder. Nevertheless, none has been done using high-RPM disintegrated Al waste can powder and ball-milled with binary and ternary mixture of different types of metals.

## 1.8 Scope of Study

- In this study, aluminum waste can powder (AWCP) was synthesized using a disintegrator. AWCP was ball-milled with activation metals to produce AWCP composites to maximize H<sub>2</sub> production in hydrolysis with alkaline solution at room temperature.
- To further optimize the system, variables such as types of alkaline solutions, different reaction temperatures, types of water sources, and different duration of disintegration time were investigated to determine the optimized conditions for the hydrolysis system.
- The disintegrated AWCP was mechano-chemical activated by ball milling. Different compositions of AWCP composites were synthesized via ball-milling to study its effect on hydrolysis, maximum H<sub>2</sub> production volume, H<sub>2</sub> production rate and total reaction time. The optimized H<sub>2</sub> system will be used for the carbon dioxide methanation to produce CH<sub>4</sub> in batch and continuous study.
- In batch methanation, the selected pure AWCP and AWCP composites were used in carbon dioxide methanation to study the H<sub>2</sub> and CO<sub>2</sub> conversions and CH<sub>4</sub> yield. In this part, the results will be studied thoroughly to identify the factors that help increased CH<sub>4</sub> yield.
- In continuous methanation, the selected samples were allowed to run the methanation continuously for 1 hour to study the CH<sub>4</sub> production in a continuous manner.

- The outlet gas was analyzed every 5 min to investigate the amount of unreacted H<sub>2</sub>, unreacted CO<sub>2</sub>, and generated CH<sub>4</sub> to determine the conversion of H<sub>2</sub>, conversion of CO<sub>2</sub>, and CH<sub>4</sub> yield.

## 1.9 Organization of Thesis

The dissertation starts with Chapter 1 on the background of the research and adds information to support the statements. It also focuses on the novelty, problem statement, objectives and scope of the work.

Chapter 2 discloses the literature review of the study which yields critical assessment of the information that has been added such as the history of the study, the past related research which has been done, the outcomes of the research and its impact to this research. It gives readers information on the developments of the topic being studied and the improvement and novelty of this research.

Chapter 3 conveys the information on the methodology and materials that were used in the conduct of the experiment. This chapter includes methodological approach of turning aluminum waste can into powder; production of binary and ternary aluminum composites from ball milling disintegrated Al waste can powder with chosen metal elements; the batch and continuous CO<sub>2</sub> methanation process to investigate the methane production from the optimized aluminum-water reaction system. This chapter also describes the method of analysis such as XRD, FESEM, XRF, BET and PSA.

Chapter 4 discusses the results of the experiment and discussion with scientific support. The characterization results of the samples were tabulated and discussed so that readers can understand the microscopic structure and other characteristic properties of the samples produced and its relationship with the hydrolysis performance and methane production yield and selectivity.

Chapter 5 puts forward the conclusion and summary of the dissertation with results provided in a concise yet precise manner. It summarizes and reflect the research and connects with the objectives that were outlined in the beginning of the research. This chapter also includes recommendations for future work on this research area.

## **CHAPTER 2**

### **LITERATURE REVIEW**

#### **2.1 Introduction**

This chapter reviews the core topics of this research such as H<sub>2</sub> energy, global warming and CO<sub>2</sub> utilization, H<sub>2</sub> and utilization of CO<sub>2</sub> by methanation. In this section the review of current techniques of H<sub>2</sub> production, types of H<sub>2</sub> production systems are analyzed and discussed. The works related to aluminum-water reaction were thoroughly discussed to reflect and report the performances of previous researches on hydrolysis of aluminum and its alloys. Lastly, CO<sub>2</sub> methanation techniques and current trends in methanation were discussed.

#### **2.2 Hydrogen Production**

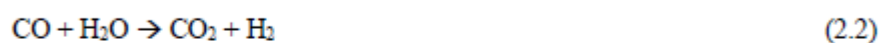
There is a growing concern towards environmental damage caused by the fossil-fuel based processes which urgently calls for carbon neutral energy systems. H<sub>2</sub> is the promising solution because it is a very clean energy. However, most of

the current H<sub>2</sub> is produced by hydrocarbons which produce significant amount of CO<sub>2</sub> to the atmosphere. Half of global H<sub>2</sub> demand is currently fulfilled by natural gas steam reforming (SMR); 30% from oil reforming, and balance 20% from coal gasification, water electrolysis, and others (Muradov and Veziroglu, 2005; Kothari, Buddhi and Sawhney, 2008; Dincer and Acar, 2015). About 95% of H<sub>2</sub> is generated by SMR and coal gasification which its feedstock is all fossil fuel based. Although these conventional methods are mature and well-established, Wang et al. (2009) commented that they should not be a deep-rooted strategy for H<sub>2</sub> production, notwithstanding the fact that they are neither sustainable nor clean.

### **2.2.1 Methane Steam Reforming (SMR)**

Methane steam reforming (SMR) produced almost 90% of the current global demand for H<sub>2</sub> at high temperature and pressure conditions (Haryanto et al., 2005). Also, about 95% of H<sub>2</sub> in the United States was produced by steam reforming in 2012 (LeValley, Richard and Fan, 2014). Steam reforming is the current most cost-effective H<sub>2</sub> production method. The feedstock for the steam reforming process can be methane, ethane, methanol, ethanol, acetone and other hydrocarbons (LeValley, Richard and Fan, 2014). Methane is the most commonly used natural gas to be used as the feedstock for steam reforming process. It is an endothermic reaction where methane is mixed with steam and heated in a steam reforming reactor or reformer at 750-1450°C and 5-25 atm over metal nickel catalyst to produce CO, CO<sub>2</sub>, H<sub>2</sub> and unreacted CH<sub>4</sub> which are

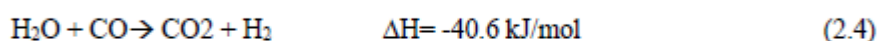
called syngas. The small amount of naturally occurring sulfur compounds in natural gas is removed by using zinc oxide adsorbent which makes the purification process easier (Muellerlanger et al., 2007). The CO is usually employed in a water-gas shift reaction (WGSR) where CO reacts with water to generate CO<sub>2</sub> and H<sub>2</sub>; therefore, more amount of H<sub>2</sub> will be formed. The final product will be fed to a pressure swing adsorption (PSA) unit for purification (Ogden, 1999; Spath and Mann, 2001). The partial and overall reactions of SMR are shown in (Eq. 2.1, Eq. 2.2 and Eq. 2.3).



### 2.2.2 Water-gas Shift Reaction (WGSR)

WGSR is a reversible and exothermic reaction between CO and water to form CO<sub>2</sub> and H<sub>2</sub>. It is a reversible reaction; therefore, upon changes in the reaction conditions, the reaction reverses, commonly known as reversed water-gas shift reaction (RWGS). WGSR is commonly employed in steam reforming and partial oxidation of hydrocarbons since both reactions produce carbon

monoxide, WGSR is employed to reduce CO levels and additionally increase H<sub>2</sub> production. Iron-based and copper-based catalysts are commonly employed in the WGSR (Newsome, 1980). Shift reactors are adiabatic with increasing temperature along the bed of the catalyst as WGSR is exothermic in nature. The reactors can be single-stage for lower purity H<sub>2</sub>; or two-stage if high purity H<sub>2</sub> was desired (Newsome, 1980). The WGSR reaction is shown in (Eq. 2.4).



### 2.2.3 Coal Gasification (CG)

Coal gasification (CG) is a process of converting carbonaceous organic matter into syngas at high temperature, at above 700°C. A consistent flow rate of oxygen and steam are both introduced into the gasifier for reaction. CG is commonly employed in regions that have limited natural gas resources and in manufacturing of ammonia and methanol (Muellerlanger et al., 2007). The syngas containing carbon monoxide can normally be integrated with a WGSR to produce more H<sub>2</sub>. The final product will be further purified in a PSA unit (Ogden, 1999; Muellerlanger et al., 2007; Pilavachi, Chatzipanagi and Spyropoulou, 2009). Gasification of coals which are fossil fuel derived is clearly a non-renewable option.

## 2.2.4 Electrolysis of Water (EW)

Electrolysis cell is used to produce H<sub>2</sub> and oxygen from water by introduction of electric current to pass between two electrodes of the cell. The water before input to the electrolyzer is pre-treated to eliminate mineral deposits and prevent any electrochemical reactions (Bhandari, Trudewind and Zapp, 2014). Electrolysis technology is well-established and being commercialized in the industry for H<sub>2</sub> production (Lodhi, 2003). The anodic and cathodic half and overall equations are shown in (Eq. 2.5, Eq. 2.6, and Eq. 2.7).

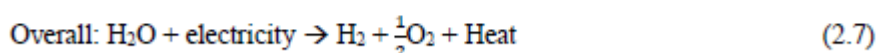


Table 2.1 shows the specifications of three major types of electrolyzers: Alkaline type, PEM and SOE. Table 2.2 systematically tabulates the conventional techniques to produce H<sub>2</sub>, its advantages and limitations which are generally fossil fuel based. Table 2.3 indicates the H<sub>2</sub> production systems with results after modifications with latest findings from literature review.

Table 2.1: Specifications of three major types of electrolyzers (Bhandari, Trudewind and Zapp, 2014; Dincer and Acar, 2015).

Specification	Alkaline	PEM	SOE
Technology maturity	Commercialized	Demonstration phase	In research
Cell temperature, °C	60-80	50-80	900-1000
Cell pressure, bar	< 30	< 30	< 30
Current density, A/cm <sup>2</sup>	0.2-0.4	0.6-2.0	0.3-1.0
Cell voltage, V	1.8-2.4	1.8-2.2	0.95-1.3
Power density, W/cm <sup>2</sup>	≤ 1.0	≤ 4.4	-
Voltage efficiency, %	62-82	67-82	81-86
Specific system energy consumption, kWh/Nm <sup>3</sup>	4.5-7.0	4.5-7.5	2.5-3.5
H <sub>2</sub> production, Nm <sup>3</sup> /hr	< 760	< 30	-
Stack lifetime, hr	< 90,000	< 20,000	< 40,000
System lifetime, yr	20-30	10-20	-
H <sub>2</sub> purity, %	> 99.8	99.999	-
Cold start up time, min	15	< 15	> 60

Table 2.2: Conventional techniques to produce H<sub>2</sub>, its advantages and limitations.

Method	Advantages	Drawbacks	References
<b>SMR</b>	<ul style="list-style-type: none"> <li>● Mature and well-established technology</li> <li>● Lowest current cost</li> <li>● Most viable approach</li> </ul>	<ul style="list-style-type: none"> <li>● High capital, operation and maintenance costs</li> </ul>	(Acar and Dincer, 2014)
<b>WGSR</b>	<ul style="list-style-type: none"> <li>● Commonly employed in steam reforming and partial oxidation of hydrocarbons to additionally convert CO to CO<sub>2</sub> and H<sub>2</sub></li> </ul>	<ul style="list-style-type: none"> <li>● Reaction which is thermodynamically limited</li> <li>● Required to operate at low temperatures</li> <li>● Higher amount of catalyst needed to achieve required CO conversions</li> </ul>	(De Falco, Piemonte and Basile, 2011)
<b>CG</b>	<ul style="list-style-type: none"> <li>● Low-cost</li> <li>● Renewable source</li> </ul>	<ul style="list-style-type: none"> <li>● High capital cost for the gasification reactor</li> <li>● Relatively lower efficiency</li> <li>● Feedstock impurities</li> </ul>	(Acar and Dincer, 2014)

Table 2.2: Continue.

Method	Advantages	Drawbacks	References
EW	<ul style="list-style-type: none"> <li>● No pollution with renewable resources such as wind and solar energy.</li> <li>● High-purity H<sub>2</sub> production</li> <li>● Less maintenance due to no moving parts.</li> </ul>	<ul style="list-style-type: none"> <li>● High capital costs</li> <li>● Low efficiency</li> </ul>	(Acar and Dincer, 2014; Bhandari, Trudewind and Zapp, 2014)

Table 2.3: H<sub>2</sub> production systems with modifications and its results.

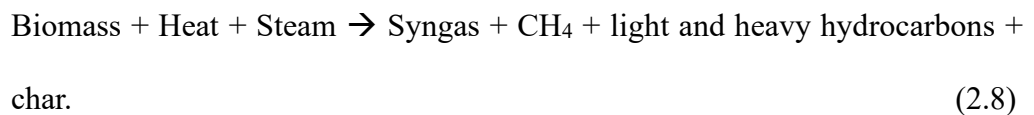
Method	Modification	Results	References
SMR	<ul style="list-style-type: none"> <li>Novel electro-catalytic SMR using Ni-based reforming catalyst, Ni-CeO<sub>2</sub>/γ-Al<sub>2</sub>O<sub>3</sub>-MgO</li> </ul>	<ul style="list-style-type: none"> <li>Reduction in reforming temperature</li> <li>Prolonged catalyst life</li> </ul>	(Lu et al., 2019)
SMR	<ul style="list-style-type: none"> <li>Using Silica-zirconia membrane supported on modified alumina for H<sub>2</sub> purification</li> </ul>	<ul style="list-style-type: none"> <li>Significant improvement in H<sub>2</sub> selectivity</li> <li>Better separation of product from CH<sub>4</sub> feed</li> </ul>	(Akbari and Omidkhah, 2019)
WGSR	<ul style="list-style-type: none"> <li>Adsorptive Reactor (AR) integrated in WGSR</li> </ul>	<ul style="list-style-type: none"> <li>Higher CO conversion</li> <li>Lower catalyst use</li> <li>Lower separator loads</li> <li>Reduced capital costs</li> <li>Improve process efficiency</li> <li>Reduced energy consumption</li> </ul>	(Karagöz et al., 2019)

Table 2.3: Continue.

Method	Modification	Results	References
CG	<ul style="list-style-type: none"> <li>● Employment of LaFeO<sub>3</sub> modified with potassium as catalyst for coal char CO<sub>2</sub> gasification</li> </ul>	<ul style="list-style-type: none"> <li>● Improved catalytic performance</li> <li>● Recyclable catalyst</li> <li>● Equipment-friendly</li> <li>● Lower initial reaction temperature</li> </ul>	(Wang et al., 2019)
EW	<ul style="list-style-type: none"> <li>● High-area chemically-modified electrodes (CME) with ternary Ru, Sb and Ta or bismuth oxides on carbon using microwave heating method</li> </ul>	<ul style="list-style-type: none"> <li>● Low cost</li> <li>● Homogenous morphology of the catalyst</li> <li>● Higher electrochemical active areas than unmodified electrodes</li> <li>● Shorter production time</li> <li>● Reduced production costs</li> </ul>	(Gonzaga et al., 2019)

### 2.2.5 Biomass Gasification (BG)

Gasification of biomass is a similar process compared to CG. The feedstock for BG derived from crops; for instance, is a renewable alternative for electricity or H<sub>2</sub> production. Few general categories of biomass resources are; for instance, industrial waste, energy crops, forestry waste, agricultural residues and municipal waste. The biomass gasification reaction equation is shown in (Eq. 2.8).



However, BG is not fully commercialized due to several technical aspects in feedstock preparation, ash removal, and gasification procedure (Muellerlanger et al., 2007; Pilavachi, Chatzipanagi and Spyropoulou, 2009).

### 2.2.6 Photovoltaic (PV) Electrolysis

PV electrolysis (PV-EL) is a water electrolysis process powered by solar power through photovoltaic cells. In PV electrolysis, the solar/H<sub>2</sub> conversion efficiency is of utmost importance. The low conversion efficiency can be made up by increasing the surface area of photovoltaic cells so as to collect more sunlight. Khaselev, Bansal and Turner (2001) reported an overall solar/H<sub>2</sub>

conversion efficiency of 7.8. However, H<sub>2</sub> production using solar energy still requires in-depth research to increase the overall solar/H<sub>2</sub> conversion efficiency.

### **2.2.7 Wind Turbine Electrolysis System (W-EL)**

H<sub>2</sub> production system using wind turbines powered by wind power to produce electricity for electrolyzer. The system is composed of a turbine, electrolyzer, H<sub>2</sub> storage device, and fuel cell. The electric power generated from wind power is utilized to generate H<sub>2</sub> from the electrolyzer. However, the development of wind-powered H<sub>2</sub> production technology is not mature enough. The major challenge in wind power is that the wind energy is also weather dependent, it is simply not a constant source of energy and geographically dependent (Li et al., 2019).

### **2.2.8 Hydropower electrolysis system (H-EL)**

H<sub>2</sub> production system from electrolyzer powered by electricity produced from hydropower. Hydropower takes advantage of the potential energy and kinetic energy stored in the water itself in order to generate electricity. Unfortunately, it is still not a mature H<sub>2</sub> production system because most of the electricity produced from hydropower will be transmitted to the national power grid. Posso et al. (2015) studied the feasibility of a hydro-powered H<sub>2</sub> production system in. However, it has limitations as well where the construction of the hydropower infrastructure will affect the environment, destroying the floras and faunas, and

therefore, a redundant idea which disobey the core values of the Paris Agreement.

Table 2.4 shows the technical data for various H<sub>2</sub> production methods such as production rate, overall efficiencies, CO<sub>2</sub> emissions, and H<sub>2</sub> production cost to compare overall of the methods.

In conclusion, SMR is carbon intensive and requires high operation and maintenance costs. WGSR requires a significant amount of catalyst to support the reaction. Both CG and EW have high capital cost with relatively low efficiency. The conventional H<sub>2</sub> production methods are energy intensive, of high capital and maintenance costs, and high emissions. On the other hand, BG has efficiency of 50-60% but CO<sub>2</sub>-capture system was not reported which requires more in-depth development. PV electrolysis has very low conversion efficiency and it is highly dependent on weather. Wind-powered has not reached mature development at this point of time. Hydro-powered H<sub>2</sub> production systems require heavy destruction of the ecosystem for its construction. In short, a sustainable, green and cost-effective H<sub>2</sub> production system is needed as an alternative solution to reduce emissions. Other promising solution to produce clean H<sub>2</sub> is urgently needed to replace fossil fuel sources.

Table 2.4: Technical data for various H<sub>2</sub> production methods.

H <sub>2</sub> production process	Production rate (m <sup>3</sup> <sub>STP</sub> /h)	Overall efficiencies (%) without CO <sub>2</sub> capture	CO <sub>2</sub> emission (kg CO <sub>2</sub> /kg H <sub>2</sub> )*	H <sub>2</sub> production cost (USD/kg H <sub>2</sub> /day)
SMR	20,000-250,000	70-80	7.33	32.75
CG	20,000-100,000	55	29.33	22.37
BG	≥57,000	50-60	5.89	23.78
Water electrolysis	1-1000	64-70	-	-
PV-EL	-	-	0	17.36
W-EL	-	-	0	36.75
H-EL	-	-	0	1.4

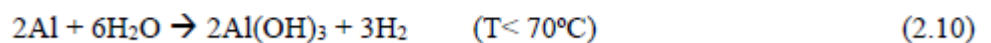
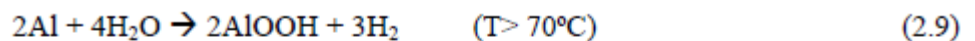
\*Excluding CO<sub>2</sub> produced in the entire process chain.

### 2.3 Aluminum-Water Reaction

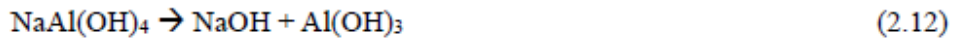
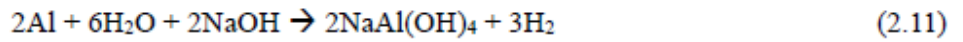
Wang et al (2009) mentioned about the technical challenges for compact and safe H<sub>2</sub> storage. The conventional methods in increasing H<sub>2</sub> storage values high-pressure compression and liquefaction at low temperatures. Albeit well-established and understood techniques aforementioned, the H<sub>2</sub> storage is not entirely safe and reliable. Nowadays, H<sub>2</sub> storage using chemical hydrides is providing solid-state storage for H<sub>2</sub> which is much safer despite slow kinetics and high temperature requirements totally restricting its industrial applications (Sakintuna, Lamari-Darkrim, and Hirscher, 2007; Wang et al., 2009). Apparently, H<sub>2</sub> storage using hydrides is not as promising as it looks in addition to its high cost. Now, reactions of reactive metals in water were reported producing significant amounts of H<sub>2</sub> and showing potentials in H<sub>2</sub> energy and storage. As a matter of fact, H<sub>2</sub> generation from displacement reactions of metals was discovered in the olden days. Wang et al. (2009) stated that the need for H<sub>2</sub> storage can be eliminated with on-demand H<sub>2</sub> generation from reactive metals. Tzimas et al. (2003) reported that water generally contains about (111 kg H<sub>2</sub>/m<sup>3</sup>) and much higher than in gasoline (84 kg H<sub>2</sub>/m<sup>3</sup> and pure liquid H<sub>2</sub> (71 kg H<sub>2</sub>/m<sup>3</sup>). Among the reactive metals such as Zn, Mg, and Al, Al has reported producing the most significant amount of H<sub>2</sub> per unit mass (Kravchenko et al., 2005; Wang et al., 2009).

### 2.3.1 Activation of Aluminum in Alkaline Condition

Aluminum is can be easily sourced due to its availability on earth. It is called the viable metal it has many favourable properties such as light weight and renewable in the sense that it can be recycled and reused (Wang et al., 2009). 1 g of Al metal is able to produce 1360 mL H<sub>2</sub> at normal room temperature (RTP) (Ho and Huang, 2016; Shmelev, Yang and Yim, 2016; Yang et al., 2019). But the formation of oxide layer on the Al surface prevents hydrolysis reaction. According to Wang et al. (2009), the hydroxide ions (OH<sup>-</sup>) in alkaline solutions will destroy the protective inert oxide layer on the Al forming aluminum oxide, Al<sub>2</sub>O<sub>3</sub>. Therefore, Al is easily dissolved in the alkaline condition even at room temperature, leading to desired H<sub>2</sub> yield, H<sub>2</sub>. The aluminum-water reaction alternative pathways are shown in (Eq. 2.9 and Eq. 2.10) at different reaction temperatures (Razavi-Tousi and Szpunar, 2014).



Whereas, the aluminum-water reaction in alkaline NaOH solution is shown in Eq. (2.11 and 2.12). NaOH depletion process is shown in Eq. 2.11 will be re-generated via decomposition of NaAl(OH)<sub>4</sub> in Eq. 2.12. Therefore, only water is being consumed throughout the process. Both Eq. 2.11 and Eq. 2.12 together will yield Eq. 2.13. The overall reaction which is expressed as follows.



According to Huang et al. (2013), the by-product  $\text{Al}(\text{OH})_3$  is non-volatile and non-corrosive. It is widely used in the ceramic industry as raw material. Besides being useful products in the ceramic industry, Al hydroxide can be utilized as an adsorbent in chromatography, ink production and glass lubricants, etc. (Huang et al., 2013).

Stockburger et al. (1992) reported the optimum temperature for Al/ $\text{H}_2\text{O}$  reaction about 70-90°C and NaOH concentration of 5.75 M. Soler et al. (2005) reported using Al foil, 260 mL/min of  $\text{H}_2$  was produced with 5M KOH solution at 75°C. Martinez et al. (2005) reported using Al waste cans to substitute commercial Al powder, the waste cans were pretreated with  $\text{H}_2\text{SO}_4$  to remove paint and plastic cover, about 12.5 mL/min/g  $\text{H}_2$  was produced using 6M NaOH solution at RTP. NaOH is a more effective alkaline solution in Al consumption than KOH and  $\text{Ca}(\text{OH})_2$  (Soler et al., 2007). Other than Al powders, Al and its alloys were reported to enhance  $\text{H}_2$  generation. Soler et al. (2007) also reported 216mL/min/g of  $\text{H}_2$  production for Al-88 wt %/Si-12 wt% alloy in  $\text{Ca}(\text{OH})_2$  alkaline solution at 75°C. Soler et al. (2007) reported production of 190 mL/min/g of  $\text{H}_2$  using Al/Si added with  $\text{NaBH}_4$  in saturated  $\text{Ca}(\text{OH})_2$  at 75 °C,

equivalent to 94% of maximum H<sub>2</sub> conversion yield. The enhanced H<sub>2</sub> production could be attributed to the increase of pH value due to hydrolysis of NaBH<sub>4</sub>, but NaBH<sub>4</sub> is expensive to be considered practically (Soler et al., 2007). Apart from the aforementioned alkaline solutions, Liu et al. (2018) employed CaO and Li/Li<sub>2</sub>O combined with Al powder to obtain a maximum H<sub>2</sub> yield of 90%. The rapid reaction was explained by the rapid consumption of OH<sup>-</sup> ions. Other than CaO and Li/Li<sub>2</sub>O, other metals that have been used were MgO, Al<sub>2</sub>O<sub>3</sub>, ZnO, La<sub>2</sub>O<sub>3</sub>, TiO<sub>2</sub> and NaAlO<sub>2</sub> with H<sub>2</sub> yield of ≤15%. There are several parameters that can affect the H<sub>2</sub> production besides reaction temperature and concentration of alkaline solution, such as employment of stirring in RPM, morphology and initial mass of metals induced, pretreatments of the metals, the mixing conditions in the reactor, and the Al-alloy composition if alloys were employed. Other approaches such as Al amalgamation with mercury (Hg) in Al/H<sub>2</sub>O reaction; however, Hg is toxic to; hence, not an applicable method in H<sub>2</sub> generation (Du Preez and Bessarabov, 2018). Kaya et al. (2021) experimented similar experiment using Al-2wt% Zn in 5M NaOH solution under room temperature conditions generated 0.46 ml/min/cm<sup>2</sup> of H<sub>2</sub>, the conclusion found out combination of pure Al and Zn metals had high corrosion ratio due to Zn's low melting point which helped reacts well in the alkaline condition when alloying with Al metal. Zn also increased production rate and yield of H<sub>2</sub> with enhanced pitting corrosion amount of Al-alloys.

### 2.3.2 Mechano-Chemical Activation of Aluminum in Neutral Condition

Besides activating Al in acidic or alkaline condition, mechano-chemical activation is an alternative activation method involving mechanical and chemical processes. For example, Al metals (Al foils, cans, rods, bars, tubes, plates, and flakes) are repeatedly fractured on the principle of impact and attrition where the Al metals are fractured into smaller powder forms via collisions between milling balls and the sample powder inside the ball milling machine (Fan, Xu and Sun, 2007). Razavi-Tousi and Szpunar (2014) synthesized Al powder of 99.8% purity with 190  $\mu\text{m}$  particle size using ball milling method. 70 mL and 80 mL of  $\text{H}_2$  produced for 4-hour and 7-hour ball milling process in Al/ $\text{H}_2\text{O}$  reaction. The longer the milling time for the powder, the higher  $\text{H}_2$  production rate can be obtained. Ball milling increases the BET active surface area value of the powder by decreasing its particle size by introducing cracks due to attrition and collisions. Also, it increased lattice imperfections which also increased the affinity of the ball-milled powder for Al/ $\text{H}_2\text{O}$  reaction. Inert oxide film on the surface of the particles was broken and fresh surfaces exposed to initiate hydrolysis reaction during ball milling process (Razavi-Tousi and Szpunar, 2014). Liang et al. (2016) ball-milled mixture of Fe, Co, and Ni metals gave  $\text{H}_2$  yield of 80 to 90% at 45°C. Kravchenko et al. (2005) utilized low melting point (l.m.p.) metals to synthesize Al-alloys such as Zn, Ga, Bi and In metals. A total  $\text{H}_2$  production volume of 1000 mL/g was obtained at 82°C for 30 minutes using Al-80 wt%, Ga-5.3 wt%, In-2.0 wt%, Sn-5.4 wt% & Zn-7.3 wt% alloy composite (Kravchenko et al., 2005). On the other hand, Fan, Xu and Sun (2007) explained and reported that ball milling method

is more effective than melting for production of Al-alloys.

940 mL/g H<sub>2</sub> was produced at RTP in ~ for 15 minutes for Al-80 wt%, Bi-5 wt%, Ga-10 wt%, & Zn -5 wt%; whereas, 1050 mL/g of H<sub>2</sub> was produced at RTP in~ for 15 minutes for Al-80 wt%, Bi-8 wt%, Zn-2 wt%, Ga-8 wt%, & CaH<sub>2</sub>-2 wt%. Addition of CaH<sub>2</sub> made the composite not to agglomerate and blend equally in the miller. (Fan, Xu and Sun, 2007). However, l.m.p. metals caused slow reaction rate at room temperature and are easily evaporated in the melting process (Fan, Xu and Sun, 2007). Du Preez and Bessarabov (2018) later improvised by reacting Al-90 wt% & 10 wt% total In & Sn at RTP attaining 96.5-99.5% maximum H<sub>2</sub> yield by ball milling for 30 minutes at 1500 RPM. Escobar-Alarcón et al. (2019) synthesized Al-9 wt% Mg by melting at 300 °C for 72 hours. It was reacted with distilled water with ultrasonic YAG laser with 1064 nm, 5 ns pulse duration and 10 Hz repetition conditions to generate 500 ml/min H<sub>2</sub> in water displacement apparatus. Zhang et al. (2018) later synthesized Al-30 wt% Sn- 10 wt % Zn ternary composite via high pressure torsion (HPT) for N= 10 turns at room temperature and at 1 RPM. The composite was reacted with pure water at room temperature conditions generated >900 ml/g H<sub>2</sub>. The addition of Zn increased the H<sub>2</sub> production speed, while addition of Sn metal in the composite increased the H<sub>2</sub> generation rate and H<sub>2</sub> yield.

### 2.3.3 Hydrogen Production using Aluminum Waste Cans

Yang et al. (2019) made use of Al waste can from Sprite cans, reported 95.3% H<sub>2</sub> yield (1297 ml H<sub>2</sub> in 360 s) with alkaline condition, 0.75M NaOH. In this study, aluminum waste cans instead of being recycled, Al waste cans are combined with activation elements such as Sn and In metals to form a composite of Al-Sn-In that is mechano-chemically prepared via ball milling, a modification from work of Du Preez and Bessarabov (2018). Yolcular, Karaoglu and Karasoglu (2020) produced Al-alloy chips powder through ball milling with by adding 20 wt% NaCl salt at 200 RPM for duration of 40 hours. The Al-alloys comprised of 90 wt% to 99.62 wt% Al and balance small amount of trace elements such as Si, Fe, Cu, Mn, Zn, Ti, and Cr which are found in most aluminum beverage cans. The hydrolysis results were 700 to 900 ml/g of H<sub>2</sub>. The maximum H<sub>2</sub> generation and H<sub>2</sub> yield would be investigated in this project using Al powder generated from Al waste cans.

Deng et al. (2005) conducted a modification on Al particle surfaces by reacting Al powder and Al(OH)<sub>3</sub> mixed with ethanol solution and introduced to ball milling for 48 hours, then sintered at 600°C in vacuum to produce porous Al/ $\gamma$ -Al<sub>2</sub>O<sub>3</sub>. The modified Al particles was able to perform hydrolysis at room temperature to produce H<sub>2</sub>. About 2000-2500  $\mu$ mol of H<sub>2</sub> was produced for Al-30wt %/ $\gamma$ -Al<sub>2</sub>O<sub>3</sub>-70wt % in 20 hrs duration (Deng et al., 2005). Adans et al. (2016) successfully synthesized  $\gamma$ -Al<sub>2</sub>O<sub>3</sub> from Al waste cans via precipitation methods with specific surface area comparable to that of commercial one about

204 m<sup>2</sup>/g. Table 2.5 shows the hydrolysis performance of Al and its alloys in alkaline conditions. Table 2.6 shows the hydrolysis performance of Al and its alloys in neutral conditions.

It can be deduced from the literature review that no research by far focused on doping Al waste can powder with activation elements to improve hydrolysis performance. Therefore, in this study, Al waste cans are to be mechano-chemically activated by different activation elemental metals to form binary and ternary Al composites. The AWCP composites are mechano-chemically prepared via ball milling machine.

Table 2.5: Hydrolysis performance of Aluminum and its alloys in alkaline conditions.

Treatment and type of metal/metal alloys	Alkaline Solution	Temperature (°C)	Maximum H <sub>2</sub> production rate	Maximum H <sub>2</sub> conversion yield	References
Atomization of Al (99.8 & 99.99% purity); Al-12%Si	10M, 1M & 0.1M NaOH	25	>500 ml/min/0.2g	100%	Belitskus, 1970
Al foil powder (99.9% purity)	0.003 – 0.1M NaOH	30-80	For aluminum foil, 40 ml/s/cm <sup>2</sup>	For aluminum foil, 0.6 μm/mm	Aleksandrov, Tsyganova and Pisarev, 2003

Paint and plastic cover removal using H <sub>2</sub> SO <sub>4</sub> -Al can strips	6M NaOH	23 ± 3	12.5 ml/min/g	-	Martinez et al., 2005
Al powder	5M KOH	75	260 ml/min	-	Soler et al., 2005
Al powder (99.9% purity)	1.0M & 5.0M NaOH	RTP	-	-	Hiraki et al., 2007
Al alloys (powder, rod, bar, foil, tube, plate & flake)	Ca(OH) <sub>2</sub>	75	216 ml/min/g for Al 88wt%/Si 12wt% alloy	76%	Soler et al., 2007

Table 2.5: Continue.

Treatment and type of metal/metal alloys	Alkaline Solution	Temperature (°C)	Maximum H <sub>2</sub> production rate	Maximum H <sub>2</sub> conversion yield	References
Addition of NaBH <sub>4</sub> Al, Al/Si, Al/Co, Al/Mg (powder/flake)	Ca(OH) <sub>2</sub>	75	190 ml/min/g (for Al/Si + NaBH <sub>4</sub> + saturated Ca(OH) <sub>2</sub> )	94%	Soler et al., 2007
Al (99% purity)	Ca(OH) <sub>2</sub> & Li(OH) <sub>2</sub>	RTP	-	90% for both CaO & Li/Li <sub>2</sub> O (X=0.05g)	Liu et al., 2018
Pretreated with concentrated H <sub>2</sub> SO <sub>4</sub> to remove paint, cut	NaOH	40	1296 ml in 0.75M NaOH	95.3%	Yang et al., 2019

into small flakes & magnetic grind into powder -Al can powder					
Al-2wt% Zn Synthesized via casting at high temperatures	NaOH	25	0.46 ml/min/cm <sup>2</sup>	-	Kaya et al., 2021

Table 2.6: Hydrolysis performance of Al and its alloys in neutral conditions.

Treatment and type of metal/metal alloys	Temperature (°C)	Maximum H <sub>2</sub> production rate / condition	Maximum H <sub>2</sub> conversion yield	References
Melting Al alloys	82	1000 ml/g in ~ for 30 min for Al-80wt%, Ga-5.3wt%, In-2.0wt%, Sn-5.4wt% & Zn-7.3wt% alloy	100%	Kravchenko et al., 2005
Ball milling Al & Al-alloys (l.m.p. metals: Zn, Ga, Bi, Pb, Sn, Mg, In, etc)	RTP	940 ml/g in ~ for 15 min for Al-80wt%, Bi-5wt%, Ga-10wt% & Zn-5wt%	100%	Fan, Xu and Sun, 2007

		1050 ml/g in ~ for 15 min for Al-80wt%, Bi-8wt%, Zn-2wt%, Ga-8wt% & CaH <sub>2</sub> -2wt%		
Ball milling Al-Bi-hydride, Al-Bi-solid salt powder	RTP	1050 ml/g in 5min of hydrolysis for 5 hours milling Al-10wt%, Bi-10wt%, MgH <sub>2</sub> mixture & Al-10wt%, Bi-10wt%, MgCl <sub>2</sub> mixture	93.4%	Fan et al., 2008
Ball milling for 20 hr at 270 RPM Ball to powder ratio 20:1 Al (99% purity) < 100μm	70	NaCl salt to aluminum mole ratio 1:5:1	95%	Alinejad and Mahmoodi, 2009

Table 2.6: Continue.

Treatment and type of metal/metal alloys	Temperature (°C)	Maximum H <sub>2</sub> production rate / condition	Maximum H <sub>2</sub> conversion yield	References
Ball milling Al/ $\gamma$ -Al <sub>2</sub> O <sub>3</sub>	RTP	Induction time ~ 3 hr for 70 vol% Al + 30 vol% $\gamma$ -Al <sub>2</sub> O <sub>3</sub>	-	Deng, Liu and Gai, 2005
Direct addition Al + $\gamma$ -Al <sub>2</sub> O <sub>3</sub>	RTP	Shortens induction from 79.2 hr to 2.4 hr	-	Gai, Fang and Deng, 2007
Ball milling for 2, 4, 7, 11 & 19 hr @ 200RPM	80	80 ml for 7-hour ball milled Al-water reaction	-	Razavi-Tousi and Szpunar, 2014

Ball to powder ratio 30:1 Al powder (99.8% purity) 190 μm particle size (without activation elements)		70 ml for 4-hour ball milled Al-water reaction		
Ball milling in low alkaline condition (NaOH) for 5 hr @ 300RPM	70	1350 ml/g for Al-Ni-Bi (wt% was not reported)	100%	Ho and Huang, 2016

Table 2.6: Continue.

Treatment and type of metal/metal alloys	Temperature (°C)	Maximum H <sub>2</sub> production rate / condition	Maximum H <sub>2</sub> conversion yield	References
Ball milling Al-M (M= Fe, Co or Ni)	35	3ml/g/min for Al-Fe (X = 0.02g); 4ml/g/min for Al-Co (X= 0.20g); 5ml/g/min for Al-Ni (X= 0.05g)	80-90%	Liang et al., 2016
Ball milling Al-M (M= Fe, Co or Ni)	45	4ml/g/min for Al-Fe (X = 0.02g); 4ml/g/min for Al-Co (X= 0.20g); 2ml/g/min for Al-Ni (X= 0.05g)	80-90%	Liang et al., 2016

Ball milling for 3 hr Al powder (99% purity) 17-19 $\mu\text{m}$	35	9.5 ml/g/sec for Al-90wt%, Bi-7.5wt% & Sn-2.5wt%	85%	Xiao et al., 2018
Ball milling for 30min @1500 RPM Ball to powder ratio 30:1 Al powder (99% purity) <200 $\mu\text{m}$	RTP	Al-90wt% & 10 wt% total In & Sn	96.5 – 99.5%	Du Preez and Bessarabov, 2018

Table 2.6: Continue.

Treatment and type of metal/metal alloys	Temperature (°C)	Maximum H <sub>2</sub> production rate / condition	Maximum H <sub>2</sub> conversion yield	References
Ball milling for 5 hr @ 250 RPM Ball to powder ratio 60:1 Al-BiOCl	RTP	1058.1 ml/g	91.6%	Zhao et al., 2019
Ball milling for 40 hr @200RPM in 1M NaOH solution Ball to powder ratio 10:1	70	Al 1050 ~ 700 ml/g in 5 min Al 6013 ~ 800 ml/g in 5 min Al 7075 ~ 900 ml/g in 10 min	-	Yolcular, Karaoglu and Karasoglu, 2020

Al chips (Al 1050, Al 6013 & Al 7075)				
Ultrasonic laser (YAG @1064 nm; 5ns pulse duration; 10 Hz repetition) Al-9wt% Mg	RTP	500 ml/min	-	Escobar-Alarcon et al., 2019
High pressure torsion (HPT) Al-30wt%Sn – 10wt% Zn	RTP	950 ml/g	69%	Zhang et al., 2018

## 2.4 Current Trends of Greenhouse Gases and Carbon Dioxide

Greenhouse gases (GHGs) are generally composed of carbon dioxide (CO<sub>2</sub>), methane (CH<sub>4</sub>), water vapour (H<sub>2</sub>O) and chlorofluorocarbons (CFCs). Figure 2.1 shows the total GHGs emissions (GT of CO<sub>2</sub> equivalent) from 1970-2012. The value increased from 27.66 GT CO<sub>2</sub> equivalent to 53.53 GT CO<sub>2</sub> equivalent from 1970-2012 (within 4 decades). The increasing CO<sub>2</sub> level is caused by rapid industrialization globally, which caused the concentration of CO<sub>2</sub> to be on the uptrend fashion from 280 ppm to 410 ppm. It is predicted to rise to 570 ppm by year 2100 (Younas et al., 2016).

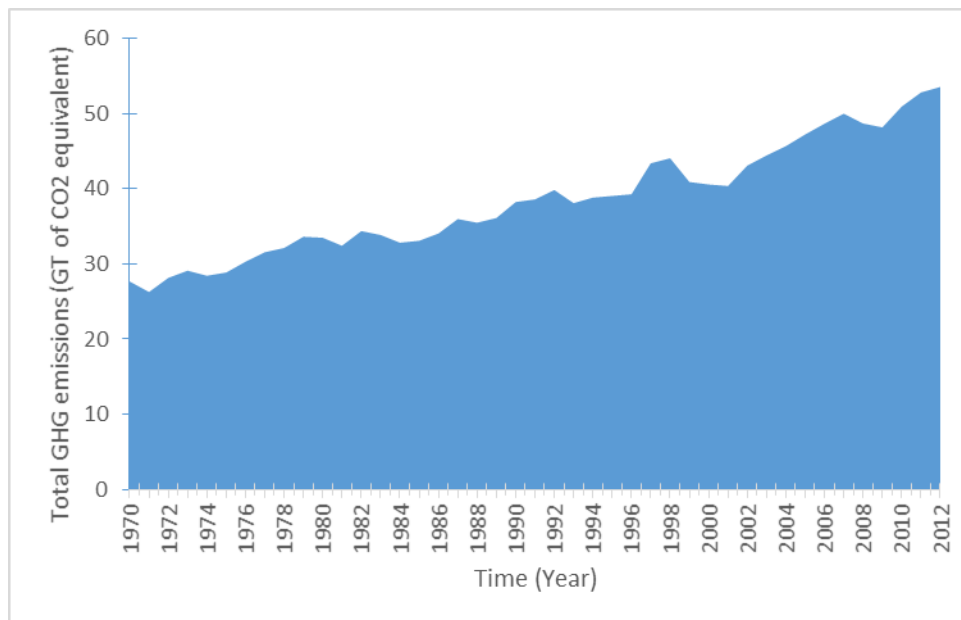


Figure 2.1: Total GHGs emissions (GT of CO<sub>2</sub> equivalent) from 1970-2012 (The World Bank, 2019).

Figure 2.2 shows the particular GHG emissions in 2017 (GT of CO<sub>2</sub> equivalent) from 1970-2012. The electricity production, transportation and industrial sectors in general accounted about 79 % of total GHGs emissions in 2017; the rest was from commercial, residential, and agricultural sectors (United States Environmental Protection Agency, 2019).

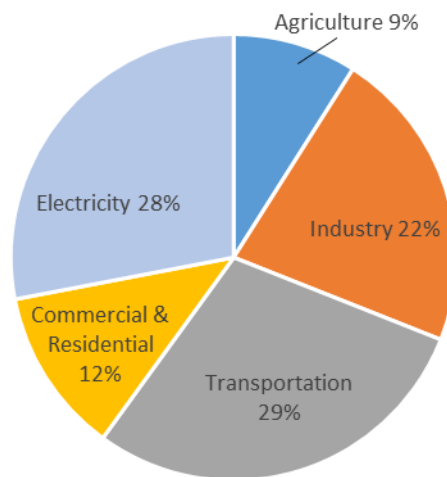


Figure 2.2: Total GHGs emissions in 2017 (equivalent to 6,457 GT CO<sub>2</sub> emissions) (United States Environmental Protection Agency, 2019).

CO<sub>2</sub> overloads the environment is a known factor for global climate change due to global warming. The global temperature increases because of the “greenhouse effect”. Therefore, CO<sub>2</sub> is one of the major contributors to greenhouse gases (GHGs). Other global environmental issues such as formation of acid rain, melting of glaciers, rise of sea levels, ocean acidification, and adverse health effects are all caused by increasing CO<sub>2</sub> level at an uncontrolled rate. On the other hand, climatic change forces some of the

regions to spend additional energy in pumping water to overcome drought problem, insufficient crops and potable water source (Kellogg and Schware, 2019). When additional energy is needed to fulfil the increasing energy demand caused by global climatic change, more CO<sub>2</sub> is produced as a by-product. Figure 2.3 shows the world's total CO<sub>2</sub> emissions (GT) from 1960-2014. From 1960-1973, the CO<sub>2</sub> emissions increased from 9.4 GT to 16.8 GT due to the Second Industrial Revolution (IR). During this period of time, coal mines, textile factories and steel work emerged due to the invention of the combustion engine (Coats and Jones, 1982). The value continuously rises to a staggering 36 GT CO<sub>2</sub> emissions in 2014; apparently due to increasing energy demand and human population as time goes by. Excessive CO<sub>2</sub> emissions will be a serious threat in both presence and future, and it needs immediate attention to curb this worrisome increasing trend.

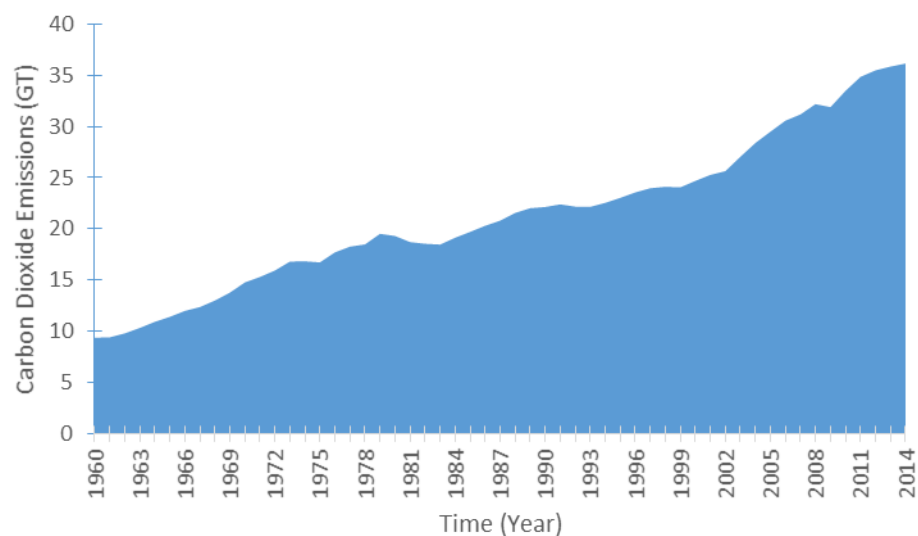


Figure 2.3: World's total CO<sub>2</sub> emission (GT) from 1960-2014 (The World Bank, 2019).

## 2.5 Technologies of Carbon Dioxide Capture

There are generally several CO<sub>2</sub> capture technologies: pre-combustion, oxy-combustion and post-combustion. Younas et al. (2016) reported 90 % of CO<sub>2</sub> capture efficiency through the aforementioned CO<sub>2</sub> capture technologies. CO<sub>2</sub> capture technologies are important for review in this research as CO<sub>2</sub> capture efficiencies affect the production of CH<sub>4</sub>, the ultimate goal of this research is to convert as much CO<sub>2</sub> and optimized H<sub>2</sub> from aluminium-water reaction to valuable CH<sub>4</sub> in a continuous manner. Li et al. (2013) reported that a total of 1297 patents are relevant to CO<sub>2</sub> capture solvents, solid sorbents and membranes (refer Figure 2.4). The aforementioned researchers later explained the likelihood of more patents on solvents and solid sorbents was due to a wider range of material availability for solvents and solid sorbents compared to that of membrane.

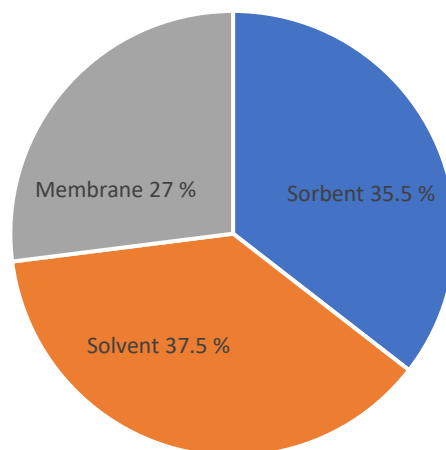


Figure 2.4: Shares of total 1297 patents on solid sorbents, membrane and solvent (Li et al., 2013).

Pre-combustion technology captures the waste CO<sub>2</sub> from syngas from reformers of upstream gasifiers (Li et al., 2013). The fuel was initially decarbonized before the combustion process. A pre-combustion system was utilized to transform solid, liquid or gaseous fuel into syngas using a gasifier or reformer. It was a well-established technology being used worldwide at chemical plants and refineries. The fuel is initially decarbonized before the combustion process. The CO<sub>2</sub> produced will be separated and undergo dehydration to remove water vapor to increase purity of CO<sub>2</sub> (Yu et al., 2012). In conclusion, for solvent, heat is not required to reverse chemicals but there would be H<sub>2</sub> loss during recovery of flash. Lastly, there is no steam load for membrane system but with H<sub>2</sub> loss at decreasing partial pressure.

Post-combustion capture (PCC) captures waste CO<sub>2</sub> from flue gas of any plant. Liquid solvents were utilized to flue gases that are low in concentration and pressure. This would result in bonding of acidic CO<sub>2</sub> with alkaline solvent such as monoethanolamine (MEA). CO<sub>2</sub> that was bonded would be released upon heating of the liquid solution (Farrell et al., 2019). The product was then cooled, compressed, purified and stored. This process did not affect the production process; it could be easily integrated into an existing process plant. Farrell et al. (2019) reported post-combustion capture being capable of producing a CO<sub>2</sub> stream of 99.9 % purity, while about 85-90 % of CO<sub>2</sub> capture efficiency. Despite the high conversion efficiencies of a post-combustion capture technology, there are few requirements of a post-combustion capture technology to be costly for implementation. For example, additional equipment is required to get rid of sulphur oxides (SO<sub>x</sub>), nitrous oxides (NO<sub>x</sub>) and some impurities such as dust

from flue gas as these impurities can damage the quality of the solvent (Farrell et al., 2019). Figure 2.5 shows the overview of post-combustion carbon capture technologies.

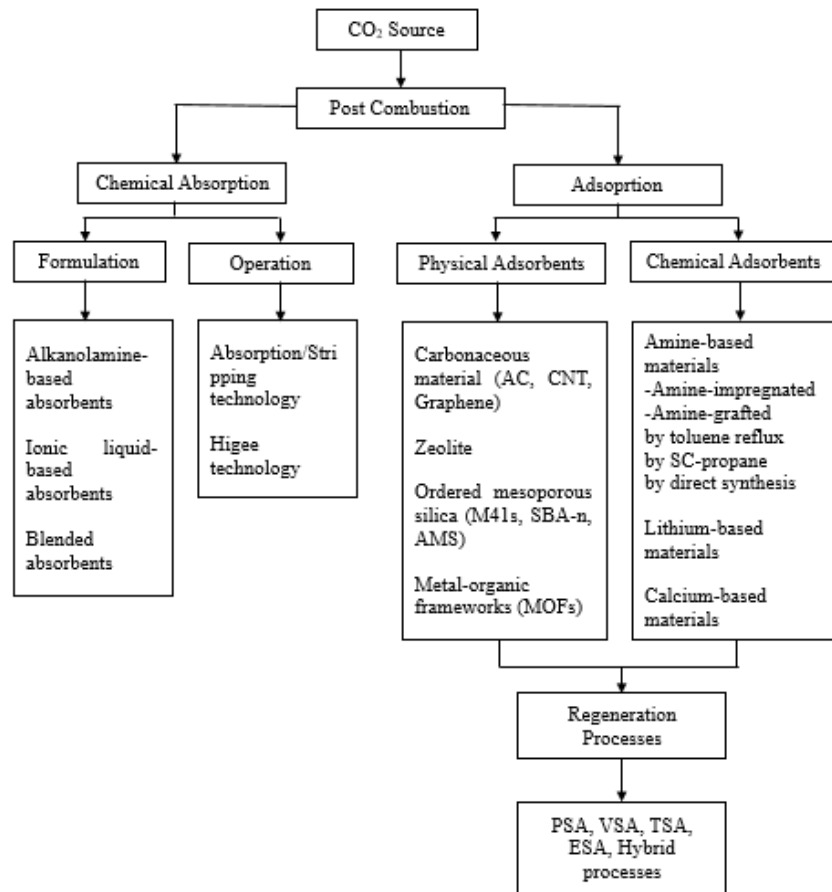


Figure 2.5: Overview of post-combustion carbon capture technologies (Yu et al., 2012).

Table 2.7 shows the advantages and downsides of post-combustion technology. In conclusion, solid sorbents CO<sub>2</sub>-capture system releases too much heat causing operational implications. Solvents, on the other hand, have a trade issue between kinetics and heat of reaction. Membranes' system has a poor economy of scale. Lastly, methanation is most promising even though it has low efficiencies at low pressures, it has the best process control among all the

systems discussed. Also, methanation is the current trend and proposed as the promising solution in the CO<sub>2</sub>-capture system.

Table 2.7: Advantages and disadvantages of post-combustion technology (National Energy Technology Laboratory, 2010).

<b>CO<sub>2</sub> capture system</b>	<b>Advantages</b>	<b>Disadvantages</b>
Solid sorbet/ Activated carbon	Large capacities and fast kinetics.	Difficult heat management creating operational issues when reaction is heat-releasing.
Solvent	High chemical potential for selective capture at low CO <sub>2</sub> partial pressure.	There is a trade-off between kinetics and heat of reaction.
Membrane	Simple modular design.	Poor economy of scale.
Methanation	Good process control as isothermal condition can be achieved.	Low efficiencies at low pressures.

## 2.6 Carbon Dioxide Methanation

Recent research has been carried out to study metal-based catalysts for CO<sub>2</sub> methanation at low temperatures and atmospheric pressure (Younas et al., 2016). Miao et al. (2016) mentioned two types of CO<sub>2</sub> methanation mechanisms that are exothermic and reversible reaction as shown in Eq. 2.14 and Eq. 2.15. One mechanism said CO<sub>2</sub> associatively adsorbed with adatom H<sub>ad</sub> forming oxygenate intermediates and hydrogenated to form CH<sub>4</sub>. Another mechanism suggested CO<sub>2</sub> dissociates to form carbonyl (CO<sub>ad</sub>) and O<sub>ad</sub>, then form CH<sub>4</sub> via carbonyl hydrogenation.



The thermochemical-route methanation occurs at the temperature of about 150-500 °C and commonly at atmospheric pressure couples with Ni-based catalysts (metal-based catalysts). The by-product of this reaction, called the Sabatier reaction, is the valuable CH<sub>4</sub>, commonly used as a fuel to generate electricity. High temperatures may cause sintering to the catalyst during the reaction; therefore, low temperatures are emphasized to improve the methanation reaction. Cheng et al. (2017) have also mentioned that Co- and Ru-based catalysts are of higher cost impact despite higher catalyst efficiencies. On the other hand, Ni-based catalysts are preferred due to its availability, lower cost and fair activity (Cheng et al., 2017). Besides, it was discovered that by adding

other metals such as Ce, La and Fe can improve catalytic activity and stability of Ni catalysts for syngas methanation process at low temperatures. Aluminum oxide, Al<sub>2</sub>O<sub>3</sub> is reported by Cheng et al. (2017) has a porous structure and high surface area. Nonetheless, Al<sub>2</sub>O<sub>3</sub> has a shortcoming which its pore structure easily collapsed during phase transformation at high temperatures. Palm shell activated carbon (PSAC) was used to prepare Ni-based methanation catalyst for methanation reaction following Younas' work (Younas et al. (2016). Palm waste is abundant in Malaysia; thus, it is more cost-effective compared to other precursor materials. No one has used nickel nitrate hexahydrate (Ni(NO<sub>3</sub>)<sub>2</sub>·6H<sub>2</sub>O) to active PSAC for CO<sub>2</sub> adsorption purpose. Younas et al. (2016) physically and chemically modified PSAC using NaOH, Ni(NO<sub>3</sub>)<sub>2</sub>·6H<sub>2</sub>O to enhance the adsorption capacity of CO<sub>2</sub>.

H<sub>2</sub> is introduced as shown in the reaction ( $\text{CO}_2 + 4\text{H}_2 \rightarrow \text{CH}_4 + 2\text{H}_2\text{O}$ ), to facilitate the methanation process. No research has been carried out to investigate the more viable H<sub>2</sub> production method. Most of the research focused on the optimization of catalysts and the methanation process. Most of the research has used the commercial H<sub>2</sub>. Therefore, it is apparently not feasible to use commercial H<sub>2</sub> which is expensive and H<sub>2</sub> is of higher calorific value gas compared to relatively lower calorific value CH<sub>4</sub>. Hence, a more economical H<sub>2</sub> production should be investigated for proposed CO<sub>2</sub> methanation, so that the CH<sub>4</sub> produced can be more cost-effective.

Table 2.8 shows a review of the methanation process done by researchers. All of the methanation experiments were using commercial H<sub>2</sub> gas from cylinder tanks. It is generally known that the commercial H<sub>2</sub> gas is cost-intensive. For instance, H<sub>2</sub> of 99.9992% purity costs about RM 24.00 - 27.00 per m<sup>3</sup> (Global Gas Report, 2020).

Therefore, we need to look into alternative H<sub>2</sub> source which is more cost-effective and cleaner since the conventional H<sub>2</sub> production method is CO<sub>2</sub>-emitting intensive. No one has mechano-chemically activated AWCP with activation metal to form AWCP composites and to react with alkaline solution at room temperature. The novelty of this work is to use the H<sub>2</sub> produced from AWCP composite hydrolysis for CO<sub>2</sub> methanation to generate CH<sub>4</sub>.

Table 2.8: A review of past methanation experiments.

Catalysts	Method	Reaction conditions	CO <sub>2</sub> conversion (%)	CH <sub>4</sub> selectivity (%)	References
Ni/SiO <sub>2</sub> -Al <sub>2</sub> O <sub>3</sub>	Incipient wetness impregnation	500 °C, 1 bar	35.0	30.0	Chang et al., 2003
15 wt% Ni/TiO <sub>2</sub>	Deposition precipitation	260 °C, 1 bar	96.0	99.0	Liu et al., 2013
12 wt% Ni/Al <sub>2</sub> O <sub>3</sub>	Incipient wetness impregnation	325 °C, 15 bar	67.3	87.0	Zhang et al., 2014
10 wt% Ni/La <sub>2</sub> O <sub>3</sub>	Incipient wetness impregnation	350 °C, 15 bar	97.1	100.0	Huanling et al., 2010
23 wt% Ni/Al <sub>2</sub> O <sub>3</sub>	Incipient wetness impregnation	400 °C, 1 bar	81.0	98.0	Mutz et al., 2015
3.7wt%Ru/CeO <sub>2</sub> /r	Incipient wetness impregnation	350 °C, 1 bar	>75.9	99.0	Sakpal, 2018
Mesoporous Rh	Wet chemical reduction	550 °C, 1 bar	98.9	81.2	Arandiyan et al., 2018
2.5 wt% Ru/TiO <sub>2</sub>	Solvothermal hydrolysis	325 °C, 1 bar	>80.0	100.0	Chai et al., 2019
5 wt% Ni/ZrO <sub>2</sub>	Plasma decomposition	350 °C, 1 bar	79.1	76.5	Jia et al., 2019

Table 2.8: Continue.

<b>Catalysts</b>	<b>Method</b>	<b>Reaction conditions</b>	<b>CO<sub>2</sub> conversion (%)</b>	<b>CH<sub>4</sub> selectivity (%)</b>	<b>References</b>
2 wt% Co/ZrO <sub>2</sub>	Incipient wetness impregnation	400 °C, 30 bar	85.0	99.0	Li et al., 2019
CO <sub>3</sub> O <sub>4</sub> nanorods	Co-precipitation	230 °C, 10 bar	70.0	~99.0	Jimenez, Wen and Lauterbach, 2019
2 wt% Ni@CeO <sub>2</sub> -ZrO <sub>2</sub>	Colloidal nanoparticle dispersion	350 °C, 1 bar	58.0	>97.5	Vrijburg et al., 2019

## CHAPTER 3

### MATERIALS AND METHODS

#### 3.1 Introduction

The research was divided to 4 phases systematically *i.e.* Phase I is to prepare the best disintegrated aluminum powder from aluminum waste cans. Phase II was to optimize the hydrolysis process. Phase 3 to activate the AWCP and Phase 4 was to analyze the CO<sub>2</sub> methanation using the H<sub>2</sub> produced. Figure 3.1 shows the overall workflow of this study.

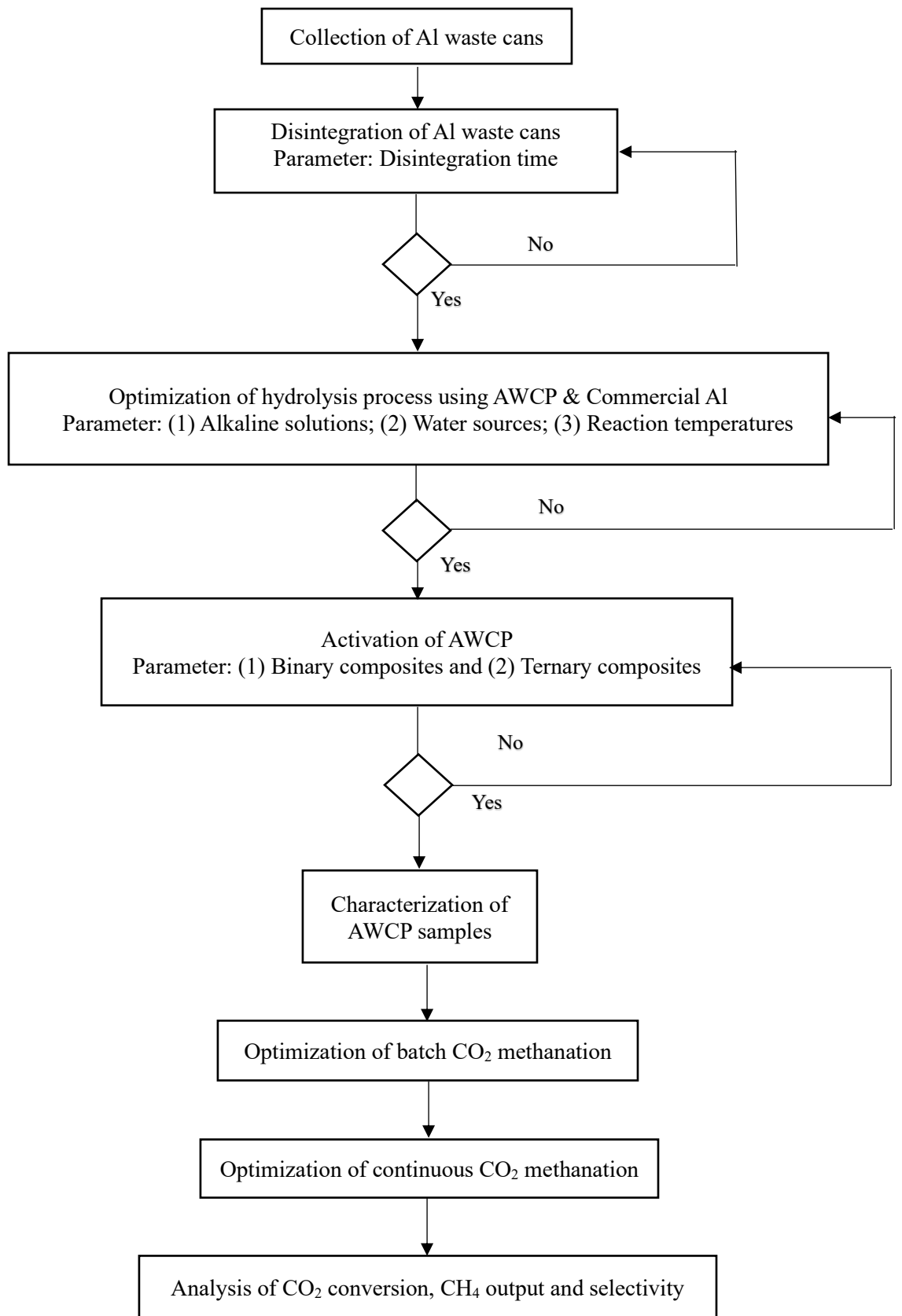


Figure 3.1: Overall workflow.

### 3.2 Materials, Chemicals and Equipment

The materials, chemicals and equipment used in this study are tabulated in Table 3.1 and Table 3.2 as shown below.

Table 3.1: List of materials

No.	Materials/Chemicals	Source/Info	Purpose of Usage
1	100 PLUS waste beverage cans	Restaurants within Kampar town	To synthesize Al waste can powder
2	Hand Dishwashing Liquid 1.5L	Sunlight Pro Hand Dishwashing Liquid 1.5L, Unilever	To wash the oil content of the aluminum waste cans
3	Commercial aluminium powder, Al (99 % purity)	Bendosen, Malaysia	To compare its hydrolysis performance with that of Al waste can powder
4	Sodium hydroxide, NaOH pellets (99 % purity)	R&M Chemicals, UK	To produce alkaline solutions to speed up Al hydrolysis reaction
5	Barium hydroxide octahydrate, Ba(OH) <sub>2</sub> .8H <sub>2</sub> O (98 % purity)	Merck, Germany	To compare its hydrolysis performance with NaOH solution
6	Potassium hydroxide, KOH pellets (99 % purity)	R&M Chemicals, UK	To compare its hydrolysis performance with NaOH solution

Table 3.1: Continued.

No.	Materials/Chemicals	Source/Info	Purpose of Usage
7	Tap water	Universiti Tunku Abdul Rahman (Kampar)	To dissolve NaOH pellets to produce alkaline solution
8	Distilled water	(Resistivity of 0.3 M $\Omega$ -cm) produced by Favorit distillation system (W4L WaterStill, Malaysia)	To dissolve NaOH pellets to produce alkaline solution
9	Deionized water	(Resistivity of 10 M $\Omega$ -cm) produced by Elga water purification system (Micra, Republic of Korea)	To dissolve NaOH pellets to produce alkaline solution
10	Ultrapure water	(Resistivity of 18.3 M $\Omega$ -cm) produced by Human Corporation water purification system (New Human UP 900, United Kingdom)	To dissolve NaOH pellets to produce alkaline solution
11	Commercial nitrogen gas, N <sub>2</sub> (99.999 % purity)	Linde, Malaysia	Used in all purging procedures
12	Commercial carbon dioxide, CO <sub>2</sub> (99.999 % purity)	Linde, Malaysia	To react with H <sub>2</sub> in methanation reaction
13	Nickel (II) nitrate hexahydrate, Ni(NO <sub>3</sub> ) <sub>2</sub> ·6H <sub>2</sub> O (>98 % purity)	GENE Chemicals, Malaysia	To synthesize methanation catalyst
14	Palm shell activated carbon, PSAC	Commercial product, unknown	To synthesize methanation catalyst

Table 3.1: Continued.

No.	Materials/Chemicals	Source/Info	Purpose of Usage
15	Tin powder, Sn (<45 $\mu\text{m}$ , 99.8 % purity)	Sigma-Aldrich, United States	To be ball-milled with Al waste can powder as an activation element
16	Lead powder, Pb (200-mesh, 99.9 % purity)	Alfa Aesar, United States	To be ball-milled with Al waste can powder as an activation element
17	Zinc granular, Zn (20-mesh, >99 % purity)	Acros Organics, United States	To be ball-milled with Al waste can powder as an activation element
18	Magnesium powder, Mg (>99 % purity)	SYSTEM, Malaysia	To be ball-milled with Al waste can powder as an activation element
19	Manganese powder, Mn (40-mesh, >99 % purity)	Acros Organics, United States	To be ball-milled with Al waste can powder as an activation element
20	Indium powder, In (100 mesh, 99.9 % purity)	Alfa Aesar, United States	To be ball-milled with Al waste can powder as an activation element

Table 3.2: List of equipment used for the study.

No.	Equipment	Brand/Model	Purpose of Usage
1	Disintegrator	Golden Bull Multi-function Disintegrator SY-04 200G	To disintegrate the Al waste can into powder form
2	Ball miller	Pulverisette 4 Vario-Planetary Mill, FRITSCH	To ball mill the Al waste can powder and the added activation element to form Al composite
3	Analytical balance	Shimadzu AY220	To weigh chemical powder
4	Sonicator bath	Cole-Parmer 8890	To sonicate the PSAC and Ni(NO <sub>3</sub> ) <sub>2</sub> ·6H <sub>2</sub> O for better impregnation
5	Rotary Evaporator	BUCHI Rotavapor R-300	To remove water content of catalyst sample
6	Oven	MEMMET 122AK3002	To dry samples
7	Carbonization unite	SAF Advance Tech	To carbonize the catalyst sample and activate PSAC
8	Command module	SDPROC Aalborg	To control the flow of CO <sub>2</sub> gas into gas rig
9	X-ray diffraction (XRD) machine	Shimadzu diffractometer XRD-6000 model	To determine the crystalline structure and phase of the samples

Table 3.2: Continued.

No.	Equipment	Brand/Model	Purpose of Usage
10	Field-emission scanning electron microscope (FESEM)	JSM 7600F FESEM, JEOL	To conduct structural morphology analyses of the samples
11	Energy Dispersive X-ray Fluorescence (EDXRF) elemental analyzer	Rigaku, Japan	To determine the elemental analysis of the samples
12	Brunauer–Emmett–Teller (BET) machine	Thermo–Finnigan Sorpmatic 1990	To measure the total active surface area of the samples
13	Particle size analyser (PSA)	Mastersizer 2000 Ver. 5.60	To determine the particle size distribution of the samples
14	Gas chromatography machine (GC)	Agilent 6890N (G1540 N) equipped with Varian capillary columns HP-PLOT/Q and HPMOLSIV	To determine the composition of the gas collected from Al/H <sub>2</sub> O reaction and the H <sub>2</sub> purity
15	125 mL stainless steel milling jar	Pulverisette 4 Vario-Planetary Mill, FRITSCH accessories	To content the Al samples for milling purpose
16	5 mm milling balls	Pulverisette 4 Vario-Planetary Mill, FRITSCH accessories	To ball mill the Al samples in the milling machine by collision
17	Metal cutter	Taparia TCS 08	To cut Al waste can into strips

Table 3.2: Continued.

No.	Equipment	Brand/Model	Purpose of Usage
18	Water bath heater	Thermo Scientific Precision GP 20	To heat the conical flask for different reaction temperatures
19	Parafilm (10 cm X 10cm)	Parafilm M	To temporarily seal the mouth of measuring cylinder during inversion process to the basin to prevent water loss

### **3.3 Preparation of Aluminum Waste Can Powder**

100 PLUS beverage aluminum waste cans were used in this study. No other types of waste cans were used to ensure the consistent chemical composition of the cans used in corresponding to the accuracy of the experiment results.

The collected aluminum waste cans were then cleaned with dishwasher to remove any impurities or oil. Then it is washed with tap water and were left to dry under the sun for 1 day. The paints on the dried aluminum waste cans were removed using sandpaper. The aluminum waste cans were cut into strips of rectangular shape (10 cm x 2 cm). They were stored in an air -tight plastic container containing inert stream of N<sub>2</sub> gas.

#### **3.3.1 Disintegration of Aluminum Waste Can Strips**

The aluminum waste cans were disintegrated using a disintegrator at a speed of 25000 rpm. During disintegration, the aluminum waste cans were being shredded by blades at high speed to produce fine AWCP. As times goes, the AWCP particle size reduced as disintegration duration prolonged. Immense amount of heat was produced from the high-speed disintegration which further activated the AWCP by removal of inert oxide layer while N<sub>2</sub> was purged into the disintegrator before disintegration started. The strips were disintegrated at different duration of time until a desired fine powder is achieved. The parameter of disintegration time was 1 min, 5 min, 10 min, 15 min and 20 min. The maximum disintegration time was fixed to 20 min due to the device limitation;

the machine was overheated after 20 min of continuous disintegration. The disintegrated particle size of AWCP were analyzed used particle size analyser (PSA) (Mastersizer 2000 Ver. 5.60) to identify the particle size of AWCP produced.

### **3.3.2 Activation of Aluminum Waste Can Powder**

The prepared AWCP was activated with different types of metal via mechano-chemical activation and prepared as a composite. A ball mill was used to mechanically activate the powder. The AWCP was ball-milled with the following metals: Tin (Sn), Magnesium (Mg), Zinc (Zn) and Indium (In).

Two types of composites are prepared *i.e.* binary and ternary. Binary composite has one type of new metal and ternary with two types of new metal added to the Al waste can powder. The binary Al composites was prepared by fixing the Al content at not less than 93 wt% of Al and varying the activation metal content from 1, 3, 5 & 7 wt%. Similarly, for ternary composite, Al composites were prepared at no lesser than 94 wt% of Al waste can powder with activation metals of not more than 6 wt%. The metals for ternary study were chosen based on the performance from the binary study. The complete parameters for the binary and ternary composites preparation are shown in Table 3.3.

Table 3.3: Composition of binary and ternary AWCP composites.

<b>Binary Composition</b>			
AWCP (99%) + Metal (1%) (Zn/Sn/Mg/In)	AWCP (96%) + Metal (3%) (Zn/Sn/Mg/In)	AWCP (95%) + Metal (5%) (Zn/Sn/Mg/In)	AWCP (93%) + Metal (7%) (Zn/Sn/Mg/In)
<b>Ternary Composition</b>			
AWCP (94%) + Combined Metal (6%)			
AWCP (1% Sn-5% Mg)		AWCP (1% Sn-5% In)	
AWCP (3% Sn-3% Mg)		AWCP (3% Sn-3% In)	
AWCP (5% Sn-1% Mg)		AWCP (5% Sn-1% In)	

The ACWP and activation metal powder were weighed according to the compositions as shown in Table 3.3 using a weighing balance. The mixtures were made into composites using a ball mill, then stored in a 125 mL stainless steel milling jar. Stainless steel milling balls of size 5 mm each were placed inside the milling jar at a ratio of 30:1 whereby 0.3 kg of milling balls per 0.1 kg powder. Inert N<sub>2</sub> gas purging was performed at the milling jar before the milling started. The mixtures were milled at speed of 1200 rpm for duration of 60 minutes (Yang et al., 2019). Once milling process ended, the milling jar was cooled down to room temperature before the composites were retrieved and stored. The produced AWCP composites were hydrolyzed immediately in view of aging and oxidation.

### 3.4 Hydrolysis Setup

The  $H_2$  is produced using a simple water displacement apparatus which consists of a conical flask, measuring cylinder, basin, tubing, rubber seal, and water bath heater (if reaction temperature is required to exceed room temperature). The set-up is illustrated in Figure 3.2. A 2 L measuring cylinder was filled with tap water completely. It took about 20 sec to completely fill the cylinder. A semi-transparent film (Parafilm) of a size of 10 cm x 10 cm was utilized to temporarily seal the opening of the measuring cylinder to avoid spillage of water when it was placed inverted onto the basin that was also filled partially with tap water. Figure 3.2 shows the actual process image.

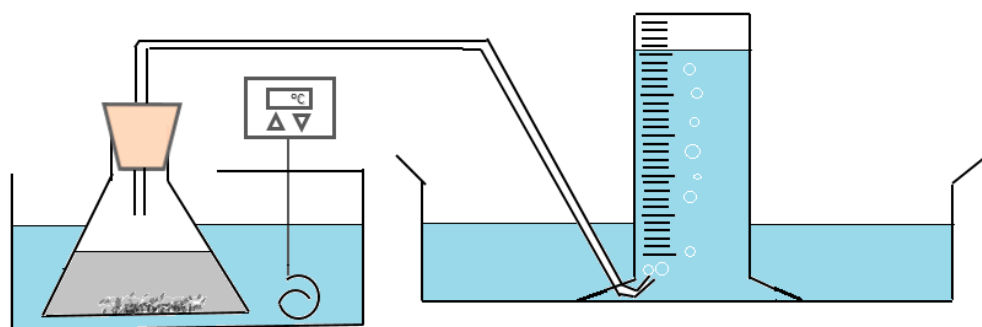


Figure 3.2: Water displacement apparatus set-up for Al hydrolysis for  $H_2$  production.

0.5 g of AWCP samples prepared were then added into the conical flask containing 200ml of 1M NaOH solution made from deionized water and it was

sealed with the rubber seal before the reaction starts to prevent loss of gas which will affect the accuracy of the H<sub>2</sub> production rate obtained. The conical flask was connected with a polymeric tubing which extended from top of the rubber seal to the mouth of the measuring cylinder that was inverted so that the gas produced was released inside the inverted measuring cylinder. The H<sub>2</sub> production was measured based on the total volume (mL) of water displaced reflecting ml of H<sub>2</sub> gas produced. The AWCP samples reacted with 200ml of alkaline solution prepared by deionized water which was suggested in section 3.8. Each set of experiment was repeated at least three times. The percentage differences in each result were less than 2 %. An average value was reported.

### **3.4.1 Hydrolysis Process Optimization**

Different types of alkaline solution, different water sources and different temperatures for hydrolysis were studied to investigate for their effect on H<sub>2</sub> production. The concentration of the alkaline solution was fixed at 1 M. The details of the parameter studied are tabulated in Table 3.4. Different parameters such as different water sources, different alkaline solutions, and different duration of disintegration time were studied on effect of total H<sub>2</sub> production volume. The parameters that produced the highest H<sub>2</sub> volume were chosen to be used as the fixed variables in H<sub>2</sub> production system for AWCP, AWCP binary and AWCP ternary composites and also for the batch and continuous methanation.

Table 3.4: Details of the parameter studied for hydrolysis optimization.

Process parameter	Details
Type of alkaline solutions	NaOH, Ba(OH) <sub>2</sub> and KOH
Hydrolysis temperatures (°C)	25° C, 50°C, 60°C, 70°C, 80°C and 100°C
Type of water source	Deionized water, distilled water, ultrapure water and tap water

### 3.4.2 Gibbs Free Energy Calculation

The initial and final temperatures of the reaction systems were recorded, and the temperature data was referred to calculate the Gibbs free energy to explain the hydrolysis mechanism. It also indicates the spontaneity of the hydrolysis reactions varied by different Al samples. The Gibbs free energy was calculated based on the equations (Eq. 3.1 and Eq. 3.2):



$$\Delta G = \Delta H - T\Delta S \quad (3.2)$$

Whereby,

$\Delta G$  = Gibbs free energy (kJ/mol)

$\Delta H$  = change in enthalpy (kJ/mol)

$T$  = change in temperature ( $^{\circ}\text{K}$ )

$\Delta S$  = change in entropy (J/mol.  $^{\circ}\text{K}$ )

### 3.5 Carbon Dioxide Methanation

Figure 3.3 shows the schematic diagram of  $\text{CO}_2$  methanation process utilizing  $\text{H}_2$  from Al hydrolysis reaction. Figure 3.4 shows actual methanation rig. The  $\text{CO}_2$  methanation reaction was carried out in a custom-made fixed-bed reactor (Diameter = 6 mm, Height= 34 cm).

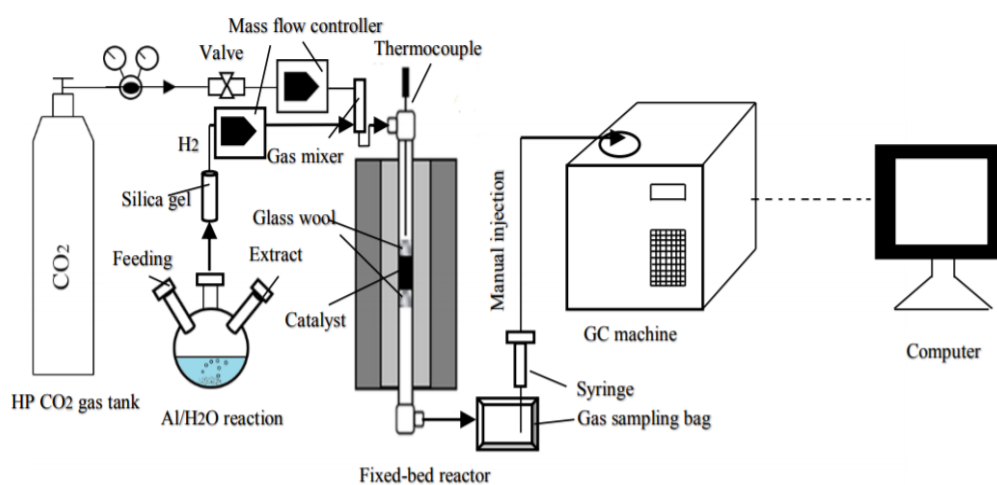


Figure 3.3: Schematic diagram of  $\text{CO}_2$  methanation process utilizing  $\text{H}_2$  produced from the Al hydrolysis.

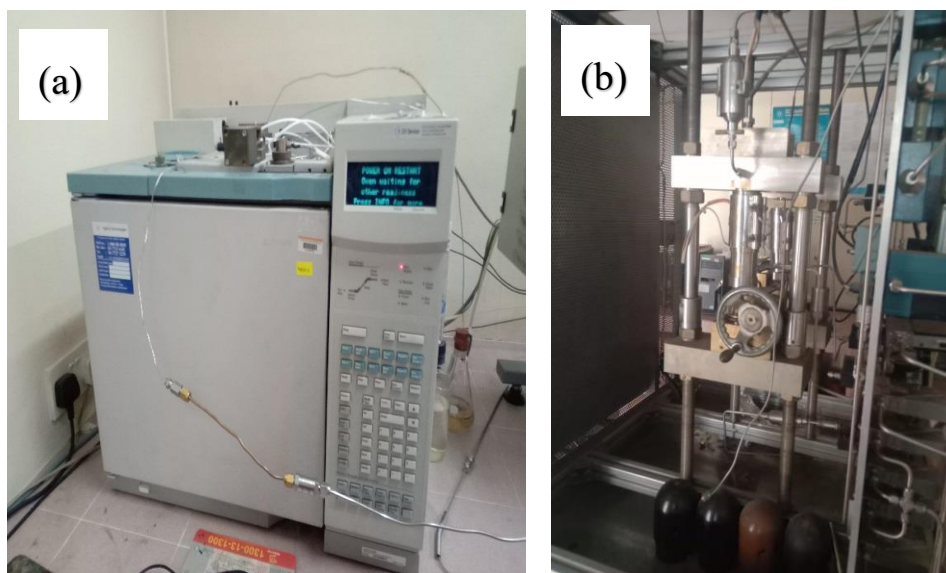


Figure 3.4: Actual methanation rig facility at PutraCAT Lab, Universiti Putra Malaysia: (a) Gas Chromatography machine and (b) Methanation Test Rig.

0.5 g of methanation catalyst (15 wt % Ni/PSAC) was inserted into the reactor system sandwiched between two glass wool to hold the catalyst in place (Younas et al., 2016). Then the fixed bed reactor was heated to 220 °C, the temperature was regulated by a temperature sensor using Type-K thermocouple. High purity lab grade CO<sub>2</sub> gas (99.9 %) from gas tank and H<sub>2</sub> generated from AWCP/NaOH/H<sub>2</sub>O reaction were introduced in excess into the methanation reactor. The H<sub>2</sub> flowrate from hydrolysis was calculated based on the best optimized hydrolysis process via the water displacement method using AWCP (100%), approximately 170 ml/min. The CO<sub>2</sub> flow rate was fixed at 50ml/min for all the experimental runs.

Both gases were pre-mixed using a gas mixer before entering the reactor system.

The reacted and unreacted gases were collected into a sampling bag for every 5 min interval. The collected gases were characterized using a gas chromatography which is equipped with varian capillary columns HP-PLOT/Q and HP-MOLSIV to determine unreacted H<sub>2</sub>, unreacted CO<sub>2</sub>, and generated CH<sub>4</sub> to obtain H<sub>2</sub> conversion, CO<sub>2</sub> conversion, CH<sub>4</sub> selectivity and CH<sub>4</sub> conversion. The collected sample was being injected to the gas chromatography. Each GC analysis took about 20 min to obtain the results. Each set of experiments was repeated at least three times. The percentage differences in each result were less than 2 %. An average value was reported.

Two types of conditions were operated for the CO<sub>2</sub> methanation process. A batch and continuous processes were tested. Batch process means a single run of methanation until the 0.5g AWCP is exhausted. Whereas, for the continuous process the methanation reaction was operated in a continuous manner for a duration of 1 hour. In this investigation, the time to re-feed AWCP into the H<sub>2</sub> production system was investigated based on the results obtained in the batch methanation system. The CO<sub>2</sub> methanation was done using the optimized H<sub>2</sub> produced parameters reached in section 3.8.

### **3.5.1 Preparation of Methanation Catalyst**

The methanation catalyst, 15 wt % Ni/PSAC was synthesized based on previous work by Younas et al. (2016). PSAC was selected as the support, while Ni was chosen as the active metal phase of the catalyst. 15%Ni/PSAC was used based

on Younas et al (2016) work. Impregnation of metallic cation  $\text{Ni}^{2+}$  in the pores of PSAC significantly enhances selectivity and  $\text{CO}_2$  adsorption capacity in the PSAC, which is due to the electrostatic interactions between  $\text{CO}_2$  and the  $\text{Ni}^{2+}$  ions (Younas et al., 2016). Figure 3.5 shows the procedural steps for 15 wt % Ni/PSAC catalyst synthesis via wetness impregnation method. Firstly, 15 wt % of nickel nitrate hexahydrate,  $\text{Ni}(\text{NO}_3)_2 \cdot 6\text{H}_2\text{O}$  was added to the distilled water to dissolve before 85 wt % PSAC was added into the solution. Then, the mixture was sonicated in a water-bath sonicator. The mixture was evaporated in the rotary evaporator and then dried in the oven overnight. The sample was then calcined using a tubular furnace at  $500\text{ }^\circ\text{C}$  with a stream of  $\text{N}_2$  gas to prevent oxidation of the sample. Finally, the samples were further calcined with argon (Ar) gas at  $400\text{ }^\circ\text{C}$  to eliminate oxygen ( $\text{O}_2$ ) as Ar is much heavier.

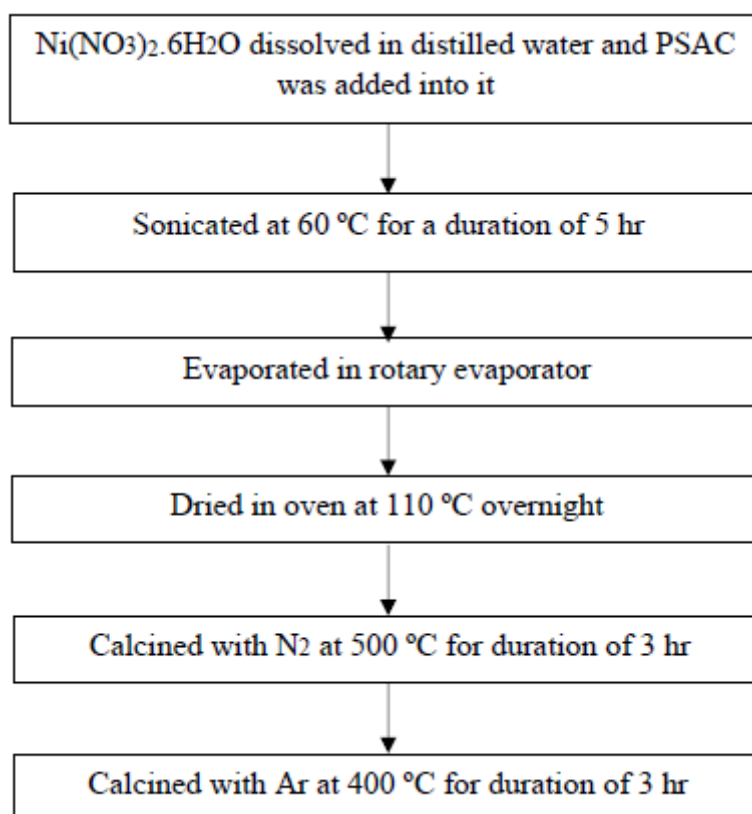


Figure 3.5: Procedural steps for 15 wt % Ni/PSAC catalyst synthesis via wetness impregnation method (Younas et al., 2016).

### 3.5.2 Catalytic Activity Calculation

The activity of the methanation catalyst is to be determined as it affects the amount of CH<sub>4</sub> produced. The conversion of CO<sub>2</sub> and H<sub>2</sub>, and selectivity and yield of CH<sub>4</sub> are defined Eq. 3.3, 3.4 3.5 and 3.6 as follows:

$$\text{H}_2 \text{ conversion, } X_{\text{H}_2} (\%) = \frac{\text{H}_{2,\text{in}} - \text{H}_{2,\text{out}}}{\text{H}_{2,\text{in}}} \times 100 \quad (3.3)$$

$$\text{CO}_2 \text{ conversion, } X_{\text{CO}_2} (\%) = \frac{\text{CO}_{2,\text{in}} - \text{CO}_{2,\text{out}}}{\text{CO}_{2,\text{in}}} \times 100 \quad (3.4)$$

$$\text{CH}_4 \text{ selectivity, } S_{\text{CH}_4} (\%) = \frac{\text{CH}_{4,\text{out}}}{\text{CO}_{2,\text{in}} - \text{CO}_{2,\text{out}}} \times 100 \quad (3.5)$$

$$\text{CH}_4 \text{ yield, } Y_{\text{CH}_4} (\%) = \frac{X_{\text{CO}_2} \times S_{\text{CH}_4}}{100} \quad (3.6)$$

Whereby,

$X_{\text{H}_2}$  = conversion for H<sub>2</sub> (%)

$X_{\text{CO}_2}$  = conversion for CO<sub>2</sub> (%)

$S_{\text{CH}_4}$  = selectivity for CH<sub>4</sub> (%)

$Y_{\text{CH}_4}$  = yield for CH<sub>4</sub> (%)

$\text{CO}_{2,\text{in}}$  = inlet CO<sub>2</sub> (ppm)

$\text{CO}_{2,\text{out}}$  = outlet CO<sub>2</sub> (ppm)

$\text{CH}_{4,\text{out}}$  = generated CH<sub>4</sub> (ppm)

### **3.6 Characterization**

Samples were characterized using Brunauer-Emmett-Teller (BET) Surface Area Measurement (BET), X-ray Diffraction Analysis (XRD), Field Emission Scanning Electron Microscopy (FESEM), Energy-dispersive X-ray Fluorescence Spectroscopy (EDXRF), and Particle Size Distribution Analysis (PSA).

#### **3.6.1 X-ray Diffraction Analysis (XRD)**

X-ray diffraction (XRD) is the main technique used to obtain information regarding the structure, crystalline phase change and the degree of crystallinity of the catalyst. The samples were analyzed by using a Shimadzu diffractometer XRD-6000 model employing Cu-K $\alpha$  radiation at 30 kV and 30 mA, produced by Philips glass diffraction X-ray tube broad-focused on 2.7 kW. The analysis was carried out at room temperature and performed at  $2\theta$  ranging over 5° to 80° at a scanning rate of 2° per min. The sample was ground and placed on the Al sample holder.

#### **3.6.2 Particle Size Distribution Analysis (PSA)**

The particle size distribution of the Al samples powder was analysed by Mastersizer 2000 Ver. 5.60 (Malvern Instruments Ltd., England). Each of the Al

samples were tested for its respective refractive index (RI) before particle size analysis. The accessories, optical unit, and computer were switched on prior to the analysis. The beaker was cleaned and filled with 800 mL of distilled water. The Mastersizer software was opened in the computer connected to the machine. Firstly, manual measurement was made using a standard operating procedure (SOP). The sample was then added into the beaker at a speed of 2000 RPM to dissolve the sample in the water. Once the correct amount of sample was added, the “START” button was pressed to initiate the actual measurement. The particle size distribution graph was obtained at the end of the analysis. The analysis was repeated for other Al samples.

### **3.6.3 Brunauer-Emmett-Teller (BET) Surface Area**

The total surface area of the catalysts was measured by using Brunauer–Emmett–Teller (BET) method. The BET analyses were conducted using Thermo–Finnigan Sorpmatic 1990 series by using N<sub>2</sub> adsorption/desorption analysis. A 0.5 g sample minimum was used for analysis. Before the analysis, the sample was degassed at 150 °C for 12 h, by applying the N<sub>2</sub> adsorption/desorption technique on the surface of the catalyst at liquid N<sub>2</sub> temperature of –196 °C and relative pressure (P/P<sub>o</sub>) ranging from 0.04 to 0.4, and a linear relationship was kept maintained.

### **3.6.4 Field Emission Scanning Electron Microscopy (FESEM)**

Structural and of the sample was analysed by field-emission scanning electron microscopy (FESEM) with an attached energy dispersive X-ray (EDX) spectrometer. Samples on the sample holder were pre-coated with element platinum (Sb, 99.99% purity) using an auto-fine coater JFC-1600, JEOL. The micrograph was taken using a JSM 7600F FESEM, JEOL with an emission current at 2.00 kV and working distance (WD) at 3.0 mm. The major elements in the catalyst sample were analysed using the EDX spectrometer model EX-230BU, JEOL with an emission current at 15.00 kV and 8.00 mm WD.

### **3.6.5 Energy-dispersive X-ray Fluorescence Spectroscopy (EDXRF)**

Energy Dispersive X-ray Fluorescence (EDXRF) elemental analyzer (Rigaku, Japan) was used to determine the elemental analysis of the samples. An X-ray fluorescence (XRF) was operated at 4 kW was used to determine the elemental composition of the disintegrated ACWP.

## CHAPTER 4

### RESULTS AND DISCUSSIONS

#### 4.1 Introduction

This chapter will review the overall results of the experiment with detailed discussion using the data obtained and scientific explanations to discuss the parameters that affect the hydrolysis performance of the samples. The characterization results on AWCP composites using BET, XRF, XRD and FESEM were discussed thoroughly. The hydrolysis performance of AWCP, AWCP binary composites and AWCP ternary composites were discussed in details. At last, the batch methanation and continuous methanation using H<sub>2</sub> produced from AWCP hydrolysis were discussed in this chapter.

#### 4.2 Disintegration of Aluminum Waste Cans

Different disintegration duration (min) will affect the particle size of the AWCP differently. Figure 4.1 (a) to (f) graphically show the particle size distribution of disintegrated AWCP at different disintegration time *i.e.* 1 min, 5 min, 10 min, 15 min, 20min, and lastly for commercial Al. Then, the Al waste can was disintegrated for 1 min, the particle size ranged from 1684-1820  $\mu\text{m}$ . When the

disintegration time was extended to 5 min, the particle size falls in the range of 371-400  $\mu\text{m}$ . When the disintegration time was further extended to 10 min, the particle size was in the range of 118-141  $\mu\text{m}$ . During disintegration, the aluminum waste cans were being shredded by blades at high speed to produce fine AWCP. As times goes, the AWCP particle size reduced as disintegration duration prolonged

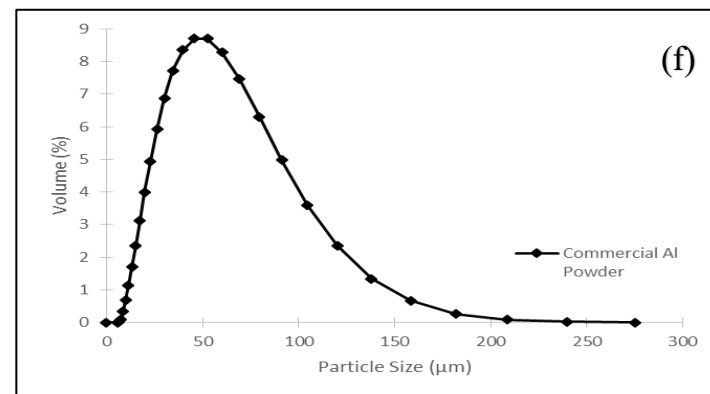
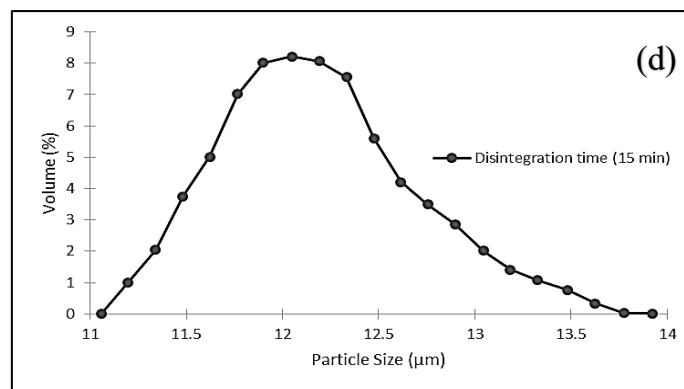
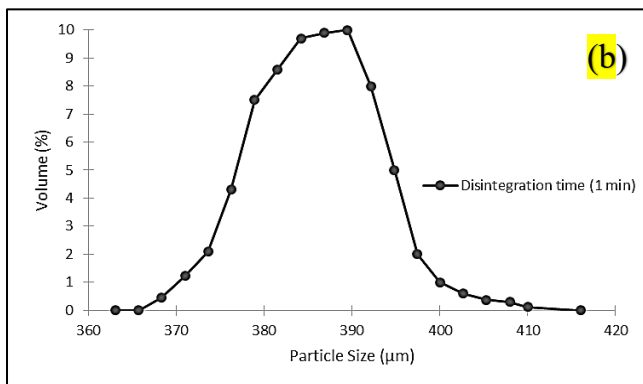
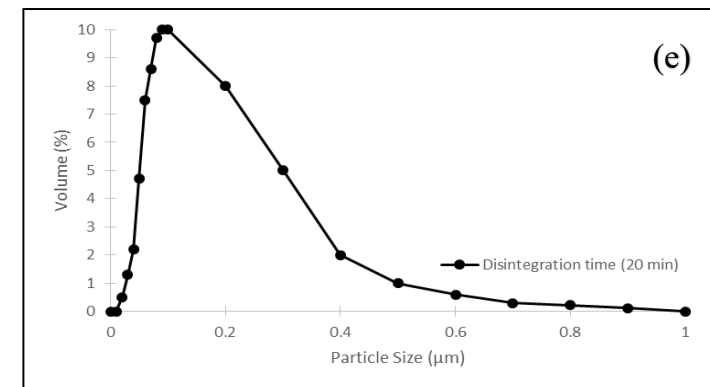
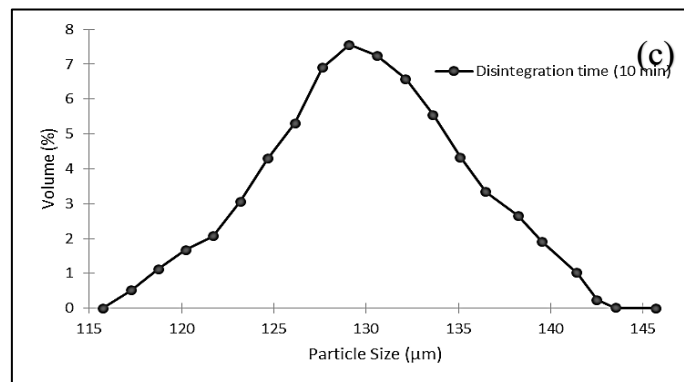
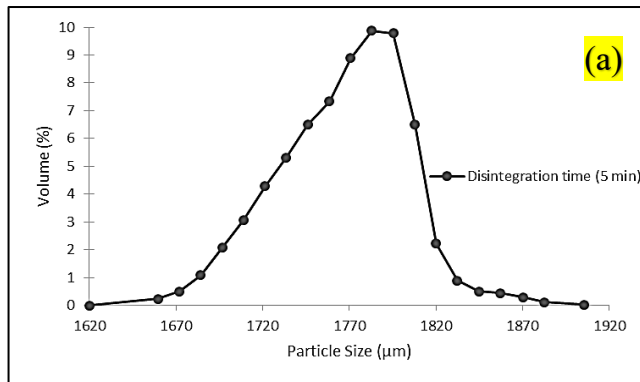


Figure 4.1: Particle size distribution for AWCP (a) 1 min (b) 5 min, (c) 10 min and (d) 15 min, (e) 20 min disintegration and (f) commercial Al.

When disintegration time was increased to 15 min, the particle size was within 11-13  $\mu\text{m}$ . Figure 4.1 (e) and (f) show the particle size distribution of AWCP result from 20 min of disintegration and commercial Al powder. Commercial Al shows a range of 10-150  $\mu\text{m}$  particle size whereas 20 min of disintegration time was within 0.01-1  $\mu\text{m}$ . Commercial Al powder was used as a control in this study for comparison. 20 min of disintegration time was chosen for the upcoming experiments as it yielded the smallest size of particles. The disintegration time was stopped at 20<sup>th</sup> minute due to device limitation. Disintegrated AWCP had better contact and surface area for the hydrolysis reaction to occur due to increased water-to-surface ratio (Yang et al., 2019).

### **4.3 Optimization of Hydrolysis Process**

The AWCP underwent a series of optimization parametric studies on the reaction conditions. Different reaction temperatures were studied with various temperatures: 25 °C, 50 °C, 60 °C, 70 °C, 80 °C and 100 °C. The next parameter studied on the type of alkaline solutions: NaOH, KOH and Ba(OH)<sub>2</sub>. Lastly, different types of water sources were experimented on disintegrated AWCP, different water sources had different value of H<sub>2</sub> generation rate and total H<sub>2</sub> volume.

### 4.3.1 Effect of Different Type of Alkaline Solution

Alkalis NaOH, KOH, and Ba(OH)<sub>2</sub> were selected to study the effect on total H<sub>2</sub> production in hydrolysis using disintegrated AWCP. The hydrolysis process condition was fixed at using 200 mL of 1 M alkaline solution prepared by deionized water. 0.5 g of Al powder was fed into the reaction system at room temperature (25 °C). Figure 4.2 shows the hydrolysis performance of disintegrated AWCP using different types of alkaline solutions. NaOH solution had the highest H<sub>2</sub> production volume due to the amount of available hydroxide ions in the aqueous solution. On the other hand, KOH solution produced 1300 ml placed second, while Ba(OH)<sub>2</sub> generated 1010 ml of H<sub>2</sub> placed last. The NaOH solution required slightly over 28 min induction time compared to KOH with 32 min. In short, Ba(OH)<sub>2</sub> is the weakest alkaline solution which needed a longer induction period. On top of that, some of the AWCP could not complete the hydrolysis reaction in Ba(OH)<sub>2</sub> solution. In conclusion, NaOH is the best alkaline solution for hydrolysis of AWCP due to lower activation energies required.

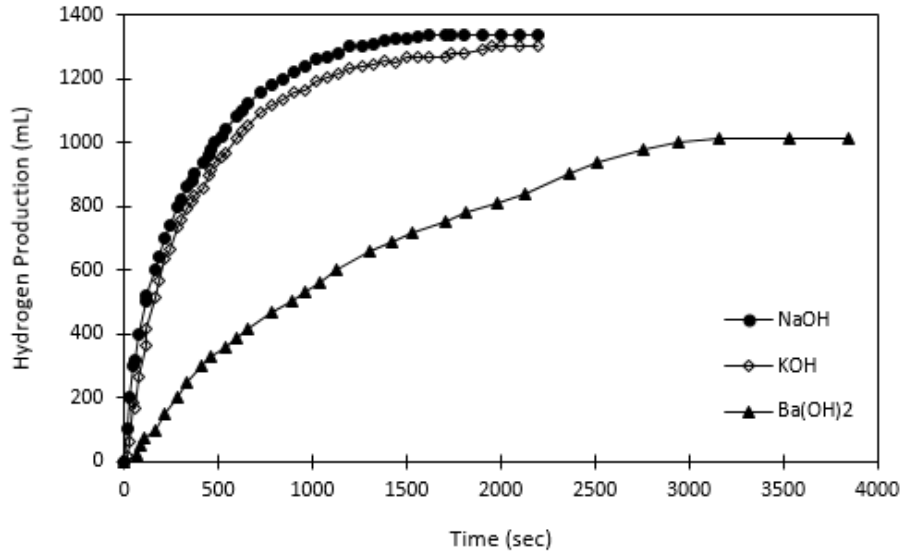


Figure 4.2: Hydrolysis performance of disintegrated AWCP using different type of alkaline solutions.

#### 4.3.2 Effect of Different Water Source

Figure 4.3 shows the hydrolysis performance of disintegrated AWCP using different types of water sources. Different types of water sources: ultrapure water, deionized water, tap water and distilled water in this parametric study. Each of these water sources was used to make 200 mL of 1.0 M NaOH solution. 1 g of Al powder was fed into hydrolysis reaction system at RTP condition. Deionized water produced highest amount of H<sub>2</sub> (1340 ml) which the hydrolysis process took 28.5 min to complete. By definition, deionized water is a form of mineralized water source. It does not contain any impurities or ions; therefore, no other side reactions would occur.

On the other hand, tap water has impurities that can affect the rate of reaction. Tap water containing chlorine may react with Al to produce aluminum chloride,  $\text{AlCl}_3$  which explained the poor hydrolysis performance (Phung, Sethupathi and Piao, 2018). Therefore, tap water is the poorest water source option available for hydrolysis. The lower the resistivity value of the water source, the higher salt concentration available. The higher the salt concentration, the higher the  $\text{H}_2$  production rate by theory. Distilled water with resistivity of  $0.3 \text{ M}\Omega\cdot\text{cm}$  should have higher total  $\text{H}_2$  production volume compared to deionized water with resistivity of  $10 \text{ M}\Omega\cdot\text{cm}$  because distilled water contains salts and ions (Yang et al., 2019). The trace elements in disintegrated AWCP such as Mn, Si, K Cr, Ga, Cl, Ca, S and P elements. These trace elements may react with the ions and salt found in distilled water which explained why deionized water was often selected compared to distilled water. Whereas, ultrapure water has the least amount of salt or ions which are not favourable for hydrolysis.

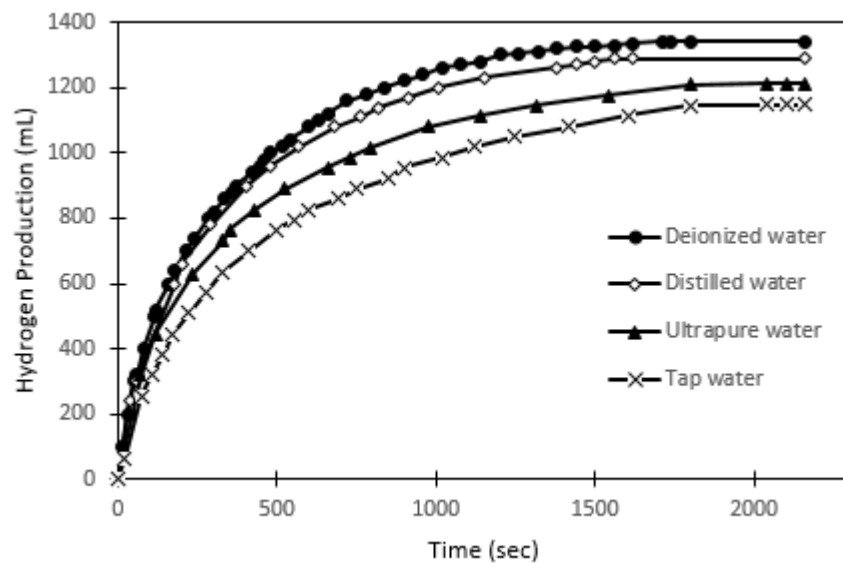


Figure 4.3: Hydrolysis performance of disintegrated AWCP using different

types of water sources.

### 4.3.3 Effect of Reaction Temperature

Different reaction temperatures will result in different hydrolysis performance affecting total H<sub>2</sub> production volume and production rate. Different temperature settings: 25°C (RTP), 50°C, 60°C, 70°C, 80°C, and 100°C were experimented on fixed variables of 200 mL of 1.0 M NaOH solution and 1 g of disintegrated AWCP powder. Figure 4.4 shows the hydrolysis performance of disintegrated AWCP at different reaction temperatures (°C). As the reaction temperature increased, the performance of hydrolysis improved. The reaction temperature plays a role in speeding up the reaction rate. However, it does not affect the total H<sub>2</sub> production rate.

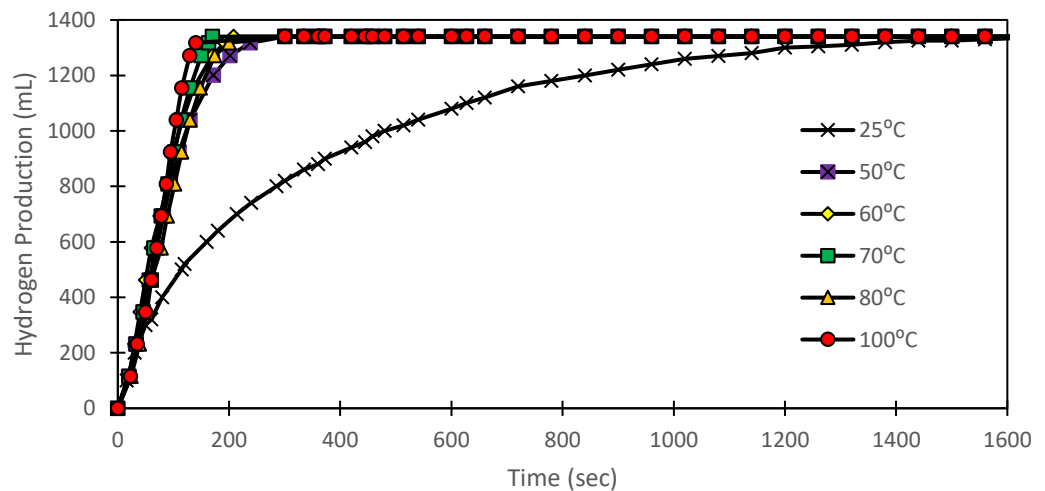


Figure 4.4: Hydrolysis performance of disintegrated AWCP at different reaction temperatures (°C).

The higher the reaction temperature, the shorter induction time. At temperatures above 50 °C, the maximum H<sub>2</sub> production of 1340 mL can be produced within 2 to 5 minutes. However, about 30 min was needed to produce the same amount of H<sub>2</sub> at RTP. The Al particles gain more kinetic energy at elevated contributed to more production of H<sub>2</sub> (Yang et al., 2019). However, 25°C room temperature was selected for AWCP hydrolysis as the temperature only speeds up reaction, it did not increase H<sub>2</sub> yield.

#### **4.4 Comparison of Hydrogen Production via Commercial Al and AWCP**

Figure 4.5 shows the H<sub>2</sub> production graph of disintegrated AWCP versus commercial Al powder. The hydrolysis process condition was fixed at 200 mL of 1 M NaOH solution prepared in deionized water with 1 g of Al powder at room temperature (25 °C). Disintegrated AWCP produced more H<sub>2</sub> (1340 ml) than that of commercial Al powder (1140 ml). This means, AWCP had 15% more H<sub>2</sub> yield. This can be explained by difference of particle size and BET active surface area values. Disintegrated AWCP has a particle size of 0.01 to 1 µm with BET value 18.54 m<sup>2</sup>/g. However, particle size of commercial Al was detected between 10 to 150 µm with BET value 0.85 m<sup>2</sup>/g.

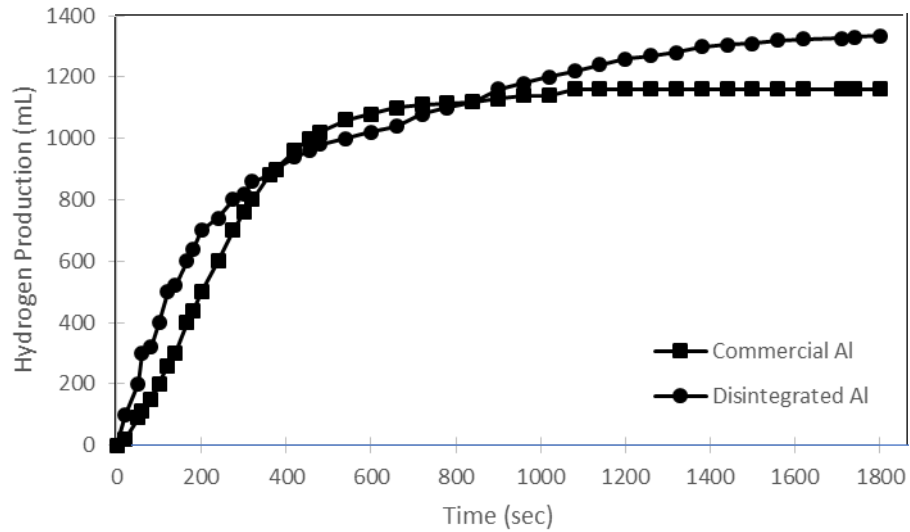


Figure 4.5: Hydrogen production of disintegrated AWCP versus commercial Al powder.

#### 4.5 Characterization of AWCP

This session will discuss the results for BET surface area and pore size; x-ray fluorescence spectroscopy (XRF) analysis results; XRD results; and FESEM results of AWCP.

##### 4.5.1 BET Surface Area and Pore Size

The effect of disintegration time (min) on the performance of AWCP was studied by determination of its respective BET active surface area and pore characteristics. Table 4.1 indicates the relationship between disintegration time (min) and the BET active surface area of the disintegrated AWCP and the characteristics of commercial Al. According to the data, the longer the

disintegration time, the higher the BET active surface area of AWCP. The highest surface area was obtained by optimized 20 min of disintegration at 25000 rpm. The optimized 20 min-disintegrated AWCP had 18.5 m<sup>2</sup>/g of multipoint BET surface area, 0.031 cc/g total pore volume and 6.7 nm average pore diameter was reported for AWCP.

Commercial Al powder has BET surface area of 0.8 m<sup>2</sup>/g. Analysis results showed that AWCP had higher BET surface area values than that of commercial Al. AWCP had higher water-to-surface ratio thus more water was able to penetrate the particle, dissolution of Al was promoted, more H<sub>2</sub> was produced as a result. AWCP was produced using a high-speed medicine blender had higher BET values compared to that reported by Ho and Huang (2016) which reported between 0.08 to 3.2 m<sup>2</sup>/g. Yang et al. (2019) reported BET surface area values between 1.6 to 2.5 m<sup>2</sup>/g for AWCP generated using a magnetic grinder. AWCP containing other trace metals such as Mn, Ga, Ca and Fe helped enhance the total H<sub>2</sub> production volume (Wang et al., 2009).

Table 4.1: BET surface area and the pore characteristics of disintegrated AWCP and commercial Al.

Disintegration time of AWCP (min)	Multipoint BET (m <sup>2</sup> /g)	DR Method micropore area (m <sup>2</sup> /g)	DR Method micropore area (cc/g)	Total pore volume (cc/g)	Average pore diameter (nm)
1	0.1	0.9	0.001	0.001	0.3
5	0.2	2.3	0.002	0.002	1.3
10	0.3	4.2	0.005	0.006	4.4
15	7.3	10.2	0.007	0.014	5.3
20	18.5	22.5	0.008	0.031	6.7
Commercial Al	0.8	5.3	0.002	0.008	4.6

Gas adsorption has been an important standard procedure to characterize the porous solids and powders. In this study, N<sub>2</sub> adsorption/desorption technique was used to characterize the porous structure of the disintegrated AWCP. Thommes et al. (2015) reported physisorption isotherms can be generally categorized into six different types. Figure 4.6 shows the N<sub>2</sub> adsorption/desorption of AWCP after 20 min of disintegration time. The corresponding N<sub>2</sub> isotherm is a Type IV (a). The BET analysis determines the average pore diameter and DR method micropore width of AWCP produced after 20 min disintegration time are 6.679 nm and 2.241 nm respectively, which its porosity can be classified as mesopores in the context of physisorption. Type IV isotherms are defined by mesoporous adsorbents. The behaviour of the adsorption in mesopores is affected by the interactions between adsorbent and adsorptive, and also the interactions between the molecules in the state of condensation (Thommes et al., 2015). In Type IV (a) isotherm, the capillary condensation is linked by hysteresis which happens when the AWCP pore width exceeded a certain critical width length. This so-called critical width relies on the adsorption system and temperatures. The Type IV(a) isotherm describes the shape of the graph for N<sub>2</sub> isotherm graph in Figure 4.6. It has a Type H5 hysteresis loop, which indicated distinctive form linked to particular pore structures which comprised of both open and partially blocked mesopores (Thommes et al., 2015).

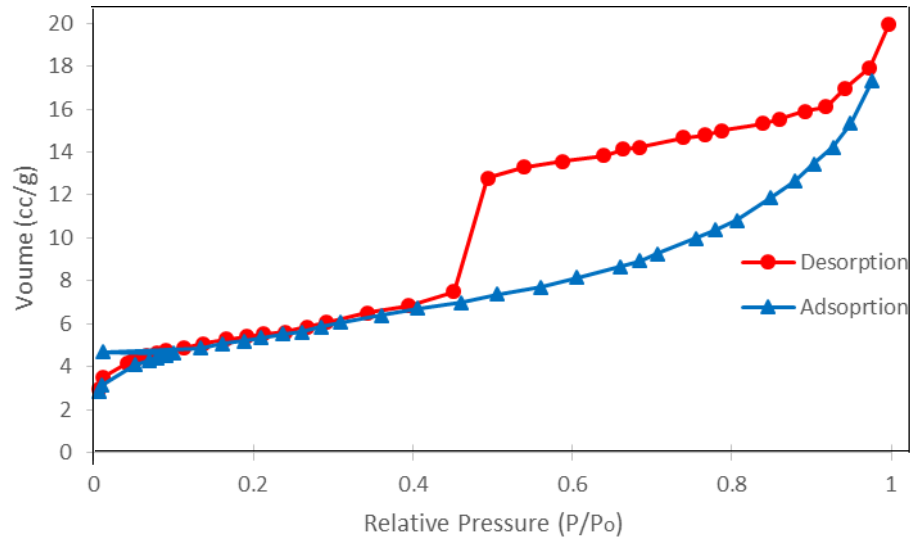


Figure 4.6: N<sub>2</sub> adsorption/desorption of AWCP after 20 min of disintegration time.

#### 4.5.2 X-ray Fluorescence Spectroscopy (XRF)

EDXRF analysis was performed on AWCP to study the elemental composition of the AWCP which the results were shown in Table 4.2. The disintegrated AWCP comprised of 96.2 wt % of Al; 1.35 wt % of Mn; 0.953 wt % of Mg; 0.734 wt % of Fe; 0.315 wt % of Cu and others in trace amount including Si, K, Cr, Ga, Cl, Ca, S and P elements.

Table 4.2: EDXRF analysis of disintegrated AWCP produced from 100 PLUS waste cans.

<b>Component</b>	<b>Result (mass %)</b>	<b>Intensity</b>
Aluminum (Al)	96.2000	95.1348
Manganese (Mn)	1.3500	3.4336
Magnesium (Mg)	0.9530	0.4830
Iron (Fe)	0.7340	2.9751
Copper (Cu)	0.3150	2.8077
Silicon (Si)	0.1510	0.0559
Potassium (K)	0.0708	0.3774
Zinc (Zn)	0.0630	0.7618
Chromium (Cr)	0.0386	0.0668
Gallium (Ga)	0.0227	0.3084
Chlorine (Cl)	0.0217	0.1280
Calcium (Ca)	0.0140	0.0886
Sulphur (S)	0.0127	0.0632
Potassium (P)	0.0079	0.0354

#### 4.5.3 X-ray Diffraction Analysis (XRD)

XRD characterization analysis test was performed on disintegrated AWCP and commercial Al to study crystal structure and crystallinity of the samples. Figure 4.7 illustrated the XRD results of AWCP and commercial Al. For AWCP, the major peaks at 38°, 44°, 65° and 78° were Al components confirmed by JCPDS card number 01-074-1119, while the other micro-peaks indicated other trace

metals. For commercial Al, the major peaks at 38°, 44°, 65° and 78° were identified as Al components and no other micro-peaks similar to that of AWCP was identified signified pure Al content.

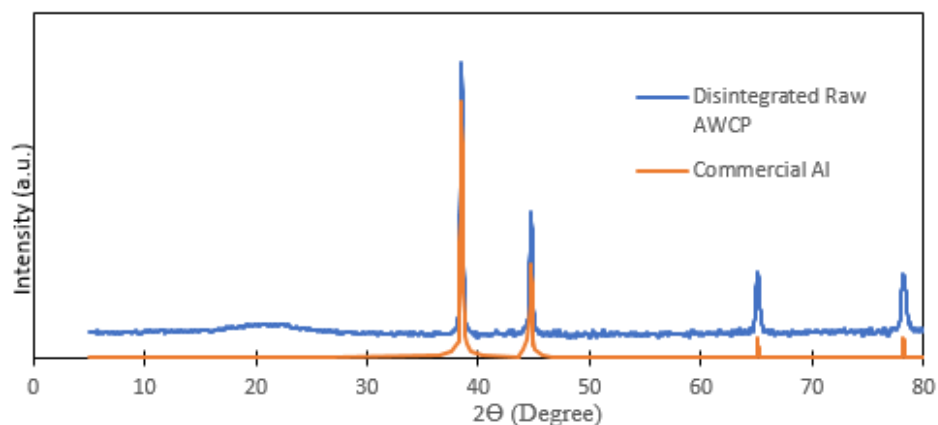


Figure 4.7: The major peaks for Al material (degree) and its corresponding intensity (a.u.) for AWCP and commercial Al.

Table 4.3: The major peaks (degree) and its corresponding intensity (a.u.) for AWCP and commercial Al.

Major peak (degree)	Intensity (a.u.) for disintegrated AWCP	Intensity (a.u.) for commercial Al
38°	1717	1488
44°	856	549
65°	508	118
78°	488	117

#### 4.5.4 Field Emission Scanning Electron Microscope (FESEM)

FESEM analysis were performed on AWCP and commercial Al to study topographical and elemental details at magnified levels. Figure 4.8 shows the FESEM images of (a) commercial Al and (b) AWCP. Commercial Al showed a well-distributed structure with numerous pores on its surface, while disintegrated AWCP which was produced by disintegration method has an irregular surface with structure that were flaky in shape. The particles underwent a cold-welding mechanism which homogenizes the mixture of particles. The particles became hardened and fractured into smaller particles which contributed to the flake-like structure (Du Preez and Bessarabov, 2018).

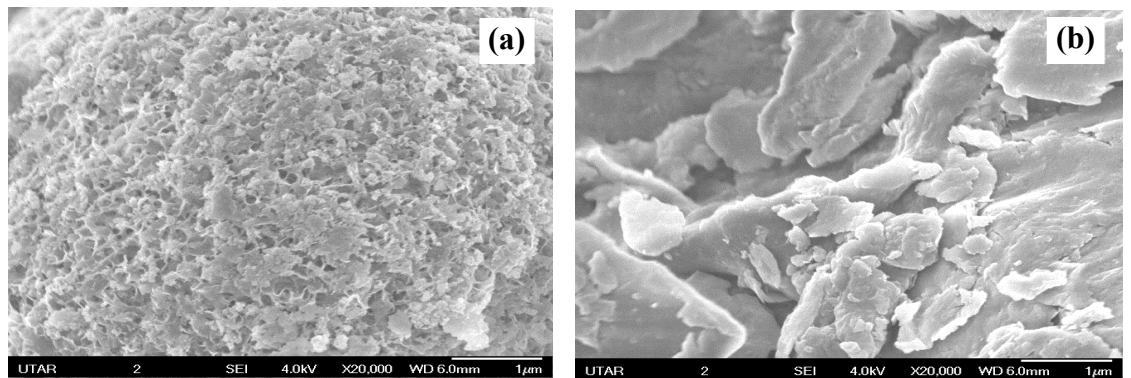


Figure 4.8: FESEM images of (a) commercial Al and (b) AWCP at 20K magnification.

#### 4.6 Hydrolysis Performance of Binary Al Composites

Upon comparing the commercial and AWCP, it was found that AWCP performed better than commercial Al. To further enhance the performance of AWCP, binary mixtures with other alloy metals was tested. 4 different metals were used *i.e.* Sn, Mg, Zn and In. Mixture ratio was prepared according to literature (du Preez and Bessarabov, 2018).

0.5 g of binary AWCP composites was introduced into the aluminum-water reaction system. The experiment was repeated three times to obtain the average results. Figure 4.9 shows the H<sub>2</sub> production (mL) versus time (sec) of the binary AWCP composites. Table 4.4 indicates the H<sub>2</sub> production performance analysis between AWCP and AWCP binary composites.

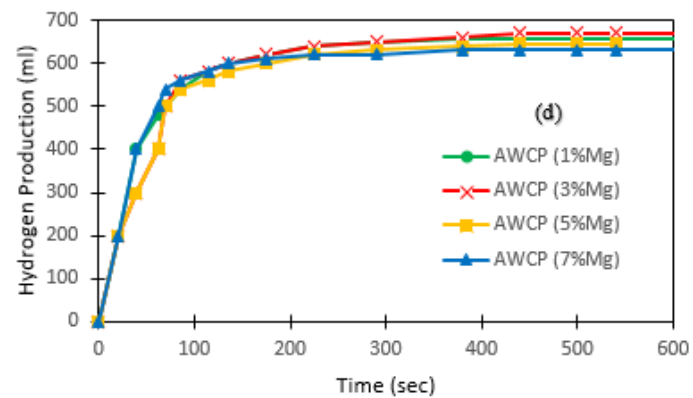
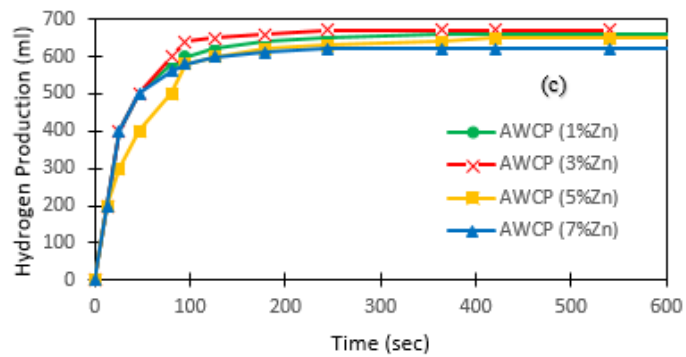
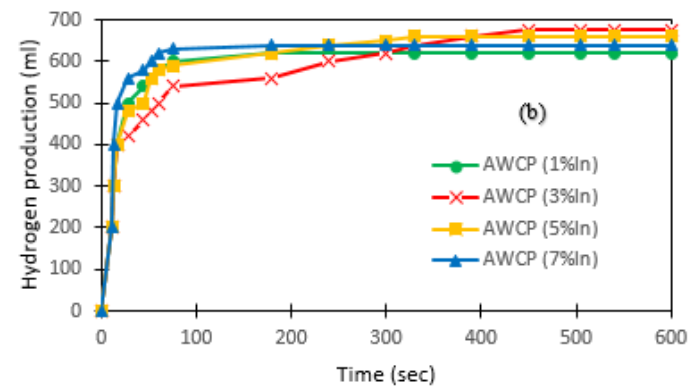
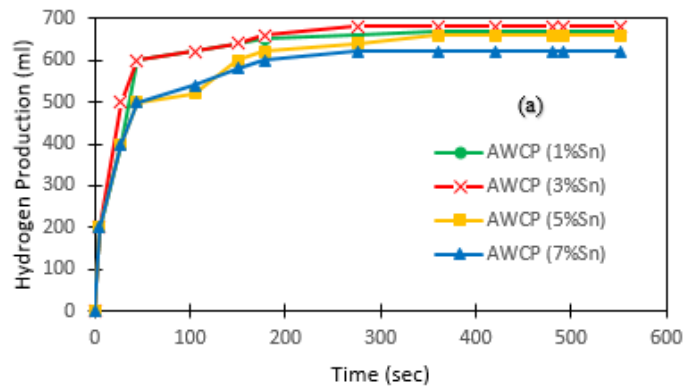


Figure 4.9: H<sub>2</sub> production graph of AWCP binary composites: a) AWCP/Sn, b) AWCP/Mg, c) AWCP/In and d) AWCP/Zn.

Table 4.4: H<sub>2</sub> production results of AWCP and AWCP binary composites.

<b>Sample</b>	<b>Maximum H<sub>2</sub> Production Volume (mL/0.5g)</b>	<b>Total Reaction Time Based on 0.5g (sec)</b>	<b>Average Maximum H<sub>2</sub> Production Rate (mL/g.sec)</b>
AWCP (100%)	670	1710	0.39
AWCP (99%)	663	1712	0.38
AWCP (97%)	650	1715	0.37
AWCP (95%)	635	1722	0.36
AWCP (93%)	623	1725	0.36
AWCP (1% Sn)	670	360	1.86
AWCP (3% Sn)	680	240	2.83
AWCP (5% Sn)	660	267	2.47
AWCP (7% Sn)	620	360	1.72
AWCP (1% Zn)	660	364	1.81
AWCP (3% Zn)	665	420	1.58

Table 4.4: Continued.

<b>Sample</b>	<b>Maximum H<sub>2</sub> Production Volume (mL/0.5g)</b>	<b>Total Reaction Time Based on 0.5g (sec)</b>	<b>Average Maximum H<sub>2</sub> Production Rate (mL/g.sec)</b>
AWCP (5% Zn)	650	420	1.54
AWCP (7% Zn)	620	240	2.58
AWCP (1% Mg)	655	380	1.72
AWCP (3% Mg)	670	432	1.55
AWCP (5% Mg)	645	540	1.19
AWCP (7% Mg)	630	385	1.63
AWCP (1% In)	660	330	2.00
AWCP (3% In)	675	330	2.04
AWCP (5% In)	640	75	8.53
AWCP (7% In)	620	180	3.44

AWCP binary composites reacted aggressively in alkaline solution between 0<sup>th</sup> to 20<sup>th</sup> second, then the reaction increased proportionally with time, and became stable after 100 seconds. AWCP (3% Sn) had the most vigorous reaction with 680 ml H<sub>2</sub> produced which only consumed total of 240 sec only (equivalent to 4 min). AWCP (3% Sn) generated 610 ml, on the other hand, AWCP (3% In) produced 560 ml, measured at 50<sup>th</sup> second.

For AWCP/Sn composite, the Sn metal promoted micro-galvanic activity between Sn and AWCP which were anode-cathode relationship in aluminum-water reaction. All binary composites had H<sub>2</sub> generation of more than the theoretical H<sub>2</sub> yield 1360 ml. The activation metal increased the H<sub>2</sub> yield and shortened total reaction time. Metals addition in the composite promoted synergistic effect. Disintegration process via medicine blender gave a larger surface area for the AWCP to react with NaOH solution with the Sn metal which can be explained by BET value (19.37 m<sup>2</sup>/g) of AWCP (3% Sn). For H<sub>2</sub> production volume from the highest to lowest: AWCP (3% Sn) > AWCP (3% In) > AWCP (3% Mg) > AWCP (3% Zn). This is because of the electrode potential difference between Al and activation metal; the larger the electrode potential difference, the higher tendency of Al potential driven towards more active direction, which promoted Al dissolution.

#### **4.7 Characterization of AWCP Binary Composites**

The binary AWCP composites were characterized using Brunauer-Emmett-

Teller (BET) Surface Area Measurement (BET), X-ray Diffraction Analysis (XRD), Field Emission Scanning Electron Microscopy (FESEM), and Energy-dispersive X-ray Fluorescence Spectroscopy (EDXRF).

#### 4.7.1 X-ray Diffraction Analysis (XRD)

XRD analysis was done on AWCP (3% Sn) binary composite to determine intermetallic phases AWCP/Sn. Figure 4.10 shows the XRD result of AWCP (3% Sn) binary composite. The major peaks which were located at degree 38°, 44°, 65° and 78° were Al components with JCPDS card number 01-074-5276. The other micro-peaks were identified Sn metal deposited on Al surface. The XRD analysis confirmed no formation of intermetallic phases which similar conclusion was reported by Preeze and Bessarabov (2018).

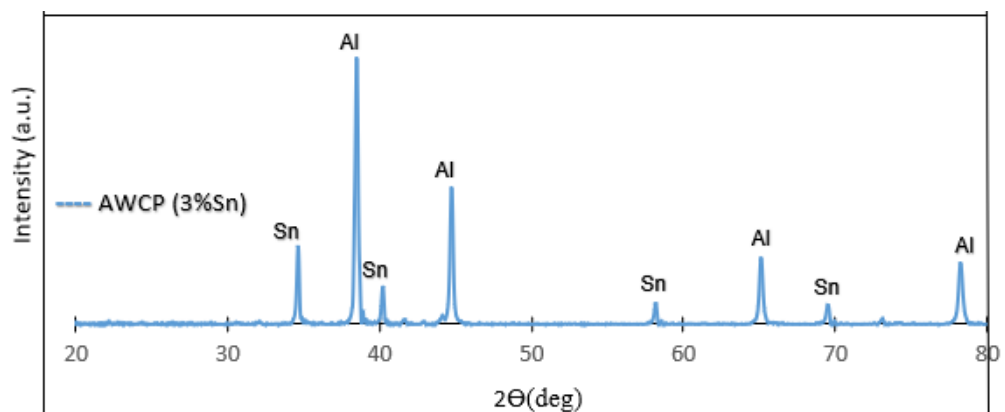
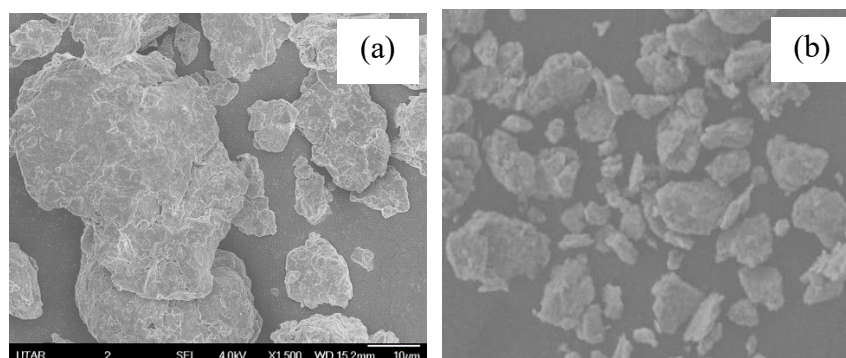


Figure 4.10: The XRD patterns of binary AWCP (3% Sn) composite.

#### 4.7.2 Field-emission Scanning Electron Microscope (FESEM)

Figure 4.13 shows FESEM images of AWCP (3% Sn) binary composite with its EDS mappings. The images showed even distribution of Sn on AWCP surface. Commercial Al in Figure 4.8 (a) shows well-distributed structure with numerous pores on its surface. Figure 4.11 shows that the AWCP (3% Sn) surface was flake-like similarly reported in AWCP FESEM analysis. The AWCP (3% Sn) particles underwent particle size reduction. Many deformities and irregularities can be seen for AWCP (3% Sn) composite particles which contributed to increased water-to-surface ratio. Size reduction alone does not guarantee Al particles to be hydrolyzed under ambient conditions. The activation metal must be equally distributed on Al particle's surface which is proved by EDS-mapping. The EDS results reported chemical composition of  $3.00 \pm 0.26\%$  Sn, coincided with the pre-determined 3 wt% Sn content in AWCP (3% Sn) binary composite.



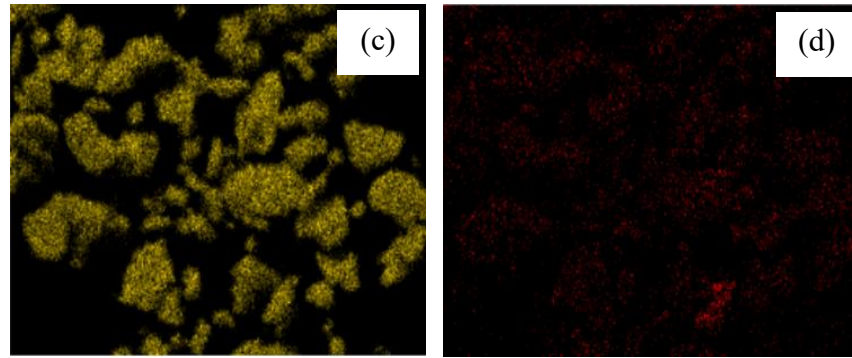


Figure 4.11: FESEM micrographs of AWCP (3% Sn) composite at X1500 magnification (a) and at X500 magnification (b); with EDS mappings of AWCP (c) and Sn (d).

#### 4.7.3 BET Surface Area

Among binary composites AWCP, AWCP (3% Sn) had the highest active surface area of  $19.37 \text{ m}^2/\text{g}$ . During ball milling process, the particles went through a cold-welding process which homogenized the mixture of particles (Du Preez and Bessarabov, 2018; Yang et al., 2019; Lim et al. 2020). During ball milling process, Al and activation metal cold-welded to one another when ball-to-ball and ball-to-jar collisions happened, forming larger coagulated particles. The larger coagulated particles then divided into smaller particles which homogenize the constituents. After certain period of plastic deformation, the ductile particles hardened and fractured into smaller particles which explained the higher BET surface area (Du Preez and Bessarabov, 2018).

Table 4.5: BET surface area of binary AWCP composites.

Al samples	BET surface area (m <sup>2</sup> /g)
Commercial Al	0.475
Disintegrated AWCP	18.54
AWCP (3%Sn)	19.37
AWCP (3%In)	18.83
AWCP (3%Mg)	18.79
AWCP (3%Zn)	18.82

#### 4.8 Hydrolysis Performance of Aluminum Ternary Composites

In the synthesis of AWCP ternary composites, Sn, Mg and In metals were selected as they have more significant production H<sub>2</sub> and rate of reaction compared to performance of AWCP binary composite doped with Zn metal. Figure 4.12 (a) and (b) indicated the H<sub>2</sub> production over time graph of AWCP ternary composites. From 0 to 200 seconds of the reaction, all ternary composites were rapid. AWCP (1% Sn-5% In) and AWCP (5% Sn-1% In) showed the highest compared to AWCP (94%) and AWCP (3% Sn-3% In). In terms of total H<sub>2</sub> production volume as shown in Table 4.9, AWCP (3% Sn-3% In) showed the highest total H<sub>2</sub> production volume with 645 ml in 360 sec despite of low H<sub>2</sub> production rate.

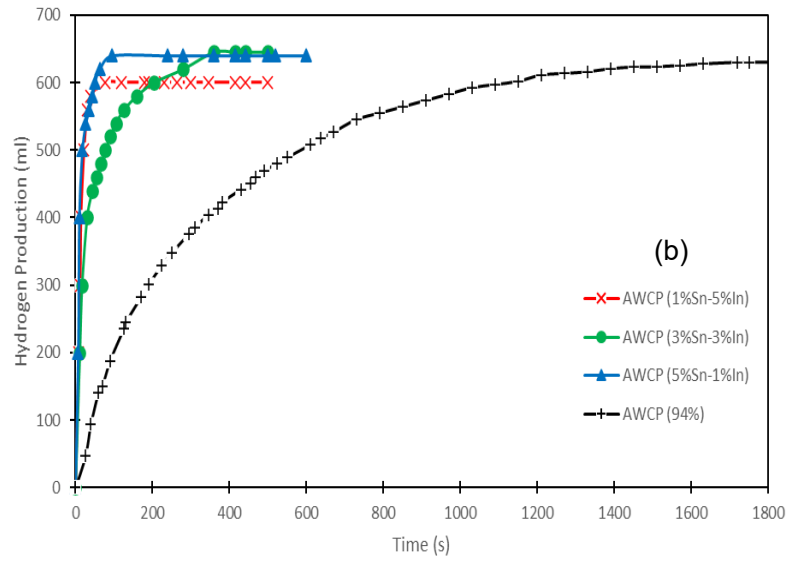
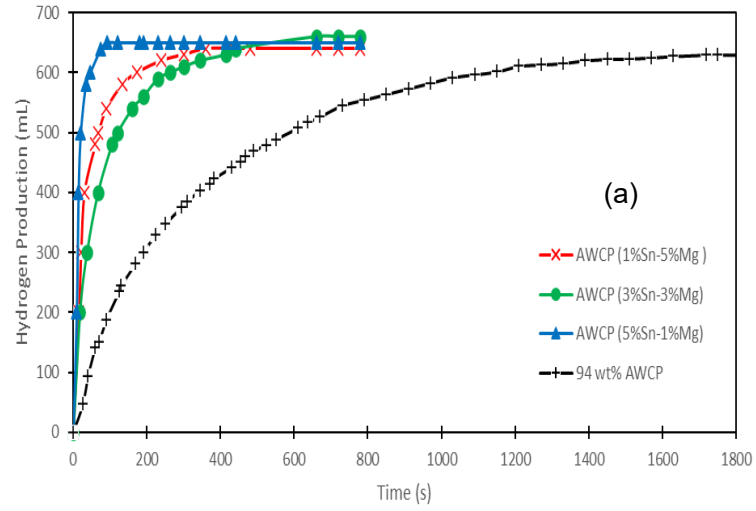


Figure 4.12: H<sub>2</sub> production graph over time of AWCP ternary composites (a) AWCP/Sn/Mg and (b) AWCP/Sn/In.

Table 4.6: H<sub>2</sub> production results of AWCP and AWCP ternary composites.

<b>Sample</b>	<b>Maximum H<sub>2</sub> Production Volume (mL/0.5g)</b>	<b>Total Reaction Time Based on 0.5g (sec)</b>	<b>Average Maximum H<sub>2</sub> Production Rate (mL/g.sec)</b>
AWCP (94%)	629	1720	0.36
AWCP (1%Sn – 5%Mg)	640	360	1.77
AWCP (3%Sn – 3%Mg)	660	660	1.00
AWCP (5%Sn – 1%Mg)	650	92	7.06
AWCP (1%Sn – 5%In)	600	77	7.79
AWCP (3%Sn – 3%In)	645	360	1.79
AWCP (5%Sn – 1%In)	640	95	6.73

For AWCP (3% Sn-3% In) composite, its reaction was slow and steady provided more room for hydrolysis and production of H<sub>2</sub>. H<sub>2</sub> production volume did not increase when Sn or In content  $\geq 5$  wt%.

AWCP (3% Sn-3% Mg) ternary composite produced 1320 ml/g H<sub>2</sub> in 660 sec. On the other hand, AWCP (3% Sn-3% In) ternary composite produced 1290 ml/g in 360 sec. In terms of total H<sub>2</sub> production, AWCP (3% Sn-3% Mg) is the best. However, in term of total evolution time required, AWCP (3% Sn-3% In) only required 360 sec to complete the hydrolysis reaction compared to 660 sec by AWCP (3% Sn-3% Mg).

Mg metal (-2.38 V) had a more negative electrode potential compared with Al (-1.663 V). The Mg metal would corrode first during the hydrolysis reaction at localized Al/Mg electrodes. The total H<sub>2</sub> generation was not only contributed by Al hydrolysis, Mg and the other metals in AWCP also suffered hydrolysis reaction. Wang et al. (2014) reported that Mg metal capable producing maximum of 1019 ml/g H<sub>2</sub> at room temperature. The localized Al/Sn would experience micro-galvanic activity. The redox reaction between Al (anode) and Sn (cathode) helped promote Al anodic dissolution. However, AWCP (3% Sn – 3% In) had lower H<sub>2</sub> generation due to electrode potential of In metal is only about -0.34 V. However, the presence of In metal in the composite significantly reduced the total reaction time.

Table 4.7: Comparison of research outcomes with literature work.

Sample	Activation Method	Temperature (°C)	Max. H <sub>2</sub> Production Rate	Max. H <sub>2</sub> Yield	Reference
Commercial Al	Alkaline -5M KOH	25	12.5 ml/g/min	NR	(Solar et al., 2005)
Commercial Al	Alkaline - Ca(OH) <sub>2</sub>	25	Not reported	90 %	(Liu et al., 2018)
Commercial Al	Ball milling – *4 hr & **7 hr at 200 RPM	80	*70 ml **80 ml	NR	(Razavi-Tousi and Szpunar, 2014)
Al-5%Bi-10%Ga-5%Zn	Ball milling – milling hr and speed NR	25	940 ml/g ~for 900 sec	70 %	(Fan, Xu and Sun, 2007)
Al-7.5%Bi-2.5%Sn	Ball milling – 3 hr, milling speed NR	35	9.5 ml/g/sec	85 %	(Xiao et al., 2018)
Al-5%Sn-5%In	Ball milling – 0.5 hr at 1500 RPM	25	1346 ml/g ~for 300 sec	99 %	(Du Preez and Bessarabov, 2018)
Commercial Al	Alkaline – 1M NaOH	25	1140 ml/g ~for 960 sec	84 %	This study
AWCP (100%)	Ball milling – 1 hr at 1200 RPM Alkaline – 1M NaOH	25	1340 ml/g ~for 1710 sec	98.5 %	This study
AWCP (3%Sn)	Ball milling – 1 hr at 1200 RPM Alkaline – 1M NaOH	25	1360 ml/g ~for 240 sec	100 %	This study
AWCP (3%Sn-3%Mg)	Ball milling – 1 hr at 1200 RPM Alkaline – 1M NaOH	25	1320 ml/g ~for 660 sec	97 %	This study

\*NR means Not Reported

Table 4.7 shows the comparison between literature work versus experimental outcome for the composites synthesized in this study in term of H<sub>2</sub> production volume and H<sub>2</sub> yield. AWCP (3%Sn) is the best among the samples in Table 4.7 based on total H<sub>2</sub> production volume 1360 ml/g with H<sub>2</sub> yield 100%. Compared to that of Al-5%Sn-5%In (Du Preez and Bessarabov, 2018), AWCP (3%Sn) not only had the highest H<sub>2</sub> production volume, it had also shortest total H<sub>2</sub> evolution time 240 sec. However, Al-5%Sn-5%In (Du Preez and Bessarabov, 2018) > AWCP (100%) > AWCP (3%Sn-3%Mg) in term of total H<sub>2</sub> production volume.

#### **4.9 Characterization of AWCP Ternary Composites**

The AWCP ternary composites were characterized using Brunauer-Emmett-Teller (BET) Surface Area Measurement (BET), X-ray Diffraction Analysis (XRD), Field Emission Scanning Electron Microscopy (FESEM), and Energy-dispersive X-ray Fluorescence Spectroscopy (EDXRF).

##### **4.9.1 X-ray Diffraction Analysis (XRD)**

XRD analysis was performed on AWCP (3%Sn – 3%Mg) ternary composites (refer Figure 4.13) to investigate the formation of intermetallic phases between AWCP, Sn and Mg. The major peaks at 38°, 44°, 65° and 78° were identified as Al component confirmed by JCPDS card number 01-074-5276. The smaller

peaks at  $34^\circ$ ,  $40^\circ$ ,  $58^\circ$  and  $69^\circ$  indicated Sn metal; while peaks at  $30^\circ$ ,  $32^\circ$ ,  $36^\circ$  and  $44^\circ$  showed Mg component. Throughout the hydrolysis, the micro-galvanic activity between Al and activation metals will remain elevated. As the AWCP was consumed, the composites would further react to produce  $H_2$  (du Preez and Bessarabov, 2018).

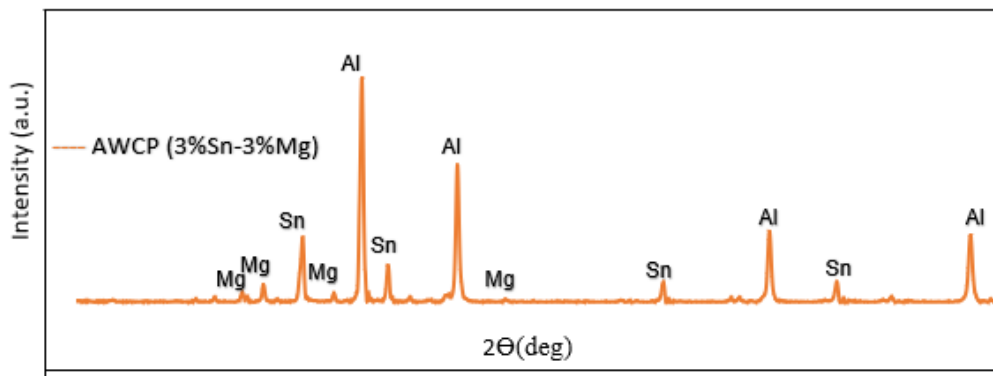


Figure 4.13: The XRD patterns of AWCP (3% Sn-3% Mg) ternary composite.

#### 4.9.2 Field-emission Scanning Electron Microscope (FESEM)

Figure 4.14 shows the FESEM pictures of AWCP (3% Sn-3% Mg) ternary composite. Micrograph showed the distribution of Sn and Mg metals were even on AWCP surface. In the ball milling process, as ball-to-ball and ball-to-jar collisions happened; the AWCP, Sn and Mg were cold-welded to one another. The metals were homogeneously distributed across the Al surface and smaller particles were formed due to constant collision and attrition. Moreover, the presence of intermetallic phase between metals promoted hydrolysis activity (du Preez & Bessarabov, 2018). Intermetallic phases between Sn/In and Sn/Mg

enhanced the hydrolysis process and increased total H<sub>2</sub> production volume. EDX result yielded an average chemical composition of 3.63 wt% Sn and 4.32 wt% Mg, well coincided with the predetermined 3 wt% Sn and 3 wt% Mg.

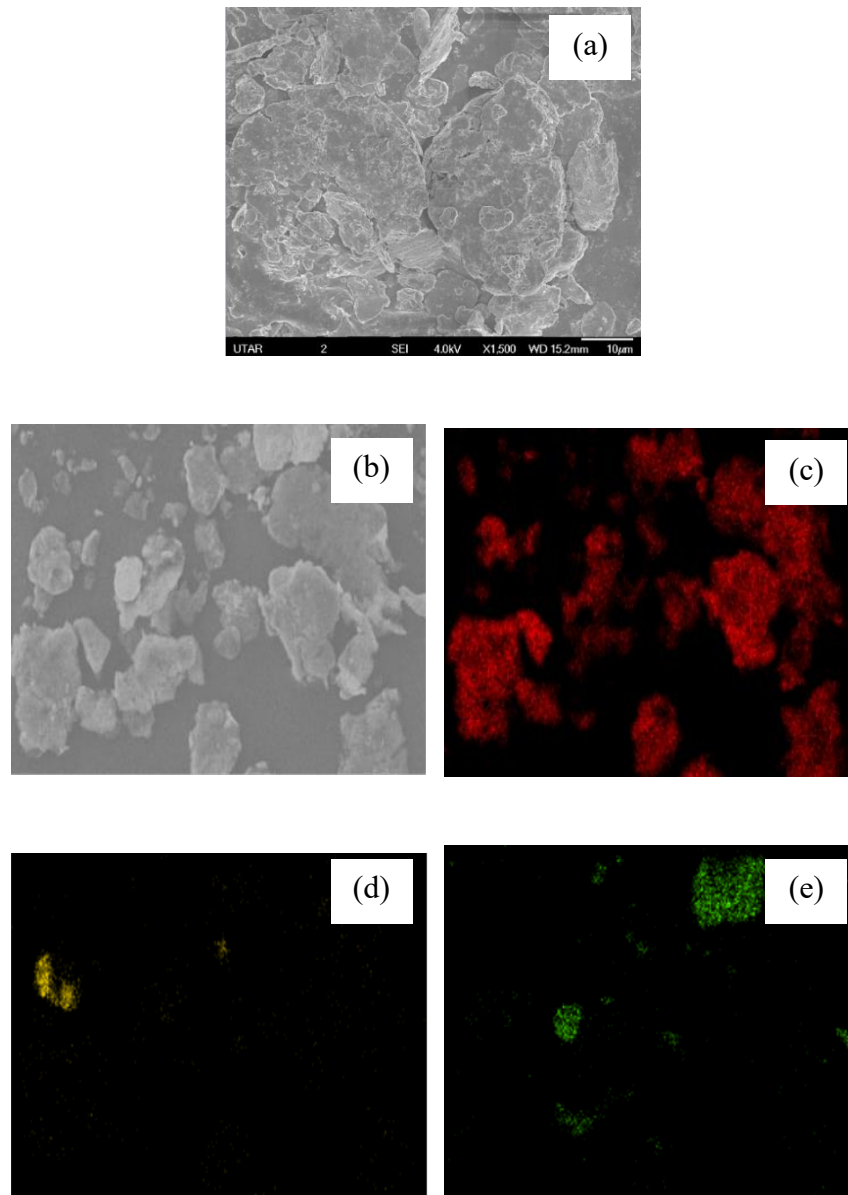


Figure 4.14: FESEM micrographs of AWCP (3% Sn-3% Mg) ternary composite at  $\times 1500$  magnification (a) and  $\times 500$  magnification (b); with EDS mappings of AWCP (c), Mg (d) and Sn (e).

### 4.9.3 BET Surface Area

Table 4.8 shows the BET surface area value of AWCP ternary composites. AWCP (3% Sn-3% Mg) had the highest BET surface area (19.43 m<sup>2</sup>/g). The random collision and aggregation during ball milling produced the random BET surface area.

Table 4.8: BET surface area of ternary AWCP composites.

Al samples	BET surface area (m <sup>2</sup> /g)
AWCP (3%Sn – 3%Mg)	19.43
AWCP (3%Sn – 3%In)	18.96

### 4.10 Gibbs Free Energy

The hydrolysis mechanism of the novel synthesized disintegrated Al waste can powder, optimized binary and ternary Al composites was studied in this section. Gibbs free energy (GFE) is defined as the thermodynamic potential energy which can be used to determine the maximum work of a thermodynamic system. The GFE was calculated based on the following equations (Eq. 4.1 and Eq. 4.2):



$$\Delta G = \Delta H - T\Delta S \quad (4.2)$$

The initial and final temperature of the hydrolysis of each sample were recorded in the experiment as the temperature data using a Hanna Instruments Checktemp digital bimetal thermometer in degree Celsius. The calculated data of Gibbs energy calculation are shown in Table 4.9. The standard-state enthalpy of formation and absolute entropy data for the reactants and products involved in aluminum-water reaction are shown in Table 4.10. The calculation of Gibbs free energy for the reaction using the Al samples aforementioned was based on the assumption of 100 % Al content. The Gibbs free energy calculated for all samples were  $\Delta G^0 < 0$ , which indicates the reactions were spontaneous and favourable in increasing temperatures.

Table 4.9: Hydrolysis results, final temperature and respective Gibbs free energy of AWCP samples.

Al samples (0.5g)	Total reaction time based on 0.5g (sec)	Hydrogen production (ml/0.5g)	Initial temperature (°C)	Final temperature (°C)	Gibbs free energy, $\Delta G$ (kJ/mol)
AWCP (100%)	1710	670	25.0	62.4	-889.06
AWCP (3%Sn)	240	680	25.0	68.5	-889.59
AWCP (3%Sn – 3%Mg)	660	660	25.0	65.9	-889.36

Table 4.10: Standard-state enthalpy of formation and absolute entropy data.

Material	$\Delta H$ (kJ/mol)	$\Delta S$ (J/mol.K)
Al	0	28.3
H <sub>2</sub> O	-285.8	69.9
H <sub>2</sub>	0	130.6
Al(OH) <sub>3</sub>	-1287.4	85.4

In ascending order of Gibbs free energy values, disintegrated ACWP (-889.06 kJ/mol), AWCP (3% Sn- 3% Mg) (-889.36 kJ/mol) and AWCP (3% Sn) (-889.59 kJ/mol). AWCP (3% Sn) had the most spontaneous reaction with the highest GFE among the samples, supported by the total reaction time (sec) data, 4min, the shortest reaction time to produce 1360 ml/g of H<sub>2</sub>. Although the ternary AWCP (3% Sn- 3% Mg) composite generated the highest total volume of H<sub>2</sub>, 1320 ml/g, the reaction consumed 660 sec.

#### **4.11 Batch Carbon Dioxide Methanation**

AWCP (100%), AWCP (97%), AWCP (94%), binary AWCP (3%Sn) composite and ternary AWCP (3%Sn-3%Mg) composite were selected to study batch methanation according to fixed hydrolysis conditions (200 ml of 1 M NaOH solution prepared by deionized water with 1 g Al sample fed at RTP).

Undoped AWCP had longer total reaction time AWCP (100%) compared to AWCP (97%) and AWCP (94%). The addition of 3% and 6% of activation metals (Zn, Mg Sn, or In) in binary and ternary composites, respectively, shortened the total reaction time compared to AWCP that was undoped. As discussed, the activation metals increased H<sub>2</sub> yield and shortened the total induction time. The hydrolysis process by undoped AWCP lasted for less than 30 min on overall.

Figure 4.15 shows the total H<sub>2</sub> and CH<sub>4</sub> production profile for batch CO<sub>2</sub> methanation for selected AWCP samples. In the first 5 min, binary composites generated the highest amount of H<sub>2</sub>, followed by ternary and others. The ternary

and binary composites generated the highest volume of CH<sub>4</sub> compared to the other samples in the first 5 min. But, after 10 minutes, AWCP (3% Sn) stopped producing CH<sub>4</sub>.

The undoped AWCP samples (AWCP (100%), AWCP (97%), and AWCP (94%)) continuously produced H<sub>2</sub> for approximately 28.5 min, these samples were continuously supplied H<sub>2</sub> for methanation to occur, leading to additional CH<sub>4</sub> production. Therefore, the undoped AWCP had more total CH<sub>4</sub> volume than the binary and ternary composites. For AWCP (100%), H<sub>2</sub> conversion ranged from 83% - 90%; it increased as H<sub>2</sub> production became less rapid as time went on because of lower GHSV resulted in higher conversion. While CO<sub>2</sub> conversion reduced from 51.3% to 0.5% from 5<sup>th</sup> – 30<sup>th</sup> min because more CO<sub>2</sub> were unreacted as less H<sub>2</sub> was produced as time went on. On the other hand, CH<sub>4</sub> selectivity increased when GHSV is low. Lastly, CH<sub>4</sub> yield reduced as less H<sub>2</sub> was produced after the rapid H<sub>2</sub> evolution. Based on Table 4.11, the trend was found similar in the undoped AWCP composites such as AWCP (97%) and AWCP (94%).

For AWCP (3% Sn), the H<sub>2</sub> production stopped at 5<sup>th</sup> min. Both H<sub>2</sub> and CO<sub>2</sub> conversion were 54.5%, CH<sub>4</sub> selectivity of 53% and lastly CH<sub>4</sub> yield of 28.9% which was higher than that of undoped AWCP composite in terms of CH<sub>4</sub> selectivity and yield. For AWCP (3% Sn – 3% Mg), the H<sub>2</sub> production stopped after 10<sup>th</sup> min. The H<sub>2</sub> conversion reduced from 82.9% to 75.3%. The CO<sub>2</sub> conversion reduced drastically from 76.6% to 5.7% because H<sub>2</sub> production was almost stopped after 5<sup>th</sup> min, but minimal H<sub>2</sub> production henceforth. However, the CH<sub>4</sub> yield was 30%, slightly higher than that of binary composite due to

lower GHSV. For binary and ternary composites, most of the H<sub>2</sub> gas produced did not react. The unreacted reactant gases passed through the methanation reactor. Sufficient time was not provided for the reactant gases (CO<sub>2</sub> + H<sub>2</sub>) to react with the catalyst to form CH<sub>4</sub>. Therefore, gas hourly space velocity (GHSV) crucially determined the total CH<sub>4</sub> production in methanation based on the flowrate of H<sub>2</sub> produced from each AWCP sample. AWCP (3%Sn -3%Mg) produced slightly higher CH<sub>4</sub> production than AWCP (3% Sn), due to additional 5 min production of H<sub>2</sub>. The undoped AWCP with lower GHSV generated much higher amount of total CH<sub>4</sub> because they had longer feed gas time even though the total amount of H<sub>2</sub> produced was lower compared to the composites. Most of the H<sub>2</sub> was not wasted and reacted efficiently to form CH<sub>4</sub>. Therefore, gas hourly space velocity (GHSV) crucially determined the total CH<sub>4</sub> production in methanation based on the flowrate of H<sub>2</sub> produced from each AWCP sample. The GHSV values for H<sub>2</sub> produced from AWCP (100%), binary AWCP (3% Sn) and ternary AWCP (3% Sn-3% Mg) are 19,951, 144,272 and 50,919 hr<sup>-1</sup>.

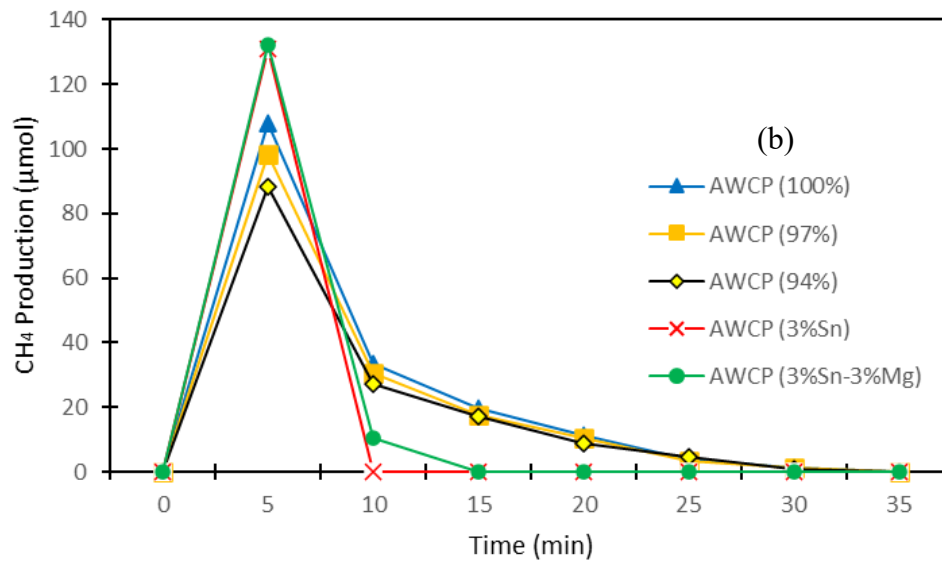
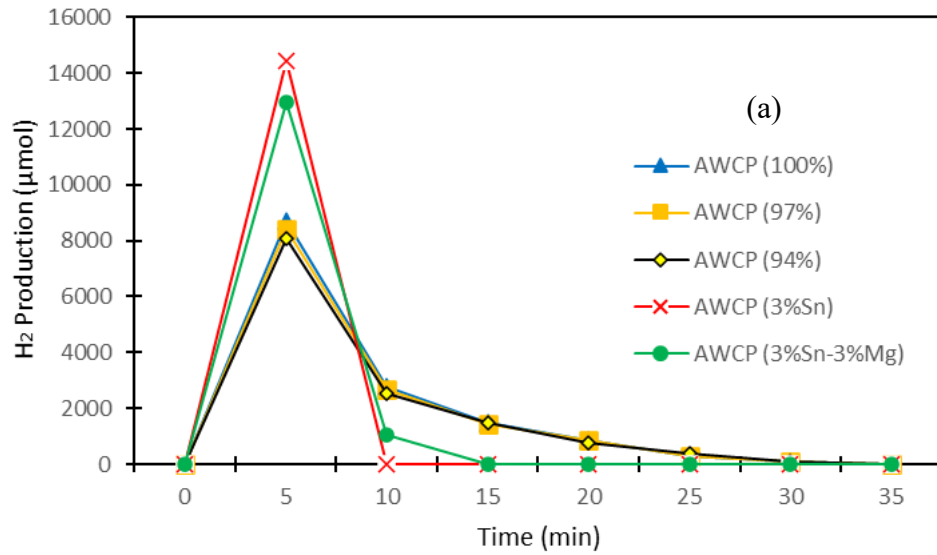


Figure 4.15: Total H<sub>2</sub> and CH<sub>4</sub> production profile for batch CO<sub>2</sub> methanation for selected AWCP samples.

Table 4.11: CH<sub>4</sub> total production and catalytic activity for batch methanation based on 0.5g sample without refeed.

Time (min)	Undoped AWCP												Binary AWCP				Ternary AWCP			
	100 wt%				97 wt%				94 wt%				(3% Sn)				(3% Sn – 3% Mg)			
	X <sub>H2</sub>	X <sub>CO2</sub>	S <sub>CH4</sub>	Y <sub>CH4</sub>	X <sub>H2</sub>	X <sub>CO2</sub>	S <sub>CH4</sub>	Y <sub>CH4</sub>	X <sub>H2</sub>	X <sub>CO2</sub>	S <sub>CH4</sub>	Y <sub>CH4</sub>	X <sub>H2</sub>	X <sub>CO2</sub>	S <sub>CH4</sub>	Y <sub>CH4</sub>	X <sub>H2</sub>	X <sub>CO2</sub>	S <sub>CH4</sub>	Y <sub>CH4</sub>
5	83.5	51.3	47.2	24.2	80.9	49.7	45.8	22.8	78.4	47.6	44.4	21.1	54.5	54.5	53.0	28.9	82.9	76.6	39.2	30.0
10	83.2	16.2	46.4	7.5	80.2	15.6	45.0	7.0	78.2	14.9	43.6	6.5	0	0	0	0	75.3	5.7	41.1	2.3
15	85.5	8.9	48.8	4.4	82.9	8.6	47.4	4.1	80.3	8.9	45.9	4.1	0	0	0	0	0	0	0	0
20	86.2	5.2	48.4	2.5	83.6	5.2	46.9	2.4	81.1	4.5	45.5	2.1	0	0	0	0	0	0	0	0
25	89.1	1.7	48.4	0.8	86.5	1.7	46.9	0.8	83.8	2.4	45.5	1.1	0	0	0	0	0	0	0	0
30	90.2	0.5	48.4	0.3	87.5	0.5	46.9	0.2	84.8	0.5	45.5	0.2	0	0	0	0	0	0	0	0
35	0	0	0	0	0	0	0	0	0	0	0	0	0	0	0	0	0	0	0	0
Total CH <sub>4</sub> produced (μmol)	176.9				161.2				147.0				130.9				142.6			
Total H <sub>2</sub> produced (μmol)	14,166.7				13,740.1				13,313.0				14,443.0				14,018.4			

The total amount of H<sub>2</sub> produced did not dictate the amount of CH<sub>4</sub> produced in methanation. Low GHSV is very important for CO<sub>2</sub> methanation reaction as it increased the contact time between the feed and the catalyst. Low GHSV also enhanced the conversion of CO<sub>2</sub> and CH<sub>4</sub> yield (Fan and Tahir, 2021). Albeit AWCP (3%Sn) produced the highest amount of H<sub>2</sub> among all samples, it has the highest GHSV which deters the methanation process and wasted the H<sub>2</sub> generated because a large amount of H<sub>2</sub> did not react with CO<sub>2</sub>. In conclusion, the CH<sub>4</sub> production of the selected samples followed this descending trend, AWCP (100%) (176.9 μmol) > AWCP (97%) (161.2 μmol) > AWCP (94%) (147 μmol) > AWCP (3%Sn -3%Mg) (130.9μmol) > AWCP (3%Sn) (142.6 μmol). Chang et al. (2003) reported 35% CO<sub>2</sub> conversion and 30% CH<sub>4</sub> selectivity based on Ni-based catalysts. The reported CH<sub>4</sub> selectivity of 50% was similar to what Younas et al. (2016) reported in his work based on the same Ni-based catalyst. However, Younas et al. (2016) used commercial H<sub>2</sub> to do the methanation process.

#### **4.12 Continuous Carbon Dioxide Methanation**

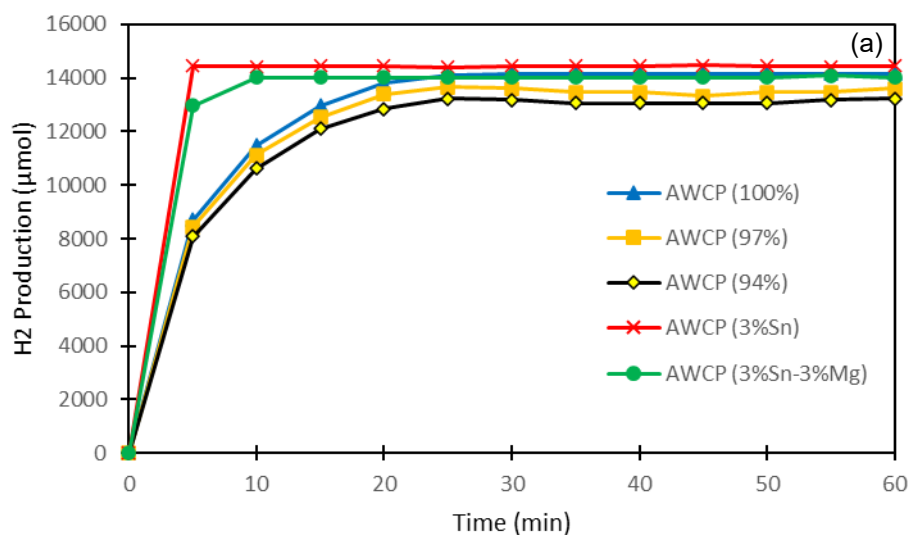
The methanation reaction would be operated in a continuous manner for a duration of 1 hr with a continuous re-feed of AWCP every 5 min.

##### **4.12.1 Continuous Carbon Dioxide Methanation via 5 min Refeed**

In continuous study, the selected AWCP samples were introduced within 1 hr of reaction. The activity study was assumed complete upon completion of the

hydrolysis and methanation processes which is 1 hour. Figure 4.22 (a) and (b) shows the continuous hydrolysis of H<sub>2</sub> and production of CH<sub>4</sub> for 1 hr respectively. Based on Fig. 4.16 (b), in the first 5 min, it is noticed that the trend of total amount of CH<sub>4</sub> produced by each sample was alike the one reported in the batch methanation because the first 5 min was by batch process before 0.5 g of AWCP sample was re-fed into the system. However, the order of total amount of CH<sub>4</sub> produced has changed. Whereby, AWCP (3%Sn) (1963.7 μmol) > AWCP (100%) (1926.7 μmol) > AWCP (3%Sn-3%Mg) (1821.9 μmol) > AWCP (97%) (1689.1 μmol) > AWCP (94%) (1481.4 μmol). For AWCP (100%), the H<sub>2</sub> conversion trend was similar in batch methanation. However, for CO<sub>2</sub> conversion, it increased from 51.3% to 86.6% as H<sub>2</sub> was supplied continuously resulted in H<sub>2</sub> reacted with CO<sub>2</sub> continuously to form CH<sub>4</sub> in reactor. The CH<sub>4</sub> selectivity was remained at 40-50% and CH<sub>4</sub> yield increased to 39.8% as time went on as H<sub>2</sub> was supplied in continuous manner. The trend remained similar for the undoped AWCP composites such as AWCP (97%) and AWCP (94%). For binary AWCP (3% Sn) composite, the H<sub>2</sub> and CO<sub>2</sub> conversion increased from 55% to 76%, CH<sub>4</sub> selectivity ranged between 48 – 58% and yield between 29.7% to 35.9%. For ternary AWCP (3% Sn – 3% Mg) composite, the H<sub>2</sub> and CO<sub>2</sub> conversion ranged approximately 70% to 80%, CH<sub>4</sub> selectivity from 40% to 50% and yield between 30% to 40%. In batch methanation process, the long residence time made methanation process favorable due to longer residence time for feed gas to form CH<sub>4</sub>. However, in continuous methanation process, the AWCP samples were re-fed into the system for every 5 min continuously for a duration of 1 hr. It is theoretically correct that the longer the residence time the feed gas had, the more time for feed gas to

form CH<sub>4</sub>. However, in continuous methanation, H<sub>2</sub> was continuously fed into the system every 5min, there is more H<sub>2</sub> being introduced for produce more CH<sub>4</sub>. Some of the H<sub>2</sub> could have pass the methanation reactor without reaction with catalyst and CO<sub>2</sub>. However, not 100% of the unreacted H<sub>2</sub> was removed from the reactor even though the outlet gas was channeled into gas sampling bag for GC analysis for every 5 min. The AWCP binary and ternary composites with higher H<sub>2</sub> production had more unreacted H<sub>2</sub> being left to further react continuously in the reactor, contributing to more formation of CH<sub>4</sub> although with shorter residence time compared to AWCP (97%) and ACWP (94%). ACWP (3% Sn) produced the highest CH<sub>4</sub> among all the candidates which was 1963.7 μmol. Therefore, for continuous methanation study further studies is needed especially on the gas hourly space velocity (GHSV) and different re-feed time of Al. This can be explored as the future of this study.



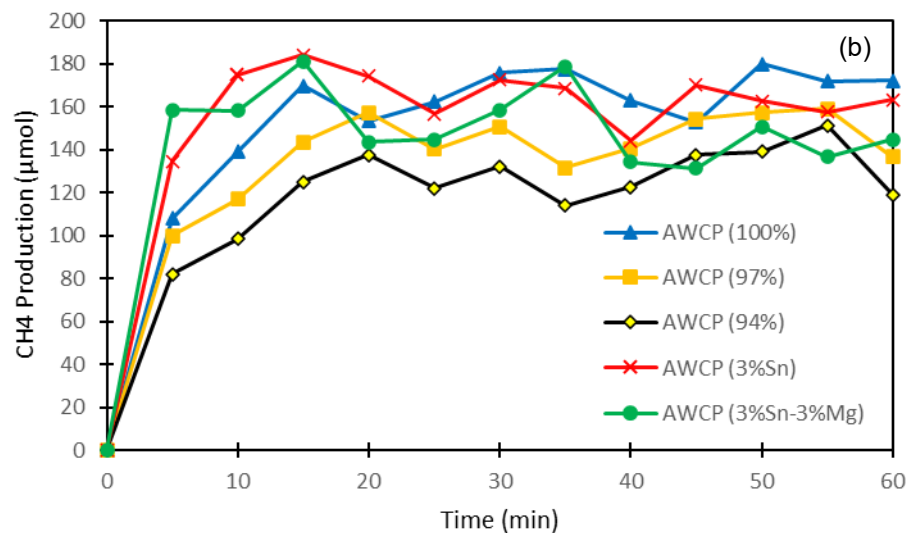


Figure 4.16: (a) H<sub>2</sub> production and (b) CH<sub>4</sub> production (µmol) from continuous CO<sub>2</sub> methanation based on every 5-min re-feed for 1 hr using AWCP (100%), AWCP (97%), AWCP (94%), AWCP (3% Sn) binary composite, and AWCP (3% Sn - 3% Mg) ternary composite.

Table 4.12: CH<sub>4</sub> total production and catalytic activity for continuous methanation based on 0.5g sample with refeed every 5 min for 1 hr.

Time (min)	Undoped AWCP												Binary AWCP				Ternary AWCP			
	100 wt%				97 wt%				94 wt%				(3% Sn)				(3% Sn – 3% Mg)			
	X <sub>H2</sub>	X <sub>CO2</sub>	S <sub>CH4</sub>	Y <sub>CH4</sub>	X <sub>H2</sub>	X <sub>CO2</sub>	S <sub>CH4</sub>	Y <sub>CH4</sub>	X <sub>H2</sub>	X <sub>CO2</sub>	S <sub>CH4</sub>	Y <sub>CH4</sub>	X <sub>H2</sub>	X <sub>CO2</sub>	S <sub>CH4</sub>	Y <sub>CH4</sub>	X <sub>H2</sub>	X <sub>CO2</sub>	S <sub>CH4</sub>	Y <sub>CH4</sub>
5	83.5	51.3	47.2	24.2	87.7	53.8	43.0	23.1	75.2	45.6	43.0	21.1	55.0	55.0	54.0	29.7	78.3	72.4	49.7	35.9
10	83.2	67.4	46.4	31.2	78.2	63.2	42.9	27.1	68.7	54.8	42.9	19.6	75.3	75.2	51.1	38.4	81.6	81.6	44.0	35.9
15	85.4	78.1	48.8	38.1	85.6	78.1	42.6	33.2	77.1	70.1	42.6	23.5	69.0	68.9	58.8	40.5	80.2	80.2	51.3	41.1
20	86.0	83.8	41.1	34.4	88.2	85.9	42.4	36.4	80.2	77.4	42.4	29.9	75.2	75.1	51.1	38.4	73.4	73.4	44.4	32.6
25	75.9	75.5	48.4	36.5	77.3	76.9	42.2	32.4	69.5	69.1	42.2	32.8	73.6	73.4	47.1	34.5	76.2	76.2	43.1	32.8
30	83.6	83.6	47.2	39.5	83.0	82.2	42.4	34.8	75.2	74.5	42.4	29.1	74.3	74.3	51.1	38.0	77.9	77.9	46.2	36.0
35	86.0	86.0	46.4	39.8	73.6	72.2	42.2	30.5	65.8	64.5	42.2	31.6	73.1	73.1	50.8	37.1	82.3	82.3	49.3	40.5
40	75.0	75.0	48.8	36.6	76.3	74.7	43.5	32.5	68.7	67.3	43.5	27.2	65.0	65.0	48.8	31.7	75.8	75.8	40.3	30.5
45	83.5	83.5	41.1	34.3	84.7	82.2	43.5	35.7	77.1	75.6	43.5	32.9	73.2	73.3	51.1	37.5	74.3	74.3	40.1	29.7
50	85.6	85.6	47.2	40.4	88.0	86.3	42.2	36.4	80.2	78.6	42.2	33.2	64.4	64.5	55.5	35.8	75.8	75.8	45.1	34.2
55	83.4	83.4	46.3	38.6	86.5	84.7	43.5	36.8	78.9	78.1	46.3	36.1	68.0	67.9	51.1	34.7	73.6	73.9	42.0	31.0
60	85.6	86.6	45.2	38.6	73.4	72.7	43.5	31.6	65.8	65.4	43.5	28.4	76.2	76.2	47.2	35.9	71.8	71.8	45.8	32.9
Total CH <sub>4</sub> produced (μmol)	176.9				161.2				147.0				130.9				142.6			
Total H <sub>2</sub> produced (μmol)	14,166.7				13,740.1				13,313.0				14,443.0				14,018.4			

## CHAPTER 5

### CONCLUSION

#### 5.1 Conclusion

The use of AWCP to produce green H<sub>2</sub> in hydrolysis reaction proved feasible for CO<sub>2</sub> methanation to generate value-added CH<sub>4</sub> in both batch and continuous fashion. EDXRF analysis showed that the AWCP comprised of 96.2 wt % of Al and other trace amounts of Mn, Mg, Fe, Cu and others. FESEM showed that the AWCP (3% Sn) surface was flake-like and irregular due to the disintegration method used to prepare the AWCP which was random and high-speed. FESEM showed that for AWCP (3% Sn – 3% Mg), the activation metals Sn/Mg were equally distributed on the disintegrated AWCP surface. AWCP, Sn and Mg were cold-welded to one another as ball-to-ball and ball-to-jar collisions occurred in ball milling process which gave homogenous distribution of activation metals and formation of smaller particles.

The disintegration method using medicine blender was a novel approach successfully synthesized the raw, binary, and ternary composites of

AWCP. Disintegration method increased the BET surface area of AWCP samples and higher H<sub>2</sub> yield compared to commercial Al. The hydrolysis reaction was optimized by studying various factors that affect the hydrolysis results. For disintegration time, the longer the Al samples were exposed to disintegration, the smaller the particle size of Al sample produced, 20 min disintegration time had the smallest particle size of 0.01 to 1 μm, beyond 20 min was neglected due to device limitation. For alkaline solution, NaOH had the best hydrolysis performance compared to Ba(OH)<sub>2</sub> and KOH due to the availability of hydroxide ions. For type of water source, deionized water was selected among other water sources such as distilled water, ultrapure water and tap water. The hydrolysis process is a success for AWCP samples using 1 g of Al sample in 200ml of 1M NaOH solution prepared by deionized water at room temperature conditions which H<sub>2</sub> production was measured by water displacement method.

The AWCP composites which were synthesized by ball milling method were capable to complete the hydrolysis reaction within 4 to 9 min which is comparably much shorter compared to other literature. The highest yield of H<sub>2</sub> (680 ml) was achieved by AWCP (3 % Sn) binary composite within 240 s with 97 wt% of AWCP content.

Nevertheless, if compared to the wt% of AWCP, the highest yield of H<sub>2</sub> (660 ml) was achieved by the ternary composite AWCP (3 % Sn - 3 % Mg) ternary composite within 660 s with only 94 wt % of AWCP content

in the mixture. The ternary AWCP composites were successfully synthesized with other pure metals via ball milling method at high rotational speed which characterization results showed homogenous distribution across the Al surface. Ternary AWCP (3% Sn – 3% Mg) ternary composite generated the highest amount of H<sub>2</sub>.

Batch and continuous methanation was a success using the H<sub>2</sub> produced from AWCP-water reaction. The highest amount of CH<sub>4</sub> produced for batch and continuous was 176.9 μmol and 1963.7 μmol respectively using AWCP (100%) and AWCP (3% Sn) respectively. AWCP (3% Sn) had the highest CH<sub>4</sub> production in continuous methanation because it had higher H<sub>2</sub> production and had more unreacted H<sub>2</sub> being left to further react continuously in the reactor, contributing to more formation of CH<sub>4</sub>. In continuous methanation, due to the rapid rate of H<sub>2</sub> production, more than 50% of the produced H<sub>2</sub> did not react in the methanation process due to lack of contact time between the reactant gases and catalyst. Low GHSV of the H<sub>2</sub> produced from AWCP was the most significant factor to have high yield of CH<sub>4</sub>. This study has given an insight on the feasibility of producing H<sub>2</sub> from pure AWCP and its composites.

## 5.2 Recommendation for Future Work

The following are recommendations for this research work to be applied in future;

- Investigate other activation method using mechano-activation method such as photocatalyst to split water for H<sub>2</sub> production.
- Utilize H<sub>2</sub> sensor which can provide more accurate H<sub>2</sub> production volume instead of water displacement method.
- Optimize the CO<sub>2</sub> methanation parameters such as pressure, temperature, catalyst and others to improve the CH<sub>4</sub> selectivity resulting in higher CH<sub>4</sub> production rate using Al produced H<sub>2</sub>.
- Different types of methanation catalyst and dosage of catalyst should be tested to optimize the methanation process.
- For continuous methanation study further studies is needed especially on the gas hourly space velocity (GHSV) and different re-feed time of Al.

## REFERENCES

- Abe, J.O., Popoola, A.P.I., Ajenifuja, E. and Popoola, O.M. (2019). Hydrogen energy, economy and storage: review and recommendation. *International Journal of Hydrogen Energy*, 44(29), pp.15072-15086.
- Acar, C. and Dincer, I. (2019) 'Review and evaluation of hydrogen production options for better environment', *Journal of Cleaner Production*. Elsevier, 218, pp. 835–849. doi: 10.1016/j.jclepro.2019.02.046.
- Acar, C., Dincer, I. and Naterer, G. F. (2016) 'Review of photocatalytic water-splitting methods for sustainable hydrogen production', *International Journal of Energy Research*. Wiley Online Library, 40(11), pp. 1449–1473.
- Acar, C. and Dincer, I. (2015). Comparative assessment of hydrogen production methods from renewable and non-renewable sources. *International Journal of Hydrogen Energy*, 39(1), pp.1-12.
- Adans, Y.F., Martins, A.R., Coelho, R.E., Virgens, C.F.D., Ballarini, A.D. and Carvalho, L.S. (2016). A simple way to produce  $\gamma$ -alumina from aluminum cans by precipitation reactions. *Materials Research*, 19(5), pp.977-982.
- Akbari, A. and Omidkhah, M. (2019). Silica-zirconia membrane supported on modified alumina for hydrogen production in steam methane reforming unit. *International Journal of Hydrogen Energy*, 44(31), pp.16698-16706.
- Al-Ogaili, A.S., Al-Shetwi, A.Q., Sudhakar Babu, T., Hoon, Y., Abdullah, M.A., Alhasan, A. and Al-Sharaa, A. (2021). Electric buses in malaysia: Policies, innovations, technologies and life cycle evaluations. *Sustainability*, 13(21), p.11577.
- Aleksandrov, Y.A., Tsyganova, E.I. and Pisarev, A.L. (2003). Reaction of Aluminum with Dilute Aqueous NaOH Solutions. *Russian Journal of General Chemistry*, 73(5).

- Alinejad, B. and Mahmoodi, K. (2009). A novel method for generating hydrogen by hydrolysis of highly activated aluminum nanoparticles in pure water. *International Journal of Hydrogen Energy*, 34(19), pp.7934-7938.
- Arandiyan, H., Kani, K., Wang, Y., Jiang, B., Kim, J., Yoshino, M., Rezaei, M., Rowan, A.E., Dai, H. and Yamauchi, Y. (2019). Correction to “Highly Selective Reduction of Carbon Dioxide to Methane on Novel Mesoporous Rh Catalysts”. *ACS Applied Materials & Interfaces*, 11(49), pp.46398-46398.
- Belitskus, D. (1970). Reaction of aluminum with sodium hydroxide solution as a source of hydrogen. *Journal of the Electrochemical Society*, 117(8), pp.1097-1099.
- Ben, H. (2019). ‘Silver Science’ Turns Aluminium Scrap Into Clean Energy Source In Farm-Shed Reactor. [online] Eandt.theiet.org. Available at: <<https://eandt.theiet.org/content/articles/2019/08/silver-science-creates-diy-zero-carbon-aluminium-hydroxide-reactor-in-a-farm-shed/>> [Accessed 30 Jan 2022].
- Bhandari, R., Trudewind, C.A. and Zapp, P. (2014). Life cycle assessment of hydrogen production via electrolysis—a review. *Journal of cleaner production*, 85, pp.151-163.
- Chai, S., Men, Y., Wang, J., Liu, S., Song, Q., An, W. and Kolb, G. (2019). Boosting CO<sub>2</sub> methanation activity on Ru/TiO<sub>2</sub> catalysts by exposing (001) facets of anatase TiO<sub>2</sub>. *Journal of CO<sub>2</sub> Utilization*, 33, pp.242-252.
- Chang, F.W., Kuo, M.S., Tsay, M.T. and Hsieh, M.C. (2003). Hydrogenation of CO<sub>2</sub> over nickel catalysts on rice husk ash-alumina prepared by incipient wetness impregnation. *Applied Catalysis A: General*, 247, pp. 309–320.
- Cheng, C., Shen, D., Xiao, R. and Wu, C. (2017). Methanation of syngas (H<sub>2</sub>/CO) over the different Ni-based catalysts. *Fuel*, 189, pp.419-427.
- Coats, A. and Jones, E. (1982). The European Miracle: Environments, Economies, and Geopolitics in the History of Europe and Asia. *The Economic History Review*, 35(2), p.329.

- da Silva Veras, T., Mozer, T., da Costa Rubim Messeder dos Santos, D. and da Silva César, A. (2017). Hydrogen: Trends, production and characterization of the main process worldwide. *International Journal of Hydrogen Energy*, 42(4), pp.2018-2033.
- Deng, Z.Y., Ferreira, J.M., Tanaka, Y. and Ye, J. (2007). Physicochemical mechanism for the continuous reaction of  $\gamma$ -Al<sub>2</sub>O<sub>3</sub>-modified aluminum powder with water. *Journal of the American Ceramic Society*, 90(5), pp.1521-1526.
- Deng, Z.Y., Liu, Y.F., Tanaka, Y., Ye, J. and Sakka, Y. (2005). Modification of Al particle surfaces by  $\gamma$ -Al<sub>2</sub>O<sub>3</sub> and its effect on the corrosion behavior of Al. *Journal of the American Ceramic Society*, 88(4), pp.977-979.
- Drage, T.C., Smith, K.M., Pevida, C., Arenillas, A. and Snape, C.E. (2009). Development of adsorbent technologies for post-combustion CO<sub>2</sub> capture. *Energy Procedia*, 1(1), pp.881-884.
- du Preez, S. and Bessarabov, D. (2018). Hydrogen generation by the hydrolysis of mechanochemically activated aluminum-tin-indium composites in pure water. *International Journal of Hydrogen Energy*, 43(46), pp.21398-21413.
- Escobar-Alarcón, L., Iturbe-García, J.L., González-Zavala, F., Solís-Casados, D.A., Pérez-Hernández, R. and Haro-Poniatowski, E. (2019). Hydrogen production by ultrasound assisted liquid laser ablation of Al, Mg and Al-Mg alloys in water. *Applied Surface Science*, 478, pp.189-196.
- El-Emam, R.S. and Özcan, H. (2019). Comprehensive review on the techno-economics of sustainable large-scale clean hydrogen production. *Journal of Cleaner Production*, 220, pp.593-609.
- Elsarrag, E., Elhoweris, A. and Alhorr, Y. (2017). The production of hydrogen as an alternative energy carrier from aluminium waste. *Energy, Sustainability and Society*, 7(1), p.9.
- Fan, M.Q., Xu, F., Sun, L.X., Zhao, J.N., Jiang, T. and Li, W.X. (2008). Hydrolysis of ball milling Al-Bi-hydride and Al-Bi-salt mixture for hydrogen generation. *Journal of Alloys and Compounds*, 460(1-2), pp.125-129.

- Fan, M., Xu, F. and Sun, L. (2007). Studies on hydrogen generation characteristics of hydrolysis of the ball milling Al-based materials in pure water. *International Journal of Hydrogen Energy*, 32(14), pp.2809-2815.
- Gonzaga, I.M.D., Andrade, A.C.A., Silva, R.S., Salazar-Banda, G.R., Cavalcanti, E.B. and Eguiluz, K.I.B. (2019). Synthesis of high-area chemically modified electrodes using microwave heating. *Chemical Engineering Communications*, 206(5), pp.647-653
- Haryanto, A., Fernando, S., Murali, N. and Adhikari, S. (2005). Current Status of Hydrogen Production Techniques by Steam Reforming of Ethanol: A Review. *Energy & Fuels*, 19(5), pp.2098-2106.
- The World Bank. (2019). CO<sub>2</sub> emissions (kt) | Data. [online] Available at: [https://data.worldbank.org/indicator/EN.ATM.CO2E.KT?end=2014&name\\_desc=false&start=1960&view=chart](https://data.worldbank.org/indicator/EN.ATM.CO2E.KT?end=2014&name_desc=false&start=1960&view=chart) [Accessed 26 Jan 2022].
- The World Bank. (2019). Total greenhouse gas emissions (kt of CO<sub>2</sub> equivalent) / Data. [online] Available at: <https://data.worldbank.org/indicator/EN.ATM.GHGT.KT.CE> [Accessed 30 Jan 2022].
- Ghani, W.W.A.K., Salleh, M.A.M., Adam, S.N., Shafri, H.M., Shaharum, S.N., Lim, K.L., Rubinsin, N.J., Lam, H.L., Hasan, A., Samsatli, S. and Tapia, J.F. (2019). Sustainable bio-economy that delivers the environment–food–energy–water nexus objectives: The current status in Malaysia. *Food and Bioproducts Processing*, 118, pp.167-186.
- Global Energy Statistical Yearbook 2019. (2019). Global Natural Gas Production | World gas natural statistics | Enerdata. [online] Available at: <https://yearbook.enerdata.net/natural-gas/world-natural-gas-production-statistics.html> [Accessed 1 Jan 2022].
- Global Energy Statistical Yearbook 2019. (2019). World Energy Primary Production | Energy Production | Enerdata. [online] Available at: <https://yearbook.enerdata.net/total-energy/world-energy-production.html> [Accessed 26 Jan 2022].
- Haraya, K., Obata, K., Hakuta, T. and Yoshitome, H. (1986). The permeation of gases through a new type polyimide membrane. *International Journal of Hydrogen Energy*, 11(1), pp.48-52.

- Ho, C.Y. and Huang, C.H. (2016). Enhancement of hydrogen generation using waste aluminum cans hydrolysis in low alkaline de-ionized water. *International Journal of Hydrogen Energy*, 41(6), pp.3741-3747.
- Huang, X., Gao, T., Pan, X., Wei, D., Lv, C., Qin, L. and Huang, Y. (2013). A review: Feasibility of hydrogen generation from the reaction between aluminum and water for fuel cell applications. *Journal of Power Sources*, 229, pp.133-140.
- Huanling, S., Jian, Y., Jun, Z. and Lingjun, C. (2010). Methanation of carbon dioxide over a highly dispersed Ni/La<sub>2</sub>O<sub>3</sub> catalyst. *Chinese Journal of Catalysis*, 31, pp. 21–23.
- Jacquemin, M., Beuls, A. and Ruiz, P. (2010). Catalytic production of methane from CO<sub>2</sub> and H<sub>2</sub> at low temperature: Insight on the reaction mechanism. *Catalysis Today*, 157(1-4), pp.462-466.
- Jia, X., Zhang, X., Rui, N., Hu, X. and Liu, C.J. (2019). Structural effect of Ni/ZrO<sub>2</sub> catalyst on CO<sub>2</sub> methanation with enhanced activity. *Applied Catalysis B: Environmental*, 244, pp.159-169.
- Jimenez, J.D., Wen, C. and Lauterbach, J. (2019). Design of highly active cobalt catalysts for CO<sub>2</sub> hydrogenation via the tailoring of surface orientation of nanostructures. *Catalysis Science & Technology*, 9(8), pp.1970-1978.
- Karagöz, S., Chen, H., Cao, M., Tsotsis, T.T. and Manousiouthakis, V.I. (2019). Multiscale model based design of an energy-intensified novel adsorptive reactor process for the water gas shift reaction. *AIChE Journal*.
- Kaya, M.F., Kahveci, O., Erol, H. and Akkaya, A. (2021). Effect of low B addition on Al-Zn alloy's hydrogen production performance. *International Journal of Hydrogen Energy*, 46(29), pp.15192-15202.
- Khaselev, O., Bansal, A. and Turner, J.A. (2001). High-efficiency integrated multijunction photovoltaic/electrolysis systems for hydrogen production. *International Journal of Hydrogen Energy*, 26(2), pp.127-132.
- Knoema. (2022). Malaysia CO<sub>2</sub> emissions per capita, 1970-2021 - knoema.com. [online] Available at: <<https://knoema.com/atlas/Malaysia/CO2-emissions-per-capita>> [Accessed 6 June 2022].

- Kothari, R., Buddhi, D. and Sawhney, R. (2008). Comparison of environmental and economic aspects of various hydrogen production methods. *Renewable and Sustainable Energy Reviews*, 12(2), pp.553-563.
- Kravchenko, O.V., Semenenko, K.N., Bulychev, B.M. and Kalmykov, K.B. (2005). Activation of aluminum metal and its reaction with water. *Journal Alloys Compound*, 397, pp.58–62.
- LeValley, T., Richard, A. and Fan, M. (2014). The progress in water gas shift and steam reforming hydrogen production technologies – A review. *International Journal of Hydrogen Energy*, 39(30), pp.16983-17000.
- Li, W., Liu, Y., Mu, M., Ding, F., Liu, Z., Guo, X. and Song, C. (2019). Organic acid-assisted preparation of highly dispersed Co/ZrO<sub>2</sub> catalysts with superior activity for CO<sub>2</sub> methanation. *Applied Catalysis B: Environmental*, 254, pp.531-540.
- Liang, J., Gao, L.J., Miao, N.N., Chai, Y.J., Wang, N. and Song, X.Q. (2016). Hydrogen generation by reaction of Al–M (M= Fe, Co, Ni) with water. *Energy*, 113, pp.282-287.
- Li, B., Duan, Y., Luebke, D. and Morreale, B. (2013). Advances in CO<sub>2</sub> capture technology: A patent review. *Applied Energy*, 102, pp.1439-1447.
- Li, Z., Guo, P., Han, R. and Sun, H. (2019). Current status and development trend of wind power generation-based hydrogen production technology. *Energy Exploration & Exploitation*, 37(1), pp.5-25.
- Lim, S.T., Sethupathi, S., Alsultan, A.G., Leong, L.K. and Taufiq-Yap, Y.H. (2020). Hydrogen Gas Production Using Aluminum Waste Cans Powder Produced by Disintegration Method. In *Key Engineering Materials* (Vol. 853, pp. 228-234). Trans Tech Publications Ltd.
- Liu, J. et al. (2013). Enhanced low-temperature activity of CO<sub>2</sub> methanation over highly-dispersed Ni/TiO<sub>2</sub> catalyst. *Catalysis Science & Technology*, 3, pp. 2627–2633.
- Liu, H., Yang, F., Yang, B., Zhang, Q., Chai, Y. and Wang, N. (2018). Rapid hydrogen generation through aluminum-water reaction in alkali solution. *Catalysis Today*, 318, pp.52-58.

- Lodhi, M. (2003). Helio-hydro and helio-thermal production of hydrogen. *International Journal of Hydrogen Energy*.
- Lu, Q., Hou, Y., Laraib, S.R., Khalifa, O., Li, K., Xie, W.L., Cui, M.S. and Yang, Y.P. (2019). Electro-catalytic steam reforming of methane over Ni-CeO<sub>2</sub>/γ-Al<sub>2</sub>O<sub>3</sub>-MgO catalyst. *Fuel Processing Technology*, 192, pp.57-64.
- Martínez, S.S., Sánchez, L.A., Gallegos, A.A.Á. and Sebastian, P.J. (2007). Coupling a PEM fuel cell and the hydrogen generation from aluminum waste cans. *International Journal of Hydrogen Energy*, 32(15), pp.3159-3162.
- MatWeb Material Property Data. (2019). MatWeb - The Online Materials Information Resource. [online] Available at: <http://www.matweb.com/search/DataSheet.aspx?MatGUID=aaaabe41a20a4ed2b48270f7f2ef1b2d&ckck=1> [Accessed 26 Jan 2022].
- Metz, B., Davidson, O., de Coninck, H. C., Loos, M., and Meyer, L.A. (2005). Carbon Dioxide Capture and Storage. Cambridge University Press: IPCC Special Report, pp.422.
- Miao, B., Ma, S.S.K., Wang, X., Su, H. and Chan, S.H. (2016). Catalysis mechanisms of CO<sub>2</sub> and CO methanation. *Catalysis Science & Technology*, 6(12), pp.4048-4058.
- Muellerlanger, F., Tzimas, E., Kaltschmitt, M. and Peteves, S. (2007). Techno-economic assessment of hydrogen production processes for the hydrogen economy for the short and medium term. *International Journal of Hydrogen Energy*, 32(16), pp.3797-3810.
- Muradov, N. and Vezirolu, T. (2005). From hydrocarbon to hydrogen-carbon to hydrogen economy. *International Journal of Hydrogen Energy*, 30(3), pp.225-237.
- Mutz, B., Carvalho, H.W.P., Mangold, S., Kleist, W. and Grunwaldt, J.D. (2015). Methanation of CO<sub>2</sub>: Structural response of a Ni-based catalyst under fluctuating reaction conditions unraveled by operando spectroscopy. *Journal of Catalysis*, 327, pp. 48–53.

- National Oceanic and Atmospheric Administration. (2019). ESRL Global Monitoring Division - Global Greenhouse Gas Reference Network. [online] Esrl.noaa.gov. Available at: [https://www.esrl.noaa.gov/gmd/ccgg/trends\\_ch4/#global](https://www.esrl.noaa.gov/gmd/ccgg/trends_ch4/#global) [Accessed 1 Jan 2022].
- Newsome, D.S. (1980). The Water-gas Shift Reaction. *Catalysis Reviews Science and Engineering*, 21(2), pp.275-318.
- Ogden, J.M. (1999). Prospects for building a hydrogen energy infrastructure. *Annual Review of Energy and the Environment*, 24, pp.227–79.
- Phung, K.K., Sethupathi, S. and Piao, C.S. (2018). Production of H<sub>2</sub> from aluminium/water reaction and its potential for CO<sub>2</sub> methanation. In *IOP Conference Series: Earth and Environmental Science* (Vol. 140, No. 1, p. 012020). IOP Publishing.
- Pilavachi, P., Chatzipanagi, A. and Spyropoulou, A. (2009). Evaluation of hydrogen production methods using the Analytic Hierarchy Process. *International Journal of Hydrogen Energy*, 34(13), pp.5294-5303.
- Porciúncula, C.B., Marcilio, N.R., Tessaro, I.C. and Gerchmann, M. (2012). Production of hydrogen in the reaction between aluminum and water in the presence of NaOH and KOH. *Brazilian Journal of Chemical Engineering*, 29(2), pp.337-348.
- Posso, F., Espinoza, J.L., Sánchez, J. and Zalamea, J. (2015). Hydrogen from hydropower in Ecuador: Use and impacts in the transport sector. *International Journal of Hydrogen Energy*, 40(45), pp.15432-15447.
- Rajaura, R. S. *et al.* (2016) ‘Role of interlayer spacing and functional group on the hydrogen storage properties of graphene oxide and reduced graphene oxide’, *International Journal of Hydrogen Energy*. Elsevier, 41(22), pp. 9454–9461.
- Razavi-Tousi, S.S. and Szpunar, J.A. (2014). Role of ball milling of aluminum powders in promotion of aluminum-water reaction to generate hydrogen. *Metallurgical and Materials Transactions E*, 1(3), pp.247-256.

- Rogelj, J., den Elzen, M., Höhne, N., Fransen, T., Fekete, H., Winkler, H., Schaeffer, R., Sha, F., Riahi, K. and Meinshausen, M. (2016). Paris Agreement climate proposals need a boost to keep warming well below 2 °C. *Nature*, 534(7609), pp.631-639.
- Sakintuna, B., Lamari-Darkrim, F. and Hirscher, M. (2007). Metal hydride materials for solid hydrogen storage: a review. *International Journal of Hydrogen Energy*, 32(9), pp.1121-1140.
- Sakpal, T.R. (2019). Structure-sensitivity in CO<sub>2</sub> methanation over CeO<sub>2</sub> supported metal catalysts. University of Twente.
- Schaaf, T., Grünig, J., Schuster, M.R., Rothenfluh, T. and Orth, A. (2014). Methanation of CO<sub>2</sub>-storage of renewable energy in a gas distribution system. *Energy, Sustainability and Society*, 4(1), p.2.
- Spath, P.L., Mann, M.K. (2001). Life cycle assessment of hydrogen production via natural gas steam reforming. *National Renewable Energy Laboratory*.
- Soler, L., Macanás, J., Munoz, M. and Casado, J. (2005). Hydrogen generation from aluminum in a non-consumable potassium hydroxide solution. In *Proceedings International Hydrogen Energy Congress and Exhibition IHEC* (pp. 13-15).
- Soler, L., Macanás, J., Munoz, M. and Casado, J. (2007). Aluminum and aluminum alloys as sources of hydrogen for fuel cell applications. *Journal of Power Sources*, 169(1), pp.144-149.
- Stockburger, D., Stannard, J.H., Rao, B.M.L., Kobasz, W. and Tuck, C.D. (1992). On-line hydrogen generation from aluminum in an alkaline solution. In *Proc Symp Hydrogen Storage Mater Batteries Electrochem* (Vol. 92, No. 5, pp. 431-44).
- TheStar. (2020). Chinese-made buses boost green public transport in Sarawak. [online] Available at: <2020. [online] Available at: <<https://www.thestar.com.my/news/regional/2020/01/21/chinese-made-buses-boost-green-public-transport-in-sarawak>> [Accessed 29 April 2020].> [Accessed 29 Jan 2022].
- Thomas, D.C. and Benson, S.M. eds. (2005). Carbon Dioxide Capture for Storage in Deep Geologic Formations-Results from the CO<sub>2</sub> Capture

Project: Vol 1-Capture and Separation of Carbon Dioxide from Combustion, Vol 2-Geologic Storage of Carbon Dioxide with Monitoring and Verification. Elsevier.

- Thommes, M., Kaneko, K., Neimark, A.V., Olivier, J.P., Rodriguez-Reinoso, F., Rouquerol, J. and Sing, K.S. (2015). Physisorption of gases, with special reference to the evaluation of surface area and pore size distribution (IUPAC Technical Report). *Pure and Applied Chemistry*, 87(9-10), pp.1051-1069.
- Tzimas, E., Filiou, C., Peteves, S.D. and Veyret, J.B. (2003). Hydrogen storage: state-of-the-art and future perspective. *EU Commission, JRC Petten, EUR 20995EN*, pp.1511-1519.
- United Nations Framework Convention On Climate Change. (2015). Paris Agreement, FCCC/CP/2015/L.9/Rev.1. Conference of the Parties, 21<sup>st</sup> session, 30 Nov – 11 Dec 2015, Paris.
- United Nations Framework Convention On Climate Change. (2019). The Paris Agreement / *UNFCCC*. [online] Available at: <https://unfccc.int/process-and-meetings/the-paris-agreement/the-paris-agreement> [Accessed 30 Jan 2022].
- United States Environmental Protection Agency (EPA). (2019). Sources of Greenhouse Gas Emissions | US EPA. [online] Available at: <https://www.epa.gov/ghgemissions/sources-greenhouse-gas-emissions> [Accessed 26 Jan 2022].
- Vega, F., Cano, M., Camino, S., Fernández, L.M.G., Portillo, E. and Navarrete, B. (2018). Solvents for Carbon Dioxide Capture. *Carbon Dioxide Chemistry, Capture and Oil Recovery*, p.141.
- Vrijburg, W.L., van Helden, J.W., Parastaev, A., Groeneveld, E., Pidko, E.A. and Hensen, E.J. (2019). Ceria–zirconia encapsulated Ni nanoparticles for CO<sub>2</sub> methanation. *Catalysis Science & Technology*, 9(18), pp.5001-5010.
- Wang, Q., Luo, C., Li, X., Ding, H., Shen, C., Cao, D. and Zhang, L. (2019). Development of LaFeO<sub>3</sub> modified with potassium as catalyst for coal char CO<sub>2</sub> gasification. *Journal of CO<sub>2</sub> Utilization*, 32, pp.163-169.

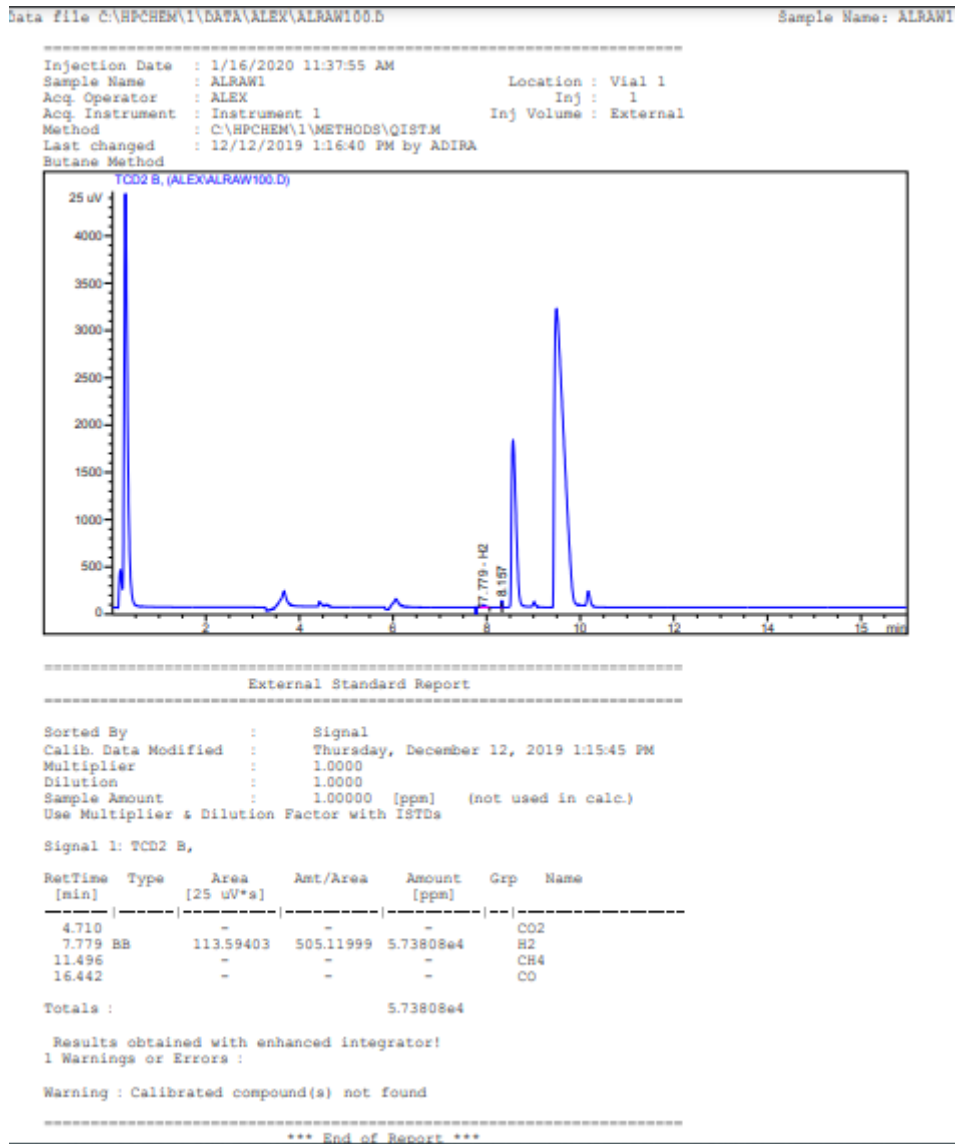
- Wang, H., Leung, D., Leung, M. and Ni, M. (2009). A review on hydrogen production using aluminum and aluminum alloys. *Renewable and Sustainable Energy Reviews*, 13(4), pp.845-853.
- Xiao, F., Guo, Y., Li, J. and Yang, R. (2018). Hydrogen generation from hydrolysis of activated aluminum composites in tap water. *Energy*, 157, pp.608-614.
- Yang, H., Zhang, H., Peng, R., Zhang, S., Huang, X. and Zhao, Z. (2019). Highly efficient hydrolysis of magnetic milled powder from waste aluminum (Al) cans with low-concentrated alkaline solution for hydrogen generation. *International Journal of Energy Research*, 43(9), pp.4797-4806.
- Younas, M., Leong, L.K., Mohamed, A.R. and Sethupathi, S. (2016). CO<sub>2</sub> adsorption by modified palm shell activated carbon (PSAC) via chemical and physical activation and metal impregnation. *Chemical Engineering Communications*, 203(11), pp.1455-1463.
- Younas, M., Loong Kong, L., Bashir, M., Nadeem, H., Shehzad, A. and Sethupathi, S. (2016). Recent Advancements, Fundamental Challenges, and Opportunities in Catalytic Methanation of CO<sub>2</sub>. *Energy & Fuels*, 30(11), pp.8815-8831.
- Yu, Z.Y., Duan, Y., Feng, X.Y., Yu, X., Gao, M.R. and Yu, S.H. (2021). Clean and affordable hydrogen fuel from alkaline water splitting: past, recent progress, and future prospects. *Advanced Materials*, 33(31), p.2007100.
- Yu, C.H., Huang, C.H. and Tan, C.S. (2012). A review of CO<sub>2</sub> capture by absorption and adsorption. *Aerosol Air Quality Retoration*, 12(5), pp.745-769.
- Zhang, J. et al. (2014). Low-temperature methanation of syngas in slurry phase over Zr-doped Ni/ $\gamma$ -Al<sub>2</sub>O<sub>3</sub> catalysts prepared using different methods. *Fuel*, 132, pp. 211–218.
- Zhang, F., Edalati, K., Arita, M. and Horita, Z. (2018). Hydrolytic hydrogen production on Al–Sn–Zn alloys processed by high-pressure torsion. *Materials*, 11(7), p.1209.
- Zhao, C., Xu, F., Sun, L., Chen, J., Guo, X., Yan, E., Yu, F., Chu, H., Peng, H., Zou, Y. and Liu, Z. (2019). A novel AlBiOCl composite for hydrogen

generation from water. *International Journal of Hydrogen Energy*, 44(13), pp.6655-6662.

,

# APPENDICES

## Appendix 1: GC result of AWCP (100%).

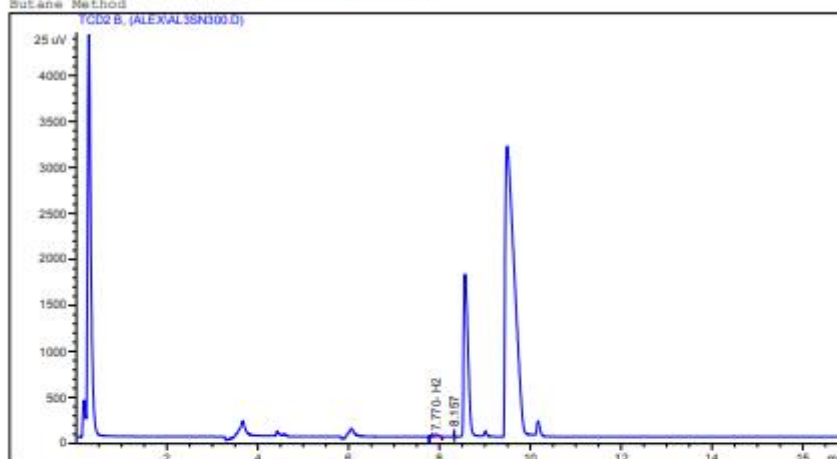


## Appendix 2: GC result of AWCP (3% Sn).

Data File C:\HPCHEM\1\DATA\ALEX\AL3SN300.D Sample Name: AL3SN

```

-----
Injection Date : 1/16/2020 2:23:01 PM
Sample Name : AL3SN3 Location : Vial 1
Acq Operator : ALEX Inj : 1
Acq Instrument : Instrument 1 Inj Volume : External
Method : C:\HPCHEM\1\METHODS\Q1STM
Last changed : 12/12/2019 1:16:40 PM by ADIRA
Butane Method
    
```



### External Standard Report

```

-----
Sorted By : Signal
Calib. Data Modified : Thursday, December 12, 2019 1:15:45 PM
Multiplier : 1.0000
Dilution : 1.0000
Sample Amount : 1.00000 [ppm] (not used in calc.)
Use Multiplier & Dilution Factor with ISTDs
    
```

Signal 1: TCD2 B,

RetTime [min]	Type	Area [25 uV*s]	Amt/Area	Amount [ppm]	Grp	Name
4.710		-	-	-		CO2
7.770	BB	113.59657	505.11199	5.73799e4		H2
11.496		-	-	-		CB4
16.442		-	-	-		CO

Totals : 5.73799e4

Results obtained with enhanced integrator!  
1 Warnings or Errors :

Warning : Calibrated compound(s) not found.

\*\*\* End of Report \*\*\*

Appendix 3: XRF result on elemental composition of AWCP (3% Sn).

Sample Information								
Sample name	Al3%Sn							
File name	UTAR Metal PowdeAl3%Sn							
Application	UTAR Metal Powde							
Date	5/6/2020 4:46:22 PM							
Analyzed by	RGSC							
Counts	1							
Comment								
Analyzed result(FP method)								
No.	Component	Result	Unit	Stat. Err.	LLD	LLQ	Element line	Intensity(cps/mA)
1	Mg	0.897	mass%	0.0072	0.0071	0.0213	4: Mg-K $\alpha$	180.122
2	Al	91.4	mass%					
3	Si	0.438	mass%	0.0025	0.0024	0.0071	4: Si-K $\alpha$	152.370
4	P	0.0169	mass%	0.0003	0.0004	0.0013	4: P-K $\alpha$	14.907
5	S	0.0127	mass%	0.0002	0.0004	0.0011	4: S-K $\alpha$	20.888
6	Ti	0.0541	mass%	0.0009	0.0018	0.0054	3: Ti-K $\alpha$	43.867
7	V	0.0066	mass%	0.0003	0.0007	0.0020	3: V-K $\alpha$	8.136
8	Cr	0.0320	mass%	0.0004	0.0006	0.0019	3: Cr-K $\alpha$	61.881
9	Mn	1.83	mass%	0.0031	0.0009	0.0027	2: Mn-K $\alpha$	1177.029
10	Fe	0.933	mass%	0.0019	0.0033	0.0098	2: Fe-K $\alpha$	937.359
11	Co	0.0089	mass%	0.0005	0.0013	0.0039	2: Co-K $\alpha$	12.375
12	Ni	0.0159	mass%	0.0002	0.0003	0.0010	2: Ni-K $\alpha$	31.578
13	Cu	0.425	mass%	0.0011	0.0003	0.0010	2: Cu-K $\alpha$	1124.702
14	Zn	0.107	mass%	0.0004	0.0002	0.0007	2: Zn-K $\alpha$	390.598
15	Ga	0.0350	mass%	0.0002	0.0002	0.0007	2: Ga-K $\alpha$	162.740
16	Ge	ND	mass%					
17	As	0.0008	mass%	<0.0001	0.0002	0.0005	2: As-K $\beta$ 1	1.139
18	Se	ND	mass%					
19	Nb	ND	mass%					
20	Mo	ND	mass%					
21	Ru	ND	mass%					
22	Rh	ND	mass%					
23	Pd	ND	mass%					
24	Ag	ND	mass%					
25	Cd	ND	mass%					
26	In	ND	mass%					
27	Sn	3.71	mass%	0.0052	0.0072	0.0217	1: Sn-K $\alpha$	2511.099
28	Sb	ND	mass%					
29	La	ND	mass%					
30	Ce	ND	mass%					
31	Pr	ND	mass%					
32	Nd	ND	mass%					
33	Hf	(0.0080)	mass%	0.0010	0.0029	0.0087	2: Hf-L $\alpha$	7.416
34	Ta	(0.0033)	mass%	0.0007	0.0020	0.0061	2: Ta-L $\alpha$	3.812
35	W	ND	mass%					
36	Ir	0.0030	mass%	0.0002	0.0004	0.0013	2: Ir-L $\alpha$	5.530
37	Pt	0.0024	mass%	0.0001	0.0002	0.0007	2: Pt-L $\alpha$	5.385
38	Au	0.0038	mass%	0.0001	0.0003	0.0009	2: Au-L $\alpha$	10.005
39	Hg	ND	mass%					
40	Tl	0.0025	mass%	<0.0001	<0.0001	<0.0001	2: Tl-L $\alpha$	8.413
41	Pb	0.0086	mass%	0.0001	0.0003	0.0010	2: Pb-L $\beta$ 1	39.617
42	Bi	ND	mass%					

Appendix 4: XRF result on elemental spectrum of AWCP (3% Sn).

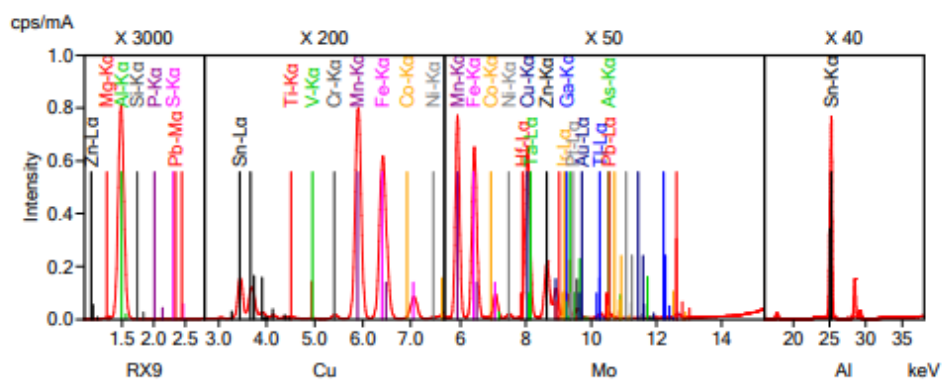
Analyzed result

Page 2/2

Sample Information

Sample name Al3%Sn  
 File name UTAR Metal PowdeAl3%Sn  
 Application UTAR Metal Powde  
 Date 5/6/2020 4:46:22 PM  
 Analyzed by RGSC  
 Counts 1  
 Comment

Spectrum



## Appendix 5: XRD result of AWCP (100%).

### Match! Phase Analysis Report

Universiti Tunku Abdul Rahman, Faculty of Science

Sample: AL01 ()

#### Sample Data

File name	LST_AL01.ORG
File path	C:\xddat\Standard\LST_AL01
Data collected	Mar 14, 2019 16:20:56
Data range	10.110° - 80.110°
Original data range	10.000° - 80.000°
Number of points	3501
Step size	0.020
Rietveld refinement converged	No
Alpha2 subtracted	No
Background subtr.	No
Data smoothed	No
2theta correction	0.11°
Radiation	X-rays
Wavelength	1.540600 Å

#### Matched Phases

Index	Amount (%)	Name	Formula sum
A	88.1	Aluminum Hydroxide Bayerite	Al (OH)3
	11.9	Unidentified peak area	

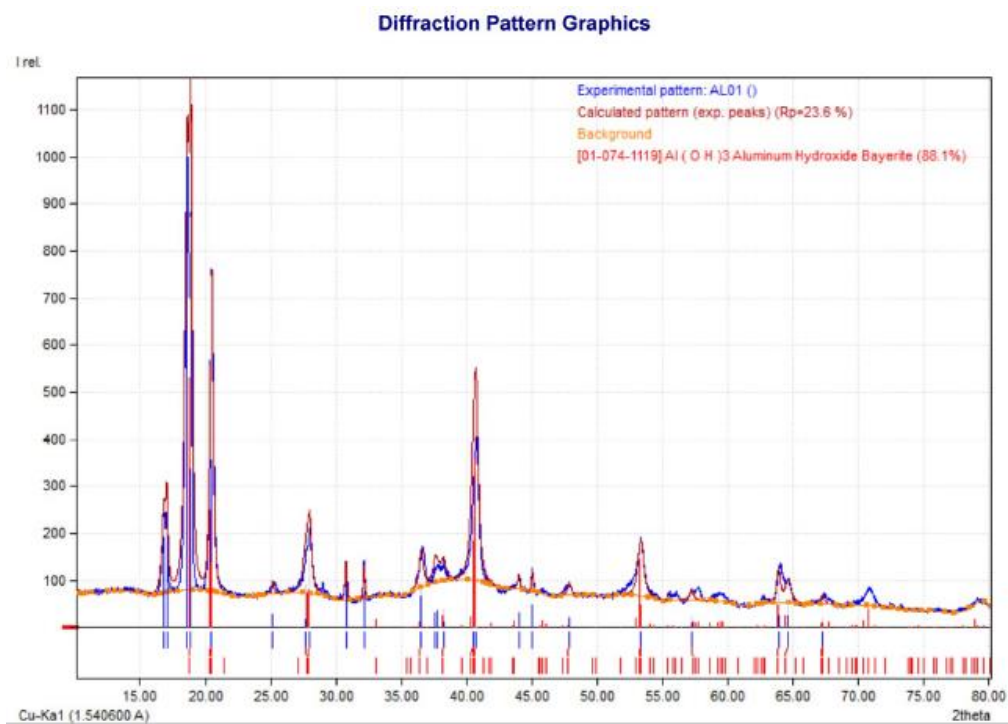
#### A: Aluminum Hydroxide

##### Bayerite (88.1 %)

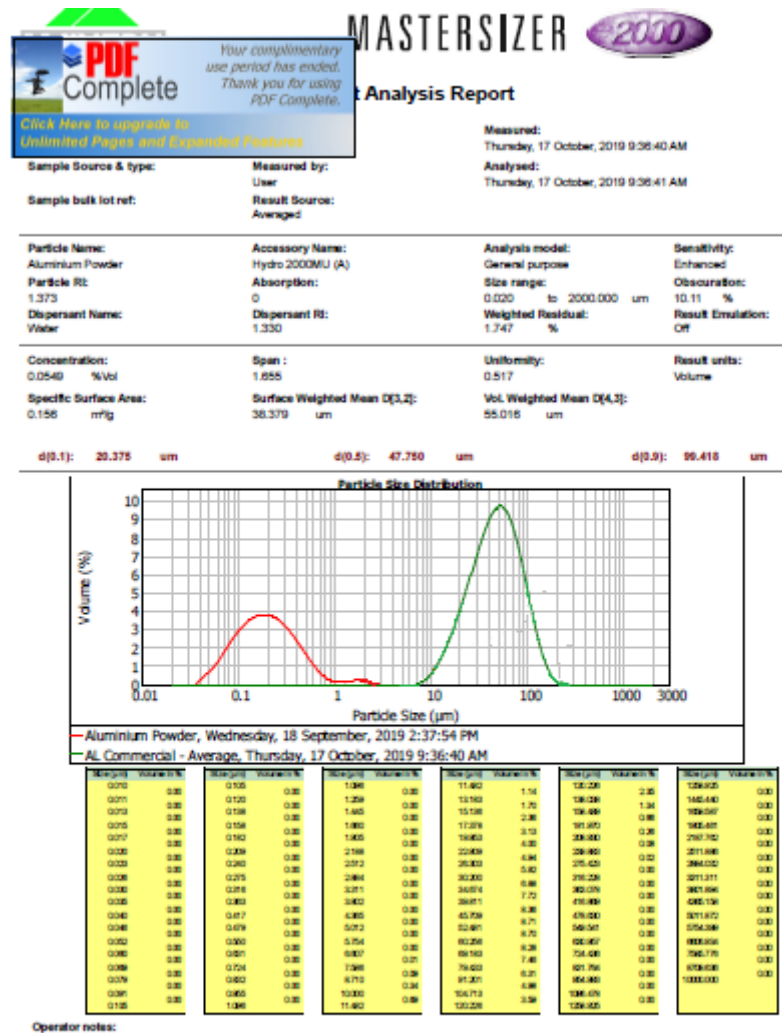
Formula sum	Al (OH)3
Entry number	01-074-1119
Figure-of-Merit (FoM)	0.876722
Total number of peaks	198
Peaks in range	198
Peaks matched	21
Intensity scale factor	0.53
Space group	P21/a
Crystal system	monoclinic
Unit cell	a= 5.0620 Å b= 8.6710 Å c= 4.7130 Å β= 90.270 °
V/c	1.33
Calc. density	2.505 g/cm <sup>3</sup>
Reference	Rothbauer, R., Zigan, F., O'Daniel, H., Z. Kristallogr., Kristallgeom., Kristallphys., Kristallchem. <b>125</b> , 317 (1967)

#### Candidates

Appendix 6: XRD pattern of AWCP (100%).



Appendix 7: PSA analysis of commercial Al and ACWP (100%).



## Appendix 8: BET analysis summary report of ACWP (3% Sn).

### Full Report Set

MicroActive for TriStar II Plus 2.03

MicroActive for TriStar II Plus Version 2.03  
Serial # 384 Unit 1 Port 2

Page 1

Sample: 000-368  
Operator: NAZRUL  
Submitter: ABDUL KAREEM  
File: C:\Users\BET\Documents\ABD...\3% SN (ABDUL KAREEM).SMP

Started: 2/26/2020 5:36:49 PM	Analysis Adsorptive: N2
Completed: 2/26/2020 10:06:39 PM	Analysis Bath Temp.: -195.800 °C
Report Time: 2/27/2020 9:54:38 AM	Thermal Correction: No
Sample Mass: 0.3359 g	Warm Free Space: 15.7668 cm <sup>3</sup> Measured
Cold Free Space: 48.4949 cm <sup>3</sup>	Equilibration Interval: 5 s
Low Pressure Dose: None	Sample Density: 1.000 g/cm <sup>3</sup>
Automatic Degas: No	

### Summary Report

#### Surface Area

Single point surface area at  $p/p^0 = 0.299467776$ : 18.8965 m<sup>2</sup>/g

BET Surface Area: 19.3702 m<sup>2</sup>/g

Langmuir Surface Area: 19.6149 m<sup>2</sup>/g

t-Plot External Surface Area: 20.9222 m<sup>2</sup>/g

#### Pore Volume

Single point adsorption total pore volume of pores  
less than 1.1445 nm width at  $p/p^0 = 0.010205277$ : 0.000105 cm<sup>3</sup>/g

Single point desorption total pore volume of pores  
less than 20.6503 nm width at  $p/p^0 = 0.900000000$ : 0.007482 cm<sup>3</sup>/g

#### Pore Size

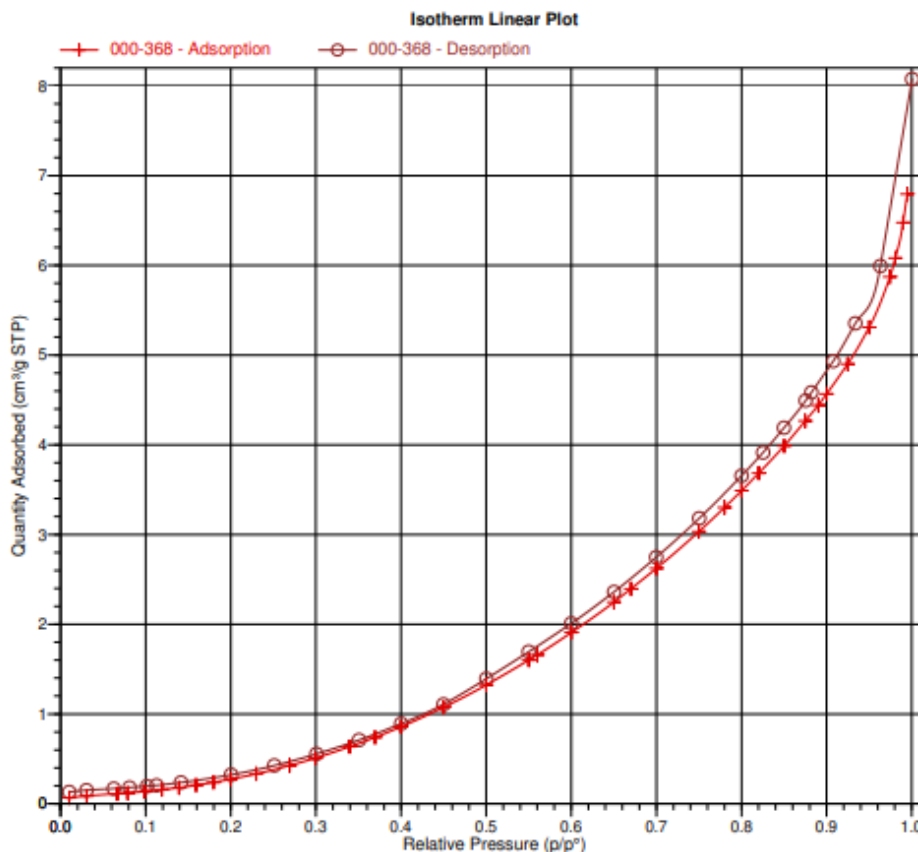
Adsorption average pore diameter (4V/A by BET): 0.20673 nm

Desorption average pore diameter (4V/A by BET): 14.77815 nm

BJH Adsorption average pore width (4V/A): 5.0799 nm

BJH Desorption average pore width (4V/A): 5.0258 nm

Appendix 9: BET isotherm linear plot of ACWP (3% Sn).



Appendix 10: BET analysis sample log message at PutraCat Lab, Universiti Putra Malaysia (UPM).

Sample log		
Date	Time	Log Message
2/26/2020	5:36:49 PM	Started analysis of file 3% SN (ABDUL KAREEM).SMP on port 2.
2/26/2020	5:36:49 PM	System volume: 13.5999 cm³
2/26/2020	5:47:31 PM	Pressure transducer zeroed.
2/26/2020	5:57:49 PM	Measured free space on port 2, Warm: 15.0049 cm³, Cold: 47.7331 cm³
2/26/2020	6:09:45 PM	Pressure transducer zeroed.
2/26/2020	6:09:45 PM	Starting p² in p² tube measurement.
2/26/2020	7:41:29 PM	p² over Sample is 758.91 mmHg.
2/26/2020	7:41:28 PM	Measured p² over sample: 758.91443 mmHg
2/26/2020	10:06:39 PM	Finished a sample analysis for C:\Users\BET\Documents\ABD...3% SN (ABDUL KAREEM).SMP on port 2.

## Appendix 11: Gibbs Free Energy Calculation.

For example, the Gibbs free energy calculation for disintegrated AWCP is as follows:

$$\begin{aligned}\Delta H^{\circ} &= \sum H_f^{\circ} (\text{Products}) - \sum H_f^{\circ} (\text{Reactants}) \\ &= [2(-1287.40) + 3(0)] - [2(0) + 6(-285.90)] \\ &= -860 \text{ kJ/mol}\end{aligned}$$

$$\begin{aligned}\Delta S^{\circ} &= \sum S^{\circ} (\text{Products}) - \sum S^{\circ} (\text{Reactants}) \\ &= [2(85.40) + 3(130.60)] - [2(28.30) + 6(69.90)] \\ &= 86.6 \text{ J/mol.K}\end{aligned}$$

$$\begin{aligned}\Delta G_{298.15^{\circ}} &= \Delta H^{\circ} - T \Delta S^{\circ} \\ &= -860 \text{ kJ/mol} - (298.15\text{K}) (86.6/1000 \text{ kJ/mol.K}) \\ &= -885.82 \text{ kJ/mol}\end{aligned}$$

$$\begin{aligned}\Delta G_{335.55^{\circ}} &= \Delta H_{298.15^{\circ}} - T \Delta S_{298.15^{\circ}} \\ &= -860 \text{ kJ/mol} - (335.55\text{K}) (86.6/1000 \text{ kJ/mol.K})\end{aligned}$$

=-889.06 kJ/mol (disintegrated AWCP)

Appendix 12: Example of catalytic activity calculation for CO<sub>2</sub> methanation.

$$\text{CO}_2 \text{ conversion, } X_{\text{CO}_2} (\%) = (\text{CO}_{2,\text{in}} - \text{CO}_{2,\text{out}}) / (\text{CO}_{2,\text{in}}) \times 100$$

$$= (7140 - 3477) / 7140 \times 100$$

$$= 51.3 \%$$

$$\text{CH}_4 \text{ selectivity, } S_{\text{CH}_4} (\%) = (\text{CH}_{4,\text{out}}) / (\text{CO}_{2,\text{in}} - \text{CO}_{2,\text{out}}) \times 100$$

$$= 1730.0631 / (0.7140 - 0.3477) \times 100$$

$$= 47.232 \%$$

$$\text{CH}_4 \text{ yield, } Y_{\text{CH}_4} (\%) = (X_{\text{CO}_2} \times S_{\text{CH}_4}) / 100$$

$$= (51.3 \times 47.232) / 100$$

$$= 24.230 \%$$

Appendix 12: Composition definition of AWCP and its composites.

Sample	Definition
0.5g AWCP (100%)	0.5g AWCP*
0.5g AWCP (97%)	0.485g AWCP
0.5g AWCP (3% Sn)	0.485g AWCP + 0.015g Sn
0.5g AWCP (3% Sn – 3% Mg)	0.47g AWCP + 0.015g Sn + 0.015g Mg

\*AWCP (optimized condition: disintegrated for 20min) in 1M NaOH solution prepared by deionized water at STP conditions.

## LIST OF PUBLICATION

No.	Type	Title	Description
1.	Conference proceeding	Hydrogen Gas Production Using Aluminum Waste Cans Powder Produced By Disintegration Method	3 <sup>rd</sup> International on Advanced Energy Materials (ICAEM 2020) – in Okinawa, Japan on 17 Feb 2020.
<p>Lim, S.T., Sethupathi, S., Alsultan, A.G., Leong, L.K. and Taufiq-Yap, Y.H., 2020. Hydrogen Gas Production Using Aluminum Waste Cans Powder Produced by Disintegration Method. In Key Engineering Materials (Vol. 853, pp. 228-234). Trans Tech Publications Ltd.</p>			
2.	WOS Journal	Hydrogen Production via Activated Waste Aluminum Cans and Its Potential for Methanation	An Energy&Fuels Published Journal in 2021.
<p>Lim, S.T., Sethupathi, S., Alsultan, A.G. and Munusamy, Y., 2021. Hydrogen Production via Activated Waste Aluminum Cans and Its Potential for Methanation. <i>Energy &amp; Fuels</i>, 35(19), pp.16212-16221.</p>			